Universidade de Aveiro
2010

Departamento de Engenharia Cerâmica e do Vidro

Joana Andreia Redondo Mendes Marques Laranjeiro

Filmes espessos de PZT para dispositivos electrónicos embutidos

Universidade de Aveiro
2010

Departamento de Engenharia Cerâmica e do Vidro

Joana Andreia Redondo Mendes Marques Laranjeiro

Filmes espessos de PZT para dispositivos electrónicos embutidos

Dissertação apresentada à Universidade de Aveiro para cumprimento dos requisitos necessários à obtenção do grau de Mestre em Engenharia de Cerâmica e do Vidro, realizada sob a orientação científica da Doutora Paula Maria Silveirinha Vilarinho, Prof.ª Doutora do Departamento de Engenharia Cerâmica e do Vidro da Universidade de Aveiro e da Doutora Aiying Wu, Investigadora Auxiliar do Centro de Investigação em Materiais Cerâmicos e Compósitos (CICECO) da Universidade de Aveiro.

Dissertation presented to the University of Aveiro in partial fulfilment of the requirements for the awarding of the master in Ceramics and Glass Engineering carried out under the supervision of Dr Paula Maria Silveirinha Vilarinho, Associated Professor at the University of Aveiro, Department of Ceramics and Glass Engineering, and Dr. Aiying Wu, Auxiliar Researcher at the Research Center for Ceramics and Composite Materials (CICECO) of the University of Aveiro

o júri

presidente

Doutor Pedro Quintanilha Mantas
Professor Auxiliar da Universidade de Aveiro

vogais

Doutor José Ramiro Fernandes
Professor Auxiliar da Universidade de Trás os Montes e Alto Douro

Doutora Paula Maria Lousada Silveirinha Vilarinho
Professora Associada da Universidade do Aveiro

Doutora Aiying Wu
Investigadora Auxiliar da Universidade de Aveiro

agradecimentos

Gostaria de expressar a minha sincera gratidão a todas as pessoas que me deram a possibilidade de terminar esta tese.
Em primeiro lugar, quero agradecer à minha orientadora e à minha coorientadora: Prof. Dr.ª. Paula Vilarinho e Dr.ª. Aiying Wu, que estiveram sempre dispostas a ouvir, discutir e dar conselhos sobre o trabalho. O seu encorajamento será sempre apreciado.
Um especial obrigado ao Professor Augusto Luis Barros Lopes, e aos Engenheiros. Marta Ferro, Conceição Costa, Célia Miranda e Jorge Corker, técnicos do Departamento de Engenharia Cerâmica e do Vidro da Universidade de Aveiro, pela ajuda prestada na utilização dos equipamentos técnico-científicos utilizados ao longo deste trabalho.
Por último, gostaria de dar os meus sinceros agradecimentos à minha família: o meu pai, mãe e irmão, João Laranjeiro, Ana Bela Laranjeiro e João André Laranjeiro, cujo amor incondicional me ajudou a completar este trabalho.

I would like to express my sincere gratitude to all of those who gave me the possibility to complete this thesis.
First of all, I want to thank my supervisors: Prof. Dr. Paula Vilarinho and Dr. Aiying Wu. They were always willing to listen, discuss and give advice throughout the work. Their encouragements and guidance will always be appreciated.
I would like to acknowledge Professor Augusto Luis Barros Lopes and Engineers Marta Ferro, Conceição Costa, Celia Miranda and Jorge Corker, technicians from the Department of Ceramics and Glass Engineering of the University of Aveiro, for their help with the utilization of the scientific and technical equipment used during this work.
Last, but not least, I would like to give my special thanks to my family: my father, mother and brother, João Laranjeiro, Ana Bela Laranjeiro and João André Laranjeiro, whose patient love and endless support enabled me to complete this work.

palavras-chave

Titanato zirconato de chumbo, PZT, Filmes Espessos, Deposição Elelectroforética, EPD, Propriedades Eléctricas, Aplicações Microelectrónicas

resumo

Pós de titanato zirconato de chumbo, com um tamanho de partícula de aproximadamente 300 nm, foram usados como material base para a deposição electroforética (EPD) de filmes espessos de PZT em substratos flexíveis de cobre. Foram preparadas, modificadas e aperfeiçoadas várias suspensões a fim de optimizar a etapa de deposição. Para diminuir a temperatura de sinterização dos filmes espessos, de forma a tornar a sua utilização compatível com o uso de substratos de cobre, recorreu-se à utilização de diferentes aditivos de sinterização, nomeadamente um vidro composto por SiO_2, PbO, Al_2O_3, B_2O_3 e uma mistura de dois óxidos (B_2O_3 e PbO). Foram então depositados por EPD filmes de PZT sobre folhas de cobre em presença destes aditivos de sinterização; primeiramente com a adição de 5, 10 e 20 % em peso de vidro e, posteriormente, com a adição de 1 e 3 % em peso de uma mistura de diferentes proporções dos óxidos B_2O_3 e PbO (90/10, 80/20 e 50/50) e os filmes foram sinterizados a diferentes temperaturas, entre 800ºC e 900ºC e em atmosfera de baixa pressão parcial de oxigénio (pO_2) (~ $5x10^{-5}$ e $8x10^{-7}$ atm). Verificou-se que a deposição em presença de pós de vidro origina filmes não uniformes, com superfícies irregulares e microestruturas porosas, o que se deve à dificuldade em obter suspensões desfloculadas e estáveis. A resposta dieléctrica dos vários filmes espessos de PZT sobre cobre foi analisada em função da frequência à temperatura ambiente. Verificou-se que a presença dos óxidos aditivos de sinterização melhorou a densificação dos filmes. A adição da mistura de 3 % em peso de 50%B_2O_3 + 50%PbO originou a melhor resposta dieléctrica de filmes sinterizados a 800 ºC e 850ºC (permitividade de ~1195 e perda dieléctrica de~0,02). Os resultados obtidos foram comparados com os da adição de uma mistura de V_2O_3 e PbO, previamente reportados. Foi então demonstrado que os filmes espessos de PZT aditivados com misturas de B_2O_3 e PbO e fabricados por deposição electroforética em substratos de cobre flexíveis são passíveis de serem usados como condensadores embutidos em circuitos da microelectrónica.

keywords

Lead Zirconate Titanate, PZT, thick films, Eletrophoretic Deposition, EPD, electric properties, microelectronic applications.
.

abstract

Powders of lead zirconate titanate with a particle size of about 300 nm, were used as base material for the electrophoretic deposition (EPD) of PZT thick films on flexible copper substrates. With these powders, several suspensions were prepared, modified and improved in order to optimize the deposition step. To lower the sintering temperature of thick films to make its employment consistent with the use of copper substrates, different sintering additives, including a glass comprising of SiO_2, PbO, Al_2O_3, and B_2O_3 and a mixture of two oxides (PbO and B_2O_3) were studied. Films were then deposited by EPD of PZT films on copper sheets in the presence of sintering additives, first with the addition of 5, 10 and 20% by weight of glass and, later, with the addition of 1 and 3% by weight of a mixture of PbO and B_2O_3 (90/10, 80/20 and 50/50) and the films were sintered at different temperatures between 800 º C and 900 º C in an atmosphere of low oxygen partial pressure (pO_2) (~ $5x10^{-5}$ and $8x10^{-7}$ atm). It was found that the deposition in the presence of glass powder causes non-uniform films with rough surfaces and porous microstructures, which is due to the difficulty in obtaining deflocculated and stable suspensions. The dielectric response of the various PZT thick films on copper was examined as a function of frequency at room temperature. It was found that the presence of oxide sintering additives improved the densification of the films. The addition of mixing 3wt% of 50% B_2O_3 + 50% PbO led to an optimized dielectric response for the films sintered at 800 º C and 850 º C (permittivity ~1195 and losses ~0.02). The results were compared with PZT films prepared with the addition of a mixture of PbO and V_2O_3, previously reported. In conclusion, PZT thick films manufactured by EPD on copper flexible substrates and sintered in the presence of PbO and B_2O_3 (as sintering aid mixtures) can be used as embedded capacitors in microelectronic circuits.

TABLE OF CONTENTS

Index

List of Symbols

d_{ij} - Piezoelectric coefficient (relates a field along the i axis to the strain in the j direction)

D_S - Dielectric breakdown strength or dielectric strength

E - Electric field

E_a - Activation energy

E_c - Coercive electric field

P - Polarization

P_r - Remnant polarization

Q - Quality factor

r_A - Ionic radius of A cation in ABO_3 perovskite

r_B - Ionic radius of B cation in ABO_3 perovskite

r_O - Ionic radius of oxygen anion in ABO_3 perovskite

t - Thickness of the dielectric

T - Temperature

T_0 - Temperature at 0ºC

T_c - Curie temperature

C – Curie Constant

ε_o - Permittivity of the vacuum

ε_r - Relative permittivity or dielectric constant

$\varepsilon_{r'}$ - The real part of the dielectric constant

$\varepsilon_{r''}$ - The imaginary part of the dielectric constant

ε_s - Static permittivity

k_{eff} – Effective coupling coefficient

k_p and k_{33}– Electromechanical coupling factor

d_{33} and d_{31} - Piezoelectric charge constant (C/N or m/V)

g_{33} - Piezoelectric voltage constant (Vm/N or m^2/C)

C – Capacitance

tan δ - Dielectric dissipation factor (dielectric loss %)

Ps - Spontaneous polarization

Psat - Saturation polarization

List of Abbreviations

AR - Anti-reflective

BNT - Sodium Bismuth Titanate ($(Bi_{1/2}Na_{1/2})TiO_3$)

BST - Barium Strontium Titanate ($Ba_{1-x}Sr_xTiO_3$)

BT - Barium Titanate ($BaTiO_3$),

BZT - Barium Zirconium Titanate ($Ba_{1-x}Zr_xTiO_3$)

CSD - Chemical Solution Deposition

CV - Capacitance Voltage curves

CVD - Chemical Vapour Deposition

d_{A-O} - Distance between A - anion and O - oxygen

d_{B-O} - Distance between B – cation and O - oxygen

DRAM - Dynamic Random Access Memory

EDS - Energy Dispersive X-ray Analysis

EPD - Electrophoretic Deposition

EETs - Explosive-to-Electrical Transducers

fcc - Face-Centered Cubic

FET - Field Effect Transistor

IR - Infrared

MEMS - Microelectromechanical Systems

MPB - Morphotropic Phase Boundary

MOD - Metalloorganic Decomposition

NEMS - Nanoelectromechanical Systems

NKN - Sodium Potassium Niobate ($(Na_{0.5}K_{0.5})\ NbO_3$)

NVRAMs - Non-volatile Random Access Memories

PbT – Lead Titanate

PbZ – Lead Zirconate

PBZT (Ba) - Lead Barium Zirconate Titanate

pH_{pzc} – Value for zero charge

pH_{iep} – Value for isoelectric charge

PLZT – Lead Lanthanum Zirconate Titanate

PNZT (Nb) - Lead Niobium Zirconate Titanate

pO_2 – Oxygen Partial Pressure

PSZT (Sn) - Lead Tin Zirconate Titanate

PVD - Physical Vapour Deposition

PWB - Printed Wiring Board

PZT – Lead Zirconate Titanate ($PbZr_{0.52}Ti_{0.48}O_3$)

R&D - Research and Development

SAW - Surface Acoustic Wave

SEM – Scanning Electron Microscopy

SONAR - Sound Navigation and Ranging

TEM - Transmission Electron Microscopy

XRD – X-Ray Diffraction

XPM - X-Ray Photoelectron Microscopy

3D – Three Dimensions

List of Figures

Figure 37: Losses versus frequency for PZT + 10 and 20 wt % Glass + 7.5 wt % PVB films sintered at 800ºC and 900ºC for 30 minutes. __ (10%), 800 ºC for 30 minutes, with 0.0046 mm of film thickness; __ (20%), 850 ºC for 30 minutes, with 0.0042 mm of film thickness; __ (20%), 900 ºC for 30 minutes, with 0.0035mm of film thickness.

Figure 38: Permittivity versus % PbO of PZT films with 1 wt % of (xB_2O_3 + (100-x) PbO), being x = 90, 80 and 50) and sintered at different sintering temperatures, 800ºC, 850ºC and 900ºC for 30 minutes.

Figure 39: Permittivity versus % PbO of PZT films with 1 wt % of (xB_2O_3 + (100-x) PbO), being x= 90, 80 and 50) and sintered at different sintering temperatures, 800ºC, 850ºC and 900ºC for 60 minutes.

Figure 40: Permittivity versus frequency for PZT films with 1wt % of (90% B_2O_3 and 10% PbO) and sintered at 800ºC, 850ºC and 900ºC for 30 and 60 minutes. __ 800 ºC for 30 minutes, with film thickness of 0.0162 mm; __ 800 ºC for 60 minutes, with film thickness of 0.0165 mm; __ 900 ºC for 30 minutes, with film thickness of 0.0172 mm; __ 900 ºC for 60 minutes, with film thickness of 0.0072 mm; __ 850 ºC for 30 minutes, with film thickness of 0.0172 mm; __ 850 ºC for 60 minutes, with film thickness of 0.0165 mm.

Figure 41: Dielectric losses (tan δ) versus frequency for PZT films with 1wt % of (90% B_2O_3 and 10% PbO) and sintered at 800ºC, 850ºC and 900ºC for 30 and 60 minutes. . __ 800 ºC for 30 minutes, with film thickness of 0.0162 mm; __ 800 ºC for 60 minutes, with film thickness of 0.0165 mm; __ 900 ºC for 30 minutes, with film thickness of 0.0172 mm; __ 900 ºC for 60 minutes, with film thickness of 0.0072 mm; __ 850 ºC for 30 minutes, with film thickness of 0.0172 mm; __ 850 ºC for 60 minutes, with film thickness of 0.0165 mm.

Figure 42: Permittivity versus frequency for PZT films with 1wt % of (80% B_2O_3+ 20% PbO) films sintered at 800ºC, 850ºC and 900ºC for 30 and 60 minutes. __ 800 ºC for 30 minutes, with film thickness of 0.0202 mm; __ 800 ºC for 60 minutes, with film thickness of 0.0146 mm; __ 900 ºC for 30 minutes, with film thickness of 0.0106 mm; __ 900 ºC for 60 minutes, with film thickness of 0.0092 mm; __ 850 ºC for 30 minutes, with film thickness of 0.0124 mm; __ 850 ºC for 60 minutes, with film thickness of 0.0265 mm.

Figure 43: Dielectric losses (tan δ) versus frequency for PZT films with 1wt % of (80 B_2O_3+ 20 PbO films sintered at 800ºC, 850ºC and 900ºC for 30 and 60 minutes. __ 800 ºC for 30 minutes, with film thickness of 0.0202 mm; __ 800 ºC for 60 minutes, with film thickness of 0.0146 mm; __ 900 ºC for 30 minutes, with film thickness of 0.0106 mm; __ 900 ºC for 60 minutes, with film thickness of 0.0092 mm; __ 850 ºC for 30 minutes, with film thickness of 0.0124 mm; __ 850 ºC for 60 minutes, with film thickness of 0.0265 mm.

Figure 44: Permittivity versus frequency for sintered PZT films with 1 and 3 wt % of (50 B_2O_3 + 50 PbO) films sintered at 800ºC, 850ºC and 900ºC for 30 and 60 minutes. __ (1wt %), 800 ºC for 30 minutes, with film thickness of 0.0238 mm; __ (1wt %), 800 ºC for 60 minutes, with film thickness of 0.0112 mm; __ (1wt %), 900 ºC for 60 minutes, with film thickness of 0.0044 mm; __ (1wt %), 850 ºC for 30 minutes, with film thickness of 0.0154 mm; __ (1wt %), 850 ºC for 60 minutes, with film thickness of 0.0130 mm; _*_ (3wt %), 800 ºC for 30 minutes, with film thickness of 0.010 mm; _'_ (3wt %), 800 ºC for 60 minutes, with film thickness of 0.009 mm; _*_ (3wt %), 850 ºC for 30 minutes, with film thickness of 0.009 mm; _*_ (3wt %), 850 ºC for 60 minutes, with film thickness of 0.009 mm.

Figure 45: Dielectric losses (tan δ) versus frequency for PZT films with 1 and 3 wt % of (50% B_2O_3+ 50% PbO) films sintered at 800ºC, 850ºC and 900ºC for 30 and 60 minutes. __ (1wt %), 800 ºC for 30 minutes, with film thickness of 0.0238 mm; __ (1wt %), 800 ºC for 60 minutes, with film thickness of 0.0112 mm; __ (1wt %), 850 ºC for 30 minutes, with film thickness of 0.0154 mm; __ (1wt %), 850 ºC for 60 minutes, with film thickness of 0.0130 mm; _*_ (3wt %), 800 ºC for 30 minutes, with film thickness of 0.010 mm; _'_ (3wt %), 800 ºC for 60 minutes, with film thickness of 0.009 mm; _*_ (3wt %), 850 ºC for 30 minutes, with film thickness of 0.009 mm; _*_ (3wt %), 850 ºC for 60 minutes, with film thickness of 0.009 mm..

Figure 46: Capacitance versus voltage PZT films with 1and 3 wt % of (50% B_2O_3+ 50% PbO) sintered at 800ºC, 850 and 900ºC for 30 and 60 minutes. __ (1wt %), 800 ºC for 30 minutes, with film thickness of 0.0238 mm; __ (1wt %), 800 ºC for 60 minutes, with film thickness of 0.0112 mm; __ (1wt %), 900 ºC for 30 minutes, with film thickness of 0.0078 mm; __ (1wt %), 850 ºC for 30 minutes, with film thickness of 0.0154 mm; __ (1wt %), 850 ºC for 60 minutes, with film thickness of 0.0130 mm; __ (3wt %), 800 ºC for 30 minutes, with film thickness of 0.010 mm; __ (3wt %), 850 ºC for 30 minutes, with film thickness of 0.009 mm

Figure 47: Permittivity versus frequency for PZT films with 1wt % of (V_2O_5 + PbO) and sintered at 800ºC, 850ºC and 900ºC and for 30 and 60 minutes. __800 ºC for 30 minutes, with film thickness of 0.007 mm; __850 ºC for 30 minutes, with film thickness of 0.010 mm; __900 ºC

for 30 minutes, with film thickness of 0.011mm; __900 ºC for 60 minutes, with film thickness of 0.009 mm.

Figure 48: Dielectric losses (tan δ) versus frequency for PZT films with 1wt % of (V_2O_5 + PbO) and sintered at 800ºC, 850ºC and 900ºC and for 30 and 60 minutes. __800 ºC for 30 minutes, with film thickness of 0.007 mm; __850 ºC for 30 minutes, with film thickness of 0.010 mm; __900 ºC for 30 minutes, with film thickness of 0.011mm; __900 ºC for 60 minutes, with film thickness of 0.009 mm

Figure 49: Dielectric permittivity and dielectric loss of PZT thick films on Cu foil sintered at 1000 ºC for 30 min at pO_2 ~5 x10^{-5} atm as a function of frequency.[32]

List of Tables

1. Introduction

Lead zirconate titanate, $PbZr_{1-x}Ti_xO_3$ (PZT) has a perovskite type structure. This structure is adopted by many functional oxides that have the chemical formula ABO_3 and several of them exhibit important and useful technological properties such as ferroelectricity, pyroelectricity, piezoelectricity, non linear optical behaviour, *inter alia*, that make them very useful in applications such as catalysts, sensors, actuators, microelectromechanical systems (MEMS), nanoelectromechanical systems (NEMS), memories, superconductors, etc.[1],[2], [7],

In PZT, Ti^{4+} and Zr^{4+} ions occupy randomly B sites of the perovskite lattice. At high temperatures PZT has the cubic perovskite structure, which is paraelectric. On cooling below the Curie point, the structure undergoes a phase transition to form a ferroelectric tetragonal or rhombohedral phase. In the tetragonal phase, the spontaneous polarization is along the <100> set of directions while in the rhombohedral phase the polarization is along the <111> set of directions. Below the Zr/Ti ratio of 95/5 the solid solution is antiferroelectric with an orthorhombic phase. On the application of an electric field to this composition a double hysteresis loop is obtained. This is because of the strong influence of the antiferroelectric $PbZrO_3$ (Lead Zirconate) phase.[3]

1.1 Lead Zirconate Titanate (PZT): General Aspects

The solid solution between $PbZrO_3$ and $PbTiO_3$ (Lead Titanate), well known as PZT, is important for electronic applications due to the peculiar electric properties displayed by some of the compositions, namely those within the morphotropic phase boundary (MPB), $PbZr_{0.52}Ti_{0.48}O_3$. MPB compositions have mixed crystallographic symmetries and therefore are easily poled in the polycrystalline form and the electromechanical properties are maximised. Above the ferroelectric phase transition T_c (being the Curie temperature) at >350ºC for the x = 0.48 MPB composition, PZT is in the paraelectric phase, with a Pm3m cubic centrosymmetric space group. Below T_c, a mixture of ferroelectric rhombohedral and tetragonal phases exists and the high dielectric permittivity (ε_r ~1000), high remanent polarization value (P_r ~30 $\mu C/cm^2$), and high piezoelectric coefficients (d_{33} ~ 350 pC/N) make it useful in a wide range of applications.[4]

Figure 1 depicts the perovskite-type PZT unit cell above the Curie temperature and its distorted unit cell below the Curie temperature.

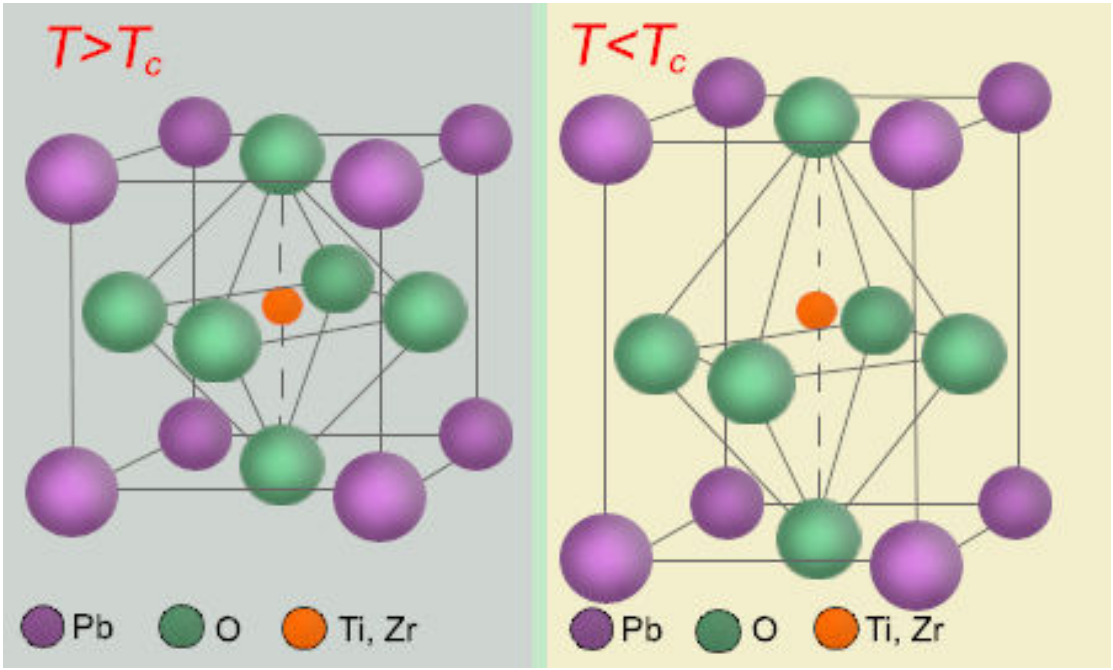

Figure 1: Perovskite lead zirconate titanate (PZT) unit cell in the symmetric cubic state, above the Curie temperature (left picture), and tetragonally distorced below the Curie temperature (right picture).[5]

PZT MPB compositions exhibit anomalously augmented dielectric and piezoelectric properties as a result of the enhanced polarizability arising from the coupling between two equivalent energy states, i.e., tetragonal and rhombohedral phases, allowing optimum domain reorientation during the poling process.[5] These properties make PZT-based compounds one of

the most prominent and useful electroceramics nowadays, in particular for electromechanical applications.

Figure 2 depicts the phase diagram of PZT[6]. Its composition is varied by altering the value x in the PZT formula. This greatly changes the properties. For example if PZT is used at 50% mol of $PbTiO_3$, then it is near the rhombohedral / tetragonal phase boundary, which allows the formation of many different polarisation states, along the <100> and <111> directions. As a consequence, there are many possible orientations for the dipole moments, originating high net polarization and easy poling.[6] Table 1 tabulates some physical characteristics of three different commercially available PZT ceramic compositions, PZT-4 ($(Pb_{0.94}Sr_{0.06})(Zr_{0.53}Ti_{0.47})O_3$)[7]; PZT-5A ($Pb_{0.988}(Zr_{0.52}Ti_{0.48})_{0.976}Nb_{0.024}O_3$)[7]; PZT-5H and of Quartz and undoped PZT for comparison. PZT-5H ceramics exhibit the highest piezoelectric properties (i.e., k_{eff}, k_p, d_{31}, and d_{33}) at room temperature, followed by the PZT-5A and PZT-4 ones, respectively. When cooled to -150 ºC, the k_{eff} (Effective Coupling Coefficient) and k_p (Electromechanical Coupling Factor) values of each composition remained relatively constant. The d_{31} and d_{33} (Piezoelectric Charge Constant) values for PZT-4 also remained relatively stable over this temperature range. The *d* constants for the PZT-5A and PZT-5H ceramics, however, decreased to approximately 50% of their room temperature values when cooled to -150ºC.[8]

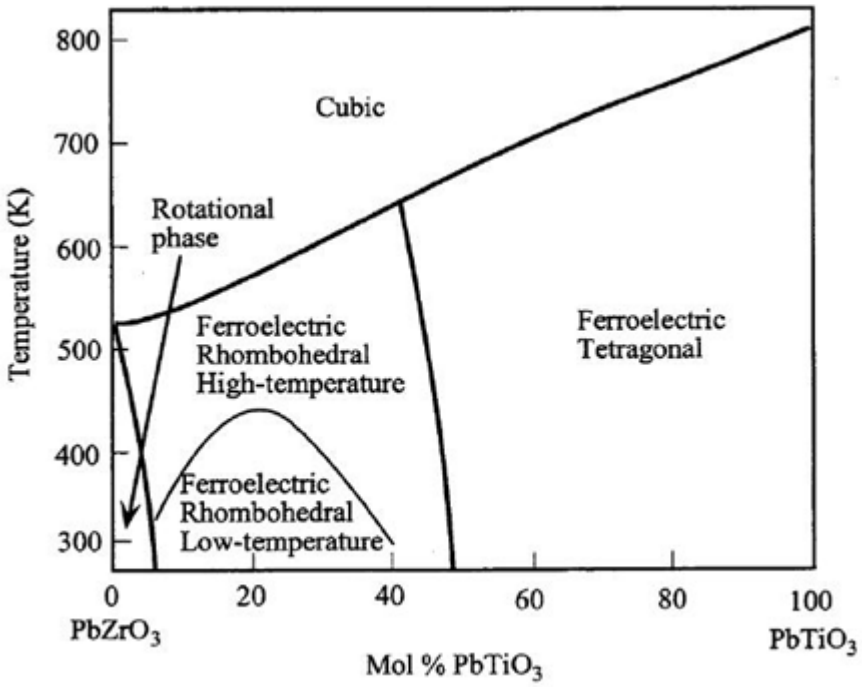

Figure 2: PZT Phase Diagram.[6]

Table1: Composition and physical properties of commercially available PZT ceramics. [9], [10], [11]

Composition	Density (g/cm^3)	T_c (ºC)	tan δ (%)	K_p	K_{33}	d_{33} ($x10^{-12}$ C/N)	d_{31} ($x10^{-12}$ C/N)	g_{33} ($x10^{-3}$ (Vm/N))	Properties	Applications
PZT - 4	7.5	328	0.4	0.58	0.7	289	-123	26.1	High amplitude vibration, maintaining low dielectric and mechanical losses	Ultrasound and sonar Recommended for applications at medium and high electric power.
PZT - 5A	7.8	365	2	0.6	0.71	374	-171	24.8	Mechanical and dielectric losses with high intensity	Low power transmitter and receiver devices, i.e. NDT (Non-destructive testing), hydrophones and accelerometers.
PZT - 5H	7.5	193	4	0.65	0.75	593	-274	23.1	Large mechanical deformations	Positioners and actuators
Quartz	2.21	350	0.013	-	-	2.3	-	57.8	Limited degree of freedom and limited fragmentation direction	Resonators for monitoring
Undoped PZT	3.63[10]	386	0.4	0.52	0.67	220	-93	-	Small domains *p*-type conductivity[11]	Limited actuators; Optical memory devices

PZT ceramics are almost always used with dopants, modifiers, or other chemical constituent to improve and optimize their basic properties for specific applications. Examples of these additives include aliovalent *donors*, such as Nb^{5+} replacing Zr^{4+} or La^{3+} replacing Pb^{2+}, to increase the electrical resistivity of PZT by at least three orders of magnitude. These additives (and vacancies) enhance for example domain reorientation; ceramics produced with some of these additives are characterized by square hysteresis loops, low coercive fields, high remanent polarization, high dielectric constants, maximum coupling factors, high dielectric loss, high mechanical compliance and reduced aging.[12]

Dopants are usually added in concentrations of ≤ 3 at%. Modifiers are substituted into the original PZT composition as solid-solution constituents in concentrations ≥ 5 at%. The most common examples of modified PZT systems are (Pb,La), $(Zr,Ti)O_3$, $(Pb,Sr)(Zr,Ti)O_3$, $(Pb,Ba)(Zr,Ti)O_3$, $Pb\text{-}(Zr,Ti,Sn)O_3$, $(Pb,La)TiO_3$, and $Pb(Mg,Nb)O_3–PbZrO_3–PbTiO_3$, among others solid-solution systems.[12]

1.2 Perovskite Crystal Structure

The perovskite crystal structure (ABO_3) is perhaps one of the most common in nature and one of the most important structures behind ferroelectricity.[13]

The structure of ABO_3 perovskite can be described in terms of a close packing of AO_3 layers, where the B-site cations occupy 100% of the resultant BO_6 oxygen octahedra. When the AO_3 layers are arranged in cubic close packing, the BO_6 octahedra are connected exclusively through corner sharing, and the structure is termed a cubic perovskite (Figure 2).

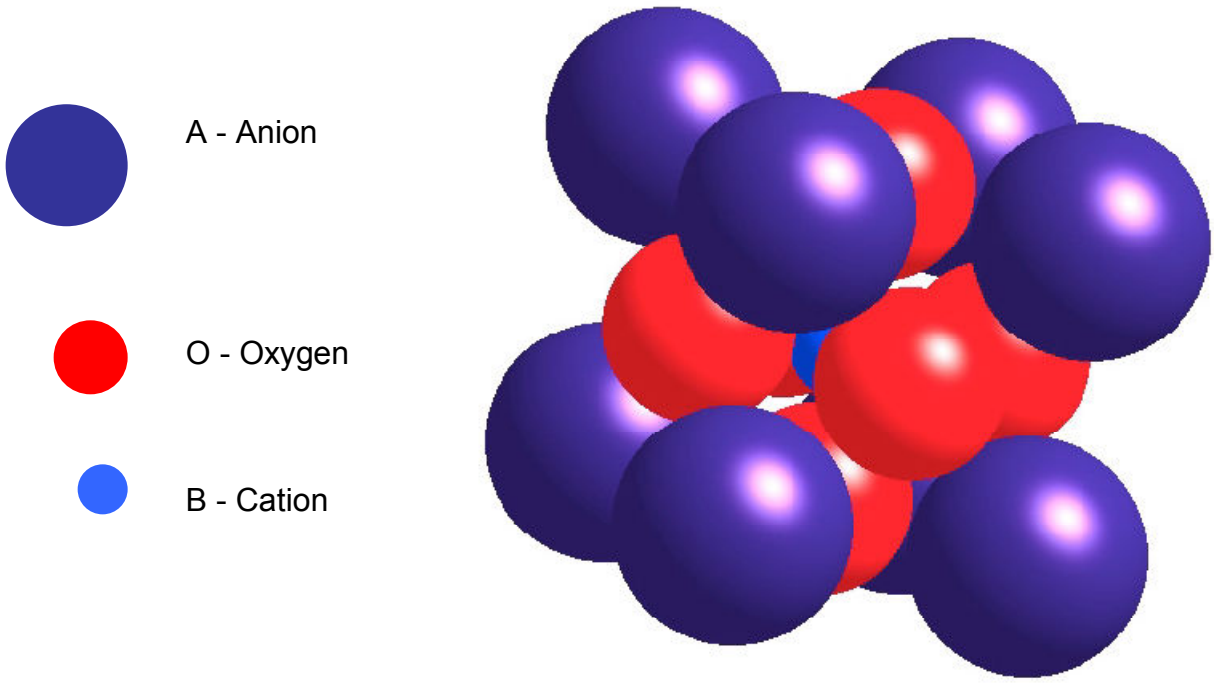

Figure 3: Prototypical perovskite unit cell (ideal cubic perovskite).[13]

In an ideal cubic perovskite, the A and B cations establish their equilibrium bond distances to oxygen without inducing any distortion of the unit cell, and $d_{A\text{-}O} = \sqrt{2}(d_{B\text{-}O})$. The resultant cubic symmetry is *Pmm* and the so-called Goldschmidt tolerance factor describes the perovskite lattice distortion and is defined as:

$$t = \frac{R_A + R_O}{\sqrt{2}(R_B + R_O)} \quad , \quad (1)$$

where R_A, R_B, and R_O stand for the ionic radii of the A-site, B-site, and anion ions respectively.

As mentioned above this is the structure assumed by PZT, with a B-cation in the center of the cube (light blue ions in Figure 3), oxygen ions at the face centres of the cube (red ions in

Figure 3), and lead ions in the cube corner. However, within this ordered perovskite structure an a extensive disorder in the direction of the B-cation distortions within their oxygen octahedral can take place. There is also disorder in the direction of the displacements of both lead and oxygen ions away from their perfect perovskite positions. It is this local disorder within the framework of the orderly perovskite lattice that gives PZT its interesting properties.[14]

1.3 Dielectric, Piezoelectricity and Ferroelectricity of Ceramic Materials

The group of functional materials (related to materials whose “function” is associated with their electric, magnetic, and or optical properties) mainly includes dielectrics, pyroelectrics, piezoelectrics, ferroelectrics, ferroelectric relaxors, incipient ferroelectrics, semiconductors, ionic conductors, superconductors, electro-optics and magnetic materials. It is common to identify the class of functional materials with applications such as Materials for Information Technology, Materials for Electrical Energy Conversion, Materials for Biologic Applications, Materials for Space Technology, among others. The application of functional materials, typified by electroactive materials including piezoelectrics, pyroelectrics and ferroelectrics, for sensing and actuation spans over most if not all industrial sectors.[15]

1.3.1 Dielectric Properties

When an electric field E is applied to an ideal insulator there is no long-range charge transport. In an insulator there is only a short-range dislocation of the positive and negative charge centre, which causes electric dipole moments in the material. The material is called a *dielectric*. The effect of the electrical field can be twofold defined:

1. The electric field *induces* electrical dipoles and aligns them in the field direction. In other words, the material does not contain electric dipoles without the electric field.

2. The electric field aligns electrical dipoles that are *already present* in the material. In other words, the material contains spontaneous electric dipoles. In this case the dipoles are randomly oriented and for zero fields the net polarization is null.

Figure 4 depicts the dielectric response of a regular dielectric material under the electric field.[16]

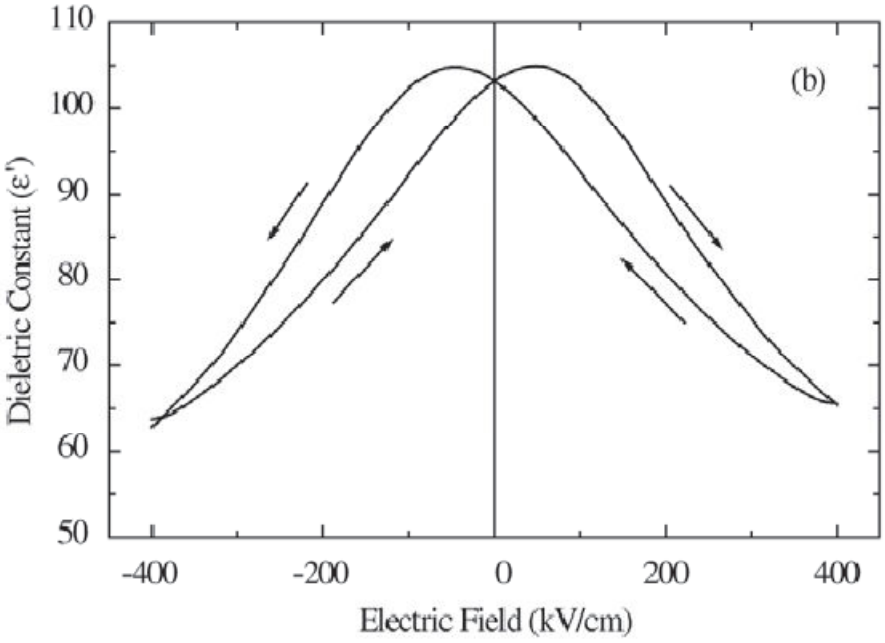

Figure 4: Dielectric constant dependence on the electric bias field.[Adapted from reference 23]

The total effect of an electric field on a dielectric material is called *polarization* (expressed in μC/cm²). Several polarization mechanisms can be identified within a material: atomic, ionic, dipolar and space charge; being each related to the nature of the charged entities, which suffer charge displacement, or to the nature of the displacement.

Dielectrics are insulators with high dielectric permittivity. Dielectric permittivity or dielectric constant is defined as the capacity of a material to store electrical charge and it gives rise to the simplest practical application of a dielectric material such as a capacitor.[16]

The permittivity of a material is commonly measured as a change in dielectric displacement, D, with applied field, E, as shown in Equation 2.

$$\varepsilon_r = \left(\frac{\partial D}{\partial E}\right)_{E=0} \quad , \quad (2)\ [13]$$

where ε_r stands for the relative permittivity, D for the dielectric displacement and E for the applied field. The dielectric displacement in turn establishes the relationship between polarization and permittivity, as in Equation 3 and results in permittivity being essentially the change in polarization with applied field as in Equation 4.

$$D = E + 4\pi P \quad , \quad (3)[13]$$

$$\varepsilon_r = 1 + 4\pi \frac{\partial P}{\partial E} \quad ; \quad (4)^{[13]}$$

where P stands for the polarization. This holds particularly true near the ferroelectric phase transition where the change in polarization with field is much larger than unity and dominates the relation.

The several polarization responses of the dielectric under an electric field are being increasingly used in micro and nanoelectronic devices.[13] The various polarization mechanisms contributing to permittivity, described in Figure 5, are: i) electronic polarization, α_e, defined as the shifting and/or stretching of the electron distribution around the nucleus; ii) ionic polarizations, α_I identified by the shifting of oppositely charged ions from their equilibrium position by an applied field; iii) dipole polarizations, α_d, which takes into account the rotation of internal dipole moments to align with an applied force; and iv) space charge polarizations $\alpha_{s.c.}$, related to the movement of charged internal defects with applied force. The sum of these polarization mechanisms gives the total change in polarization and thus the total contribution to permittivity. These contributions are generally frequency dependent, revealing a dispersive behaviour, with all polarizations mechanisms active at low frequencies and only electronic polarizations active at high frequencies.[13]

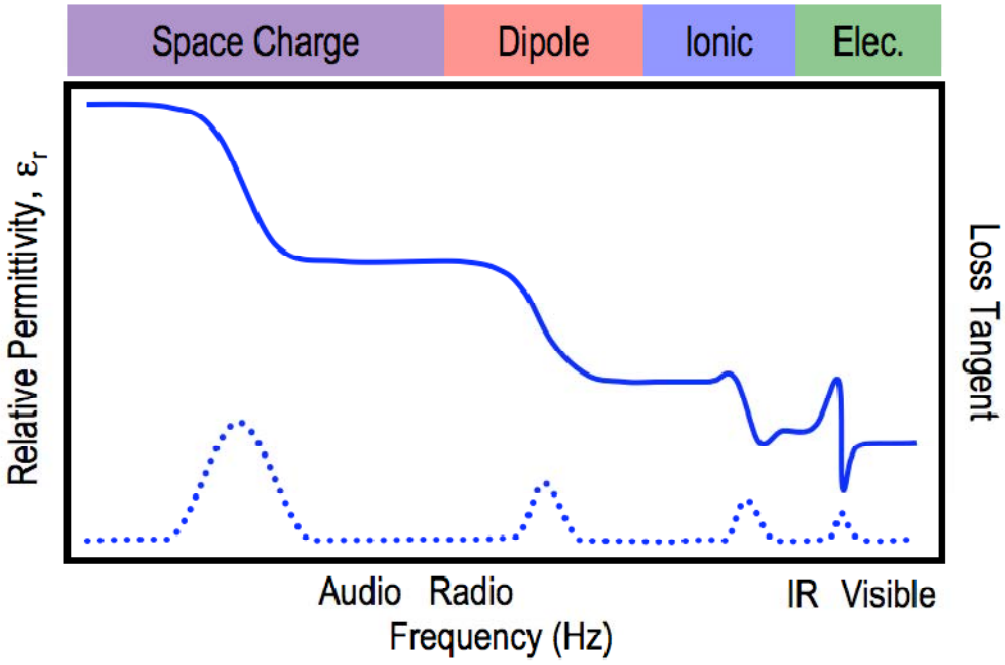

Figure 5: Frequency dispersion of a dielectric showing all possible polarization mechanisms and the expected frequencies for their inactivation.[16]

As each polarization mechanism reaches its frequency limit, subsequent increase in loss is observed. This loss increase can be attributed to a dissipation of heat energy by friction of the space charges and dipoles as they move under the applied field.[13] Electronic and ionic

polarizations show loss peaks over much finer frequency ranges than space charge and dipole polarizations. The peaks here are not so strongly related to internal friction, but are due to resonance of the bound electrons to the nuclear cores by high frequency electromagnetic radiation.[13]

There is an intimate relationship between loss and the permittivity of a material. If the relative permittivity is expressed as a complex function, Equation 5, one may identify two main components to the permittivity: the real part, ε', and the imaginary part, ε'':

$$\varepsilon_r = \varepsilon' - i\varepsilon'' \quad , \qquad (5)$$

The loss in the material can then be expressed in terms of a phase angle between the polarizing field and the response of the material commonly called the dissipation factor or loss tangent delta (Equation 6)

$$\tan\delta = \frac{\varepsilon''}{\varepsilon} \quad , \quad (6)$$

where δ stands for the phase angle of impedance as shown in Figure 6. For perfect insulators the phase angle is 90°, while for perfect conductors the phase angle is 0°. Real materials have values intermediate between the two extremes.[13]

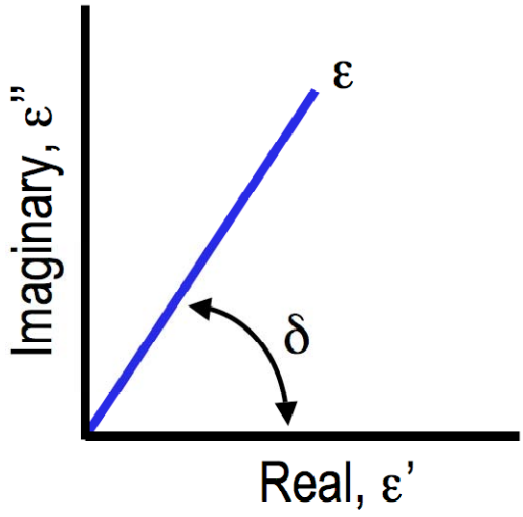

Figure 6: Schematic representation of the real versus imaginary components of the permittivity separated by a phase angle δ.[13]

The parameter tan δ is a measure of the energy dissipated per cycle and the energy stored in the dielectric and a quality factor Q (Equation 7) can be defined as:

$$Q = \frac{1}{\tan \delta} \quad , \quad (7)$$

which represents an important design parameter for practical applications.[16]

1.3.2 Piezoelectric and Ferroelectric Properties

In piezoelectric materials there is a coupling between electrical and mechanical energies and mechanical energy can be converted in electrical energy and vice-versa. [17] The direct effect (designated as a generator) is identified with the phenomenon whereby electrical charges (polarization) are generated from a mechanical stress (first part of Figure 7, designated as piezoelectric effect), whereas the converse effect (designated as a motor) is associated with the mechanical movement generated by the application of an electrical field (second part of Figure 7 and designated as reverse piezoelectric effect).[12]

The direct piezoelectric effect was originally discovered in 1880 by Jacques and Pierre Curie. Piezoelectrics did not come into widespread use until the First World War, when quartz was used in SONAR (Sound Navigation and Ranging). Quartz was replaced in the Second World War by Barium Titanate, and this has become one of the most important piezoelectric materials of the modern era. They are both now commonly used in many ways.[6]

Ferroelectrics are polar dielectrics for which the dipole moment can be switched between two or more equilibrium symmetry equivalent states by the application of an appropriate electric field.[17]

Of the 32 point groups of the crystal structures, 20 can be characterized as *piezoelectric*, that is, upon the application of a mechanical stress, an electronic displacement can be induced in the crystal. Equivalently, an applied electric field can induce a mechanical strain, a property known as the converse piezoelectric effect. The 20 point groups, which can support piezoelectricity, are non-centrosymetric. While the lack of a centre of symmetry is a necessary condition for piezoelectricity, it is not sufficient to observe a piezoelectric effect.[13]

Further categorization of the piezoelectric point groups reveals that in ten out of the twenty, the electronic polarization is spontaneous, remaining finite in the absence of an applied stress or electric field. This spontaneous polarization is characteristic of pyroelectricity and is a consequence of the atomic arrangement within the unit cell where the positive and negative charge centres is not coincident, thus establishing a resultant spontaneous electric dipole.[13]

Under an electric field, ions undergo asymmetric displacement and results in a small change in the crystal dimension, which is proportional to the applied field. Such electric field - induced strain (or piezoelectricity) has found extensive applications in actuators and sensors.[17]

The knowledge of the ferroelectric nature of ceramic $BaTiO_3$ proved to be very useful when it was discovered by Gray (in 1945) that an external electric field could orient the domains within the grains, thus producing a ceramic material that acted very similar to a single crystal possessing both ferroelectric and piezoelectric properties. This electrical aligning, or "poling" process as it has come to be called, was thus correctly identified as the key to turning an inert ceramic into an electromechanically active material with a multitude of industrial and commercial uses.[12]

With poling the ceramic becomes extremely useful, provided however that it is not heated above its Curie temperature (T_C), where it loses its polarization and all of the orientation of the polarization produced by the poling process.

a) Piezoelectric effect b) Reverse Piezoelectric effect

Figure 7: Piezoelectric effect and reverse piezoelectric effect.[Adapted from reference 9]

All ferroelectric materials are pyroelectric, however, not all pyroelectric materials are ferroelectric. Below the transition temperature (Curie temperature, Tc) ferroelectric and pyroelectric materials are polar and have a spontaneous polarization or electric dipole moment. For ferroelectric materials this polarity can be fully, in part reoriented or reversed through the application of an electric field. Complete reversal of the spontaneous polarization is called "switching".[13]

The reverse polarization can be observed by measuring the ferroelectric hysteresis as it is shown in Figure 8. As the electric field strength is increased, the polar domains start to align in the positive direction giving rise to a rapid increase in the polarization (OB). At very high field levels, the polarization reaches a saturation value.[3]

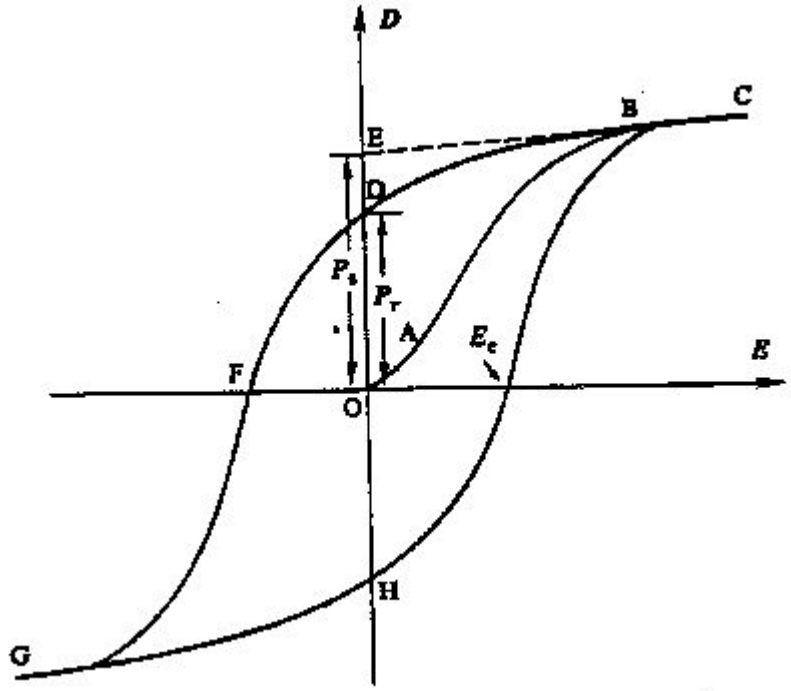

Figure 8: Polarization versus electric field (P-E) hysteresis loop for a typical ferroelectric crystal.[3]

The polarization does not fall to zero when the external field is removed. At zero external fields, some of the domains remain aligned in the positive direction; hence the crystal will show a remnant polarization (P_r). The crystal cannot be completely depolarized until a field of magnitude OF is applied in the negative direction. The external field needed to reduce the polarization to zero is called the coercive field (E_c). If the field is increased to a more negative value, the direction of polarization flips and hence a hysteresis loop is obtained. The value of the spontaneous polarization (P_s) (OE) is obtained by extrapolating the curve onto the polarization axes (CE).[3]

The relative dielectric constant, in equation 8, increases as the temperature approaches the Curie point. In this region the dielectric constant is most sensitive to the magnitude of the applied electric field. Above T_c, permittivity decreases with temperature and often exhibits Curie-Weiss behaviour. This is shown in Equation 8,

$$\varepsilon_r = \varepsilon_0 + \frac{C}{T - T_0} \quad , \quad (8)$$

where *C* stands for the Curie constant. In the paraelectric regime, the spontaneous polarization is zero but the permittivity remains high. This effect is illustrated in the following figure (Figure 9).[13], [16]

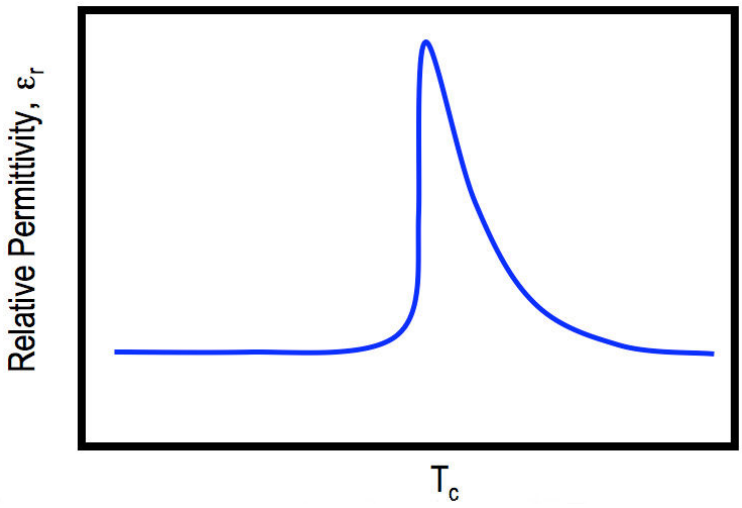

Figure 9: Temperature dependence of the relative permittivity for a ferroelectric with a first order phase transition displaying Curie-Weiss type behaviour.[13]

1.4 The Importance of Piezoelectrics and Ferroelectrics

1.4.1 General Applications of Piezoelectrics and Ferroelectrics

Due to the peculiar electrical properties of piezo -, piro - and ferroelectrics, that include high dielectric permittivity, high piezo and pyroelectric coefficients, in some cases low dielectric losses, high tunability of the permittivity with the electrical field, hysteretic response of the polarization, these materials find applications in a wide variety of electronic and microelectronic applications (as stated before), as indicated in Figure 10. These applications range from sensors and actuators, to electro optic based devices, having a particular relevance as dielectrics for capacitors and memories applications that *per s*e cover utilization areas from telecommunications, electronics and engineering to healthcare. Some applications of piezoelectric ceramics are: medical ultrasound transducers, gas igniters, displacement transducers, piezoelectric transformers and impact printer heads.[3]

Specific applications for ferroelectric ceramics are in capacitors, explosive-to-electrical transducers (EETs)[12], pyroelectric detectors and surface acoustic wave substrates[3], high dielectric constant capacitors, infrared detectors, piezoelectric transducers, optical modulators, optical waveguides, non-volatile memory chips and capacitors for dynamic random access memories (DRAM). Therefore they can be used to transform acoustic waves to electrical signal in sonar detectors and to convert electric field into motion in actuators and mechanical scanners requiring fine control. In a broader sense, ferroelectric materials can be used for pyroelectric and piezoelectric sensors (as mentioned before), voltage tunable capacitors, infrared detectors, surface acoustic wave (SAW) devices, microactuators, and nonvolatile random-access memories (NVRAMs), including the potential production of one transistor memory cells, and applications requiring nonlinear optic components. Another set of potential applications seeks to exploit the ferroelastic properties in stacked templates where they are justaposed to ferromagnetic materials.[3], [12], [18]

Some of these applications are more appropriate for bulk materials and others for films and some for both bulk and films, as indicated in Figure 10. Similar to most materials, the successful application of these piezoelectric, pyroelectric, ferroelectric, electrostrictive, and electro optic ceramics and films is highly dependent on the relative ease of adaptation to useful and reliable devices. This is, to a great extent, the reason why they have been so successful over the years in finding an increasing number of applications. Their simplicity, compact size, low cost, and high reliability are very attractive features to the design engineer and have guaranteed a continuous increase of their applications.

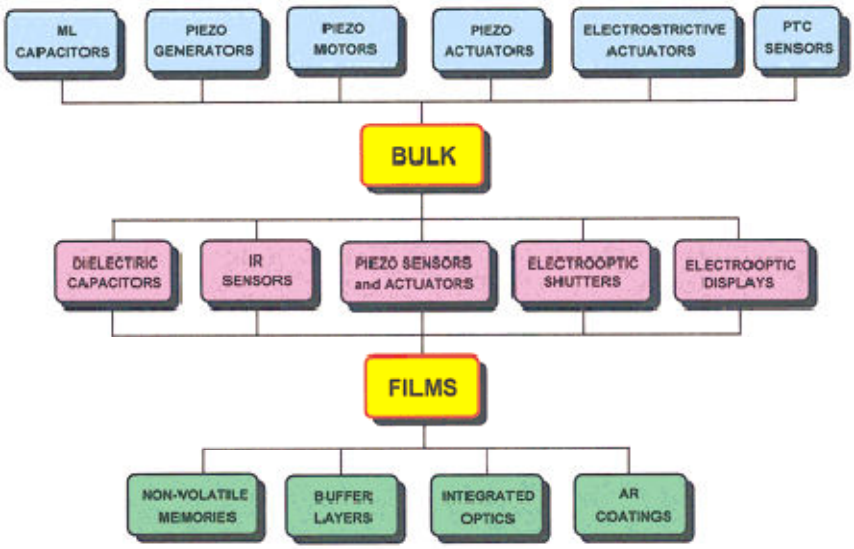

Figure 10: Applications of bulk and film ceramic electronic materials.[12]

1.4.2 Applications for PZT Materials

Piezoelectrics based on PZT show the broadest range of individual applications ranging from applications on health-care, consumer electronics and environment monitoring,[3], [19] as microsensors and actuators for medical, military, telecommunication, environmental, vehicle and office automation industries (once again similarity as ferro- and piezoelectric applications).[3], [21]. PZT-based compounds are primarily used in the manufacturing of ultrasound transducers. A secondary use is in the manufacturing of ceramic capacitors and microelectronic chips. PZT films have been widely investigated for applications in non-volatile random access memories (NVRAMs) (similar with piezoelectrics and ferroelectrics applications), as well field effect transistors (FETs), ultrasonic vibrators, filters, microactuators and microsensors, dielectric capacitors; IR sensors, buffer layers, integrated optics, electro optic shutters, AR coatings and electrooptic displays.[15]

Due to its lead content and to the environmental restrictions associated with its use, there is the need to find alternative materials to PZT. There are currently several R&D (Research and Development) programs for the search of lead free alternatives to PZT, but until now none of the barium titanate ($BaTiO_3$), sodium potassium niobate ($(Na_{0.5}K_{0.5})NbO_3$) and or sodium bismuth titanate ($(Bi_{1/2}Na_{1/2})TiO_3$) based compositions demonstrate similar properties to the ones of PZT.[4] The so far reported properties for these several alternative materials are considerably inferior (as one can witness from table 2). This is the reason why PZT is still the most important piezoelectric material and is still considered, even for modern applications such as composite structures with multiferroics. [15]

Table 2: Electrical properties comparison between current major lead-free systems and PZT.[20]

	Perovskite type structure ferroelectrics			
	$BaTiO_3$	$(Bi_{1/2}Na_{1/2})TiO_3$	$(Na_{0.5}K_{0.5})NbO_3$	PZT
Curie Temperature (°C)	120	320	420	300~400
d_{33} (pC/N)	190	120~200	100~416	200~500
d_{31} (pC/N)	-78	-7.5	-30~-152	-130
Dielectric Constant (at 1 kHz)	1500~6000	~1700	200~500	1000~4000

1.5 Fabrication of Piezoelectric and Ferroelectric Films

1.5.1 Bulk versus Films and Thin versus Thick Films

The current trend in microelectronics industry is towards device miniaturization, increased functionalization and greater reliability with low processing costs. Films respond better to these requirements than their bulk counterparts.

Thin films normally refer to layers with thickness below ~1μm and thick films above this range. However, the prime difference lies in the manufacturing process of the films.[21]. Thin and thick films of dielectric materials are being considered to replace the dielectric components presently in use in the form of bulk ceramics. This has been the driving force for the search for fabrication processes for mass-produced dielectric films with repeatable performance at low costs.[15]

For some of the applications (communication industry, resonators, filters and antennas), thick films are required, rather than thin films, as these are volume devices that store electromagnetic energy within the dielectric volume. Furthermore, the ability to process thick films conformably on substrates, and also directly on metallic foils, opens up the possibility of innovative structures and designs.[12] However, for thick films the required high sintering temperatures present a challenge for processing on base metal substrates.[3]

The techniques employed to prepare films are considerably different form the techniques used to prepared bulk ceramics and several techniques for making films are presently available. These can be divided into two main categories: physical deposition techniques, such as physical vapour deposition (PVD), and chemical techniques, which include chemical vapour deposition (CVD) and chemical solution deposition (CSD).[3] For the case of physical methods, the way the particles (atoms or ions) are removed from the target results in various deposition methods, such as radio frequency sputtering, ion beam sputtering, evaporation, electron beam and laser ablation, among others.[21], [22]

Advantages of PVD techniques include: dry processing, high levels of purity, the possibility of growing epitaxial films, and compatibility with the processing of semiconductor integrated circuits. Nevertheless, the difficulty in controlling the stoichiometry of multicomponent films, the slow rates of deposition, the need to high-temperature deposition annealing crystallization and the high costs to purchase equipment and maintenance are the main disadvantages of these methods for the preparation of functional coatings.[21]

The second group of technical processes (chemical) does not require a vacuum environment. Chemical methods are generally characterized by higher deposition rates, good control of stoichiometry, the production of large area defect free films and lower equipment costs. These advantages make chemical processes, for example, chemical vapour deposition, very attractive in terms of industrial production. However, CVD techniques are currently limited

due to the availability and toxicity of the precursor sources for functional materials what presents a major weakness of this technology. On the other hand, the methods of chemical solution deposition technique, such as sol-gel, are becoming increasingly important for the preparation of films of piezo, pyro - and ferroelectric materials.[23]

The wet chemical methods involve three distinct steps: the preparation of a solution, the deposition of the solution onto the substrate by dip or spin coating and the subsequent thermal treatment of the deposited layer to remove the organics, to crystallize the desired phase and to densify the coatings. The details of experimental routines and chemical reactions, including the choice of precursors, the choice of pressure and temperature, and reactions of polymerization, make the difference among the several methods: sol-gel route, metalloorganic decomposition (MOD) and hydrothermal routes. Chemical methods provide a very convenient, economic and rapid processing methodology for the preparation of films or coatings on a variety of substrates.[21]

The methods described before are mainly used for the preparation of thin films. The preparation of films with thicknesses between 10 and 100 μm requires different technologies, since thick films prepared by PVD and CVD become very expensive.[21]

The simplicity and versatility of sol-gel technique also makes it attractive for the preparation of thick films but has several problems. For instance there is a severe limitation related to the thickness of the coating that can be obtained from the conventional sol-gel spin or dip-coating process. Depending on the concentration and viscosity of the solutions the thickness of single layer is in the range of hundreds of nm. In order to reach the thickness of 10 μm the process of layer deposition has to be repeated many times. The deposition of a 10 μm thick green film will require several layers, making the process time consuming, tedious and cost-ineffective. Moreover the probability of creating defects (cracks, pores, and inclusions) in the films increases with to the number of layers.

Defect-free films of PZT with thickness lower than 1 μm are relatively easy to fabricate.[39, 41] Therefore, other methods have been used to prepare thick films and in particular piezoelectric thick films. Most of the techniques described are based on the densification of powder films. The powder layer is usually obtained after the deposition of a slurry onto the substrate. The powder can be delivered to the substrate by various techniques such as tape casting, screen-printing, inkjet or electrophoretic methods. Dense films are then obtained after sintering. In all of these technologies, the sintering is a critical step because of the large surface area exposed to the environment and because of the relatively small thickness. Moreover, the films are under the influence of a controlled sintering process restricted due to the presence of the substrate below. In the case of lead piezoelectrics for which a sintering temperature above 800° C is usually required, the evaporation of volatile elements (Pb) and problems of consolidation may occur.[21]

Tape casting is an ordinary process for making laminated thick layers of multilayer structures, like multilayer capacitors and actuators of PZT[12] and 1-3 PZT-based piezoelectric composites, used as transducers for ultrasonic devices, naval sonar systems, medical diagnosis and non - destructive testing of materials. Although a low-cost process that allows mass productions of laminates, tape casting is not easily compatible with the deposition onto rigid substrates and the suspension and firing without deflection are very difficult.[15] The screen-printing method is one of the most appropriate technologies to prepare thick films with thickness ranging from 10 to 30 μm. In the screen printing technique the powder is also suspended in an organic solution composed of a solvent, a dispersant and a plasticizer. The suspension or ink is applied, with the aid of a racket, on the substrate through a screen. The thickness of the deposited layer depends on the viscosity of the suspension, rate of deposition, pressure applied on the screen, among other experimental variables.[21]

1.5.2 The Electrophoretic Deposition

Another thick film processing technique is the electrophoretic deposition (EPD) that utilizes a colloidal suspension of ceramic powders. The deposition by electrophoresis combines two processes: electrophoresis itself, in which the charged particles suspended in the solution move under the influence of an electric field (Figure 11) and, in a dc field, this motion results in the particle accumulation near the oppositely charged electrode; the deposited particles are attached by van der Waals forces or by chemical bonds and thus constitute a consolidated layer, forming a solid deposit. This particulate deposit can then be densified by a sintering step and form structures suitable for many applications.[24]

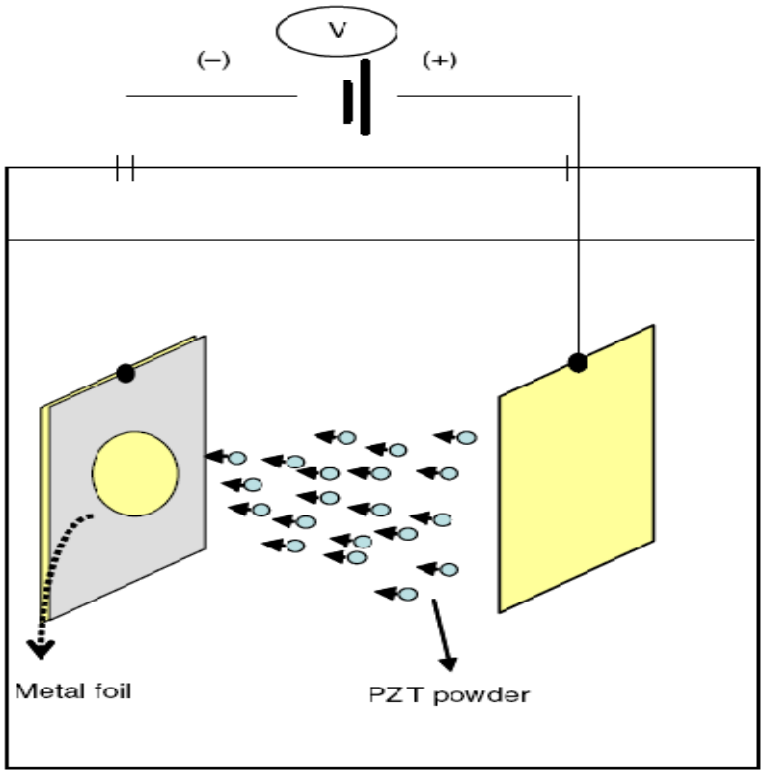

Figure 11: Schematic representation of the Electrophoretic Deposition process. After sintering, the coating densifies and becomes useful for example for piezoelectric applications.[25]

Successful EPD requires the development of stable suspensions composed of electrostatically charged particles suspended in a suitable solvent where specific mechanisms are active keeping the particles from flocculating or agglomerating.[26]

Among thick film production processes electrophoretic deposition (EPD) technology possesses a set of unique advantages. EPD is very versatile since it can be modified easily for a specific application. For example, deposition can be made on flat, cylindrical or any other shaped substrate with only minor changes in the electrode design and positioning. In principle, EPD can be applied to any solid and any material class that is available in the form of a fine

powder or a colloidal suspension including metals, polymers, carbides, oxides, nitrides and glasses.[26]

Despite being a wet process, EPD offers easy control of the thickness and morphology of a deposited film through simple adjustment of the deposition time and applied potential.[26] The interest in the EPD technique is based not only on its high versatility to be used with different materials and combinations of materials but also because EPD is a cost-effective method usually requiring simple equipment. With EPD, particulate deposits can be made in seconds on suitable surfaces of planar or more complex geometry. Moreover EPD has high potential for being scaled up to large product volumes and sizes, as well as to a variety of product shapes and 3D complex structures.[26]

EPD has been quite investigated in the fabrication of high performance functional thick/thin films, such as $(Ba,Sr)TiO_3$,[16] $BaTiO_3$,[13] $Pb(Zr,Ti)O_3$,[29] and more recently in the manufacturing of thick films for high frequencies, such as $BaO\text{-}Ln_2O_3\text{-}TiO_2$,[29], [27] and tellurium based compositions (such as $TiTe_3O_8$).[30]

1.6 Current Demands for Piezoelectrics and Ferroelectrics

1.6.1 Miniaturization and Low Processing Costs

Advanced functional components are made of materials systems rather than of discrete materials, therefore integration issues increase in importance. This is particularly true in miniaturized systems where interfaces play a very important role. Integration issues comprise both the integration of electroceramics thin films with the substrates and the semiconductor chips as well as the combination of bulk ceramics for different kinds and/or other materials such as metals, glass or polymers to form compound devices.[19]

The key words associated with the current trends of microelectronic industry are: miniaturization, optimal performance, high integration and low costs (as alleged ahead of). [3] Miniaturization of systems such as planar circuits, antennas, filters and couplers are an example of a requirement and because of that it has been the driving force for the search for fabrication processes for mass-produced dielectric films with repeatable performance at low costs. Indeed, the advances attained over the recent years in thick-film technology have permitted this inexpensive process to become significantly useful in electronics manufacturing.[20]

The growing need of the microelectronics industry for small, lightweight, multifunctional devices that use less battery power and have low manufacturing costs has also been the driving force behind the search for optimized materials. Thick films of materials with improved properties and capable of fabrication at low temperatures to replace the currently used bulk dielectric components are presently of paramount importance.[30]

The manufacturing of ferroelectric films on metal foils is an important mission for devices integrated into electronic packaging, an approach that is currently receiving considerable attention due to cost and space advantages. One of the significant costs in the manufacture of electroceramics is the energy consumed during thermal processing. The other one is associated with the high price of the substrates (Si based) and under layers (noble metals). From this perspective low sintering temperatures for the materials are desirable.[31]

1.6.2 Processing Compatibility with Metals

Base metals are commercially attractive because of their low cost and simple patternability. However their compatibility with the current fabrication techniques of functional materials is difficult and sometimes impossible.

Table 3: Physical properties for some of the metals used as electrode materials.[32]

Physical Properties	Copper	Gold	Platinum	Aluminium	Nickel
Density (g/cm^{-3})	8.94	19.30	21.45	2.70	8.91
Liquid density (g/cm^{-3})	8.02	17.31	19.77	2.38	7.81
Melting Point (ºC)	1085	1064	1768	660	1453
Boiling Point (ºC)	2562	2856	3825	2519	2732
Heat of fusion ($kJ\ mol^{-1}$)	13.26	12.55	22.17	10.71	17.47
Heat of vaporization ($kJmol^{-1}$)	300.4	324	469	294	377.46
Specific heat capacity (25ºC) ($Jmol^{-1}K^{-1}$)	24.44	25.42	25.86	26.20	26.07
Electrical conductivity (20ºC) (Sm^{-1})	$59.6x10^6$	$45.2x10^6$	$9.66x10^6$	$37.8x10^6$	$14.3x10^6$

Copper presents an excellent electrical conductivity, as referred in Table 3, and has extensive use as an electrical and heat conductor, as a building material and as a component of various alloys. Copper does not react with water (H_2O). Instead it reacts slowly at room temperature with the oxygen from air to form a layer of copper oxide on copper metal.

Cu foils with thickness of several tens of micrometers are attractive substrates for thin and thick ferroelectric film deposition due to its low cost and high conductivity. The deposition of a high-permittivity material on Cu is promising for embedded capacitor applications in printed wiring boards (PWBs). Besides cost reduction, the required wiring board area is greatly reduced by replacing the surface - mount components with pre-embedded capacitive layers. This offers indeed advantages for electronic miniaturization.[33]

Compared to platinum, which is widely used as an electrode material in many oxide thin-film devices, the low cost and high conductivity of Cu makes it a promising candidate to replace Pt for non-volatile ferroelectric memories, other ferroelectric, complex oxide thin and thick film-based devices (as is demonstrated in Table 2). However, the utilization of Cu foils as substrates for films poses several important problems. Cu is easily oxidized at high temperatures and the oxygen partial pressure (pO_2) needs to be controlled to avoid oxidation of Cu. Moreover, ferroelectric films usually need to be annealed at high temperatures in oxygen atmosphere to

obtain the desired crystalline phase. Hence, success depends on finding deposition conditions that fulfil both requirements.[34]

The successful use of Cu foils as substrates for the preparation of ferroelectric lead based and lead-free thin films have been reported by some authors.[32, 33] $BaTiO_3$ thin films with high dielectric permittivity have been deposited by sol-gel technique directly on Cu foils for embedded component applications. Cu foils were also used for the preparation of sputtered $Ba_{1-x}Sr_xTiO_3$ (BST) thin films for tunable capacitors for radio frequency/microwave applications. The feasibility of the preparation of sol–gel-derived $Ba_{1-x}Zr_xTiO_3$ (BZT) thin films on Cu foils was also recently demonstrated for tunable capacitors with radio frequency/microwave applications.[12] High-resolution TEM cross-section microscopy studies of these films revealed no interfacial reactions. According to the authors, the success in the preparation of $BaTiO_3$ based capacitors on Cu is related to the very low oxygen partial pressures required to reduce TiO_2 and BaO, compatible with the conditions under which Cu oxidizes. However, a different situation occurs for Pb-based systems. Due to the tendency of PbO to reduce at higher oxygen partial pressures than BaO, the processing window of PbO based films on Cu foils is comparatively narrow. Two approaches have been reported to avoid the oxidation of Cu. The first approach involves the use of a Ni/Ni phosphide interface layer between the Cu foil and the $Pb(Zr,Ti)O_3$ (PZT) and PLZT films. High-resolution cross-section microscopy studies revealed the formation of a NiO layer[34] and consequently, a linear dielectric capacitor with a reduced capacitance density was obtained. Although useful for embedded capacitors, this solution is not suitable when higher dielectric permittivity responses are required. The alternative approach involves the control of pO_2 within a narrow processing window predicted by thermodynamics. High quality sol–gel-derived PZT thin films deposited directly on Cu foils with an accompanying ferroelectric fatigue resistance were reported.[34] Within that window the stability of Cu against oxidation is compatible with the stability of PZT against reduction. Generally, the annealing temperature for sol–gel PZT thin films on Cu does not exceed 700ºC. However, for thick films deposited on Cu, a much higher temperature is required to achieve sintering of the PZT particles. Hence, besides oxidation, problems such as diffusion, adhesion and interaction between film and substrate at such a temperature are envisaged.

From the phase diagram of the Cu–Pb binary system, there also exists a eutectic point above 955ºC (Figure 12). It is considered therefore that this may also be a critical temperature in the processing of thick films containing Pb. The copper-lead phase diagram has a eutectic point at 326 ºC for 99.94 % Pb and as a result terminal solid solutions of most pure lead (0.007 % Cu) and pure copper (0.005 % Pb) are formed at room temperature.[35] There are three important parts to consider: (1) the liquid that is miscible in all proportions at higher temperatures, but develops a miscibility gap below about 1000ºC; (2) the face-centered cubic (fcc) solid solution (Cu), with very limited solubility of Pb, and (3) the fcc solid solution (Pb), with

presumably negligible solubility of Cu.[36] The most important feature of this diagram is the monotetic invariant reaction at 46 % Pb and 955ºC. At the monothetic point (100% Cu), L1 (46% Pb) and L2 (87% Pb) can coexist. Copper and lead are essentially insoluble in each other.[37]

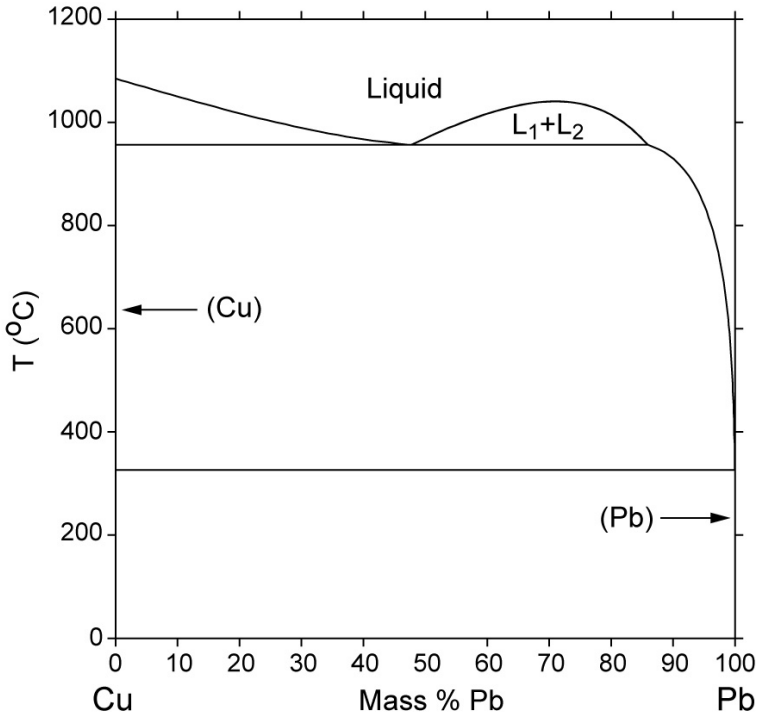

Figure 12: Phase diagram of the Cu–Pb binary system.[37]

Previous studies on the manufacture of thick PZT films on Cu by electrophoretic deposition (EPD) have shown, for the films sintered under a nitrogen based atmosphere at 950-1000 ºC with controlled pO_2, the formation of a Pb-Cu alloy at the Cu /PZT interface which migrates into the bulk of the film causing the PZT decomposition into ZrO_2 and lead titanate (PT) rich PZT. The dielectric permittivity and remanent polarization responses are consequently deteriorated when compared with the properties of PZT thick films deposited on inert metal foils, such as, Pt. These studies clearly point to the need to decrease the sintering temperature of PZT thick films on Cu.[4]

1.6.3 Sintering Aids

As well explained above, because of the need of expensive electrode materials such as platinum and palladium in many co-fired multilayer devices, imposed by the high sintering temperatures and the environmental concerns over PbO volatilization at these temperatures, much attention has been paid at reducing the sintering temperature of a wide range of electroceramics products such as barium titanate (BT) and lead zirconate titanate (PZT).

Sintering ceramics at low temperature has been done by using for example liquid phase additives. Liquid phase sintering aids melt below the sintering temperature. Ideally, the sintering aid should be chosen so that the ceramic particles are both wetted by, and practically soluble in it. Wetting of the particles by the liquid, results in curved liquid meniscus surfaces on witch capillarity forces act tending to drown the particles together. When solubility of the solid occurs, a higher diffusivity into the liquid may increase the rate of mass transport and shrinkage. Porosity is also reduced by residual liquid filling the pores.[26]

For BT, $PbO–B_2O_3$ and $Bi_2O_3–B_2O_3$ glass sintering aids have been commonly utilized.[31] For the case of $PbTiO_3$ ceramics it has been demonstrated that borate- and silicate-based glasses which contain a high mol% of TiO_2 and PbO act well as sintering aids.

The most studied additives for PZT have been: $Pb_5Ge_3O_{11}$, $PbO\text{-}B_2O_3$, $B_2O_3–Bi_2O_3$—CdO, PbO- Cu_2O, $Li_2CO_3–Bi_2O_3$ and borate- and silicate-based glasses.[4] Literature also refers the use of low melting oxides such as V_2O_5 and glass frits. The addition of glass frit enhanced density significantly to ~92% of the theoretical density, due to the low melting of the glass frit which helps densification during the initial and intermediate stages of the sintering. [1] However, deteriorating effects on the piezoelectric and dielectric properties were reported.

From the phase diagram of $PbO\text{-}B_2O_3$ (Figure 13) several eutectic points at low temperatures can be identified, making these compositions suitable to be used as sintering aids. Indeed, in some works $4PbO{\cdot}B_2O_3$ frit was added because of its low melting temperature and high polarizability, which was helpful to the dielectric and piezoelectric properties of the system. If small amounts of $4PbO{\cdot}B_2O_3$ glass powder are added to the calcined PZT ceramics, the formed liquid phase increases the surface diffusion and enhances the grain growth during sintering. Hence, the sintering temperature can be reduced and the piezoelectric and dielectric properties are enhanced.[38]

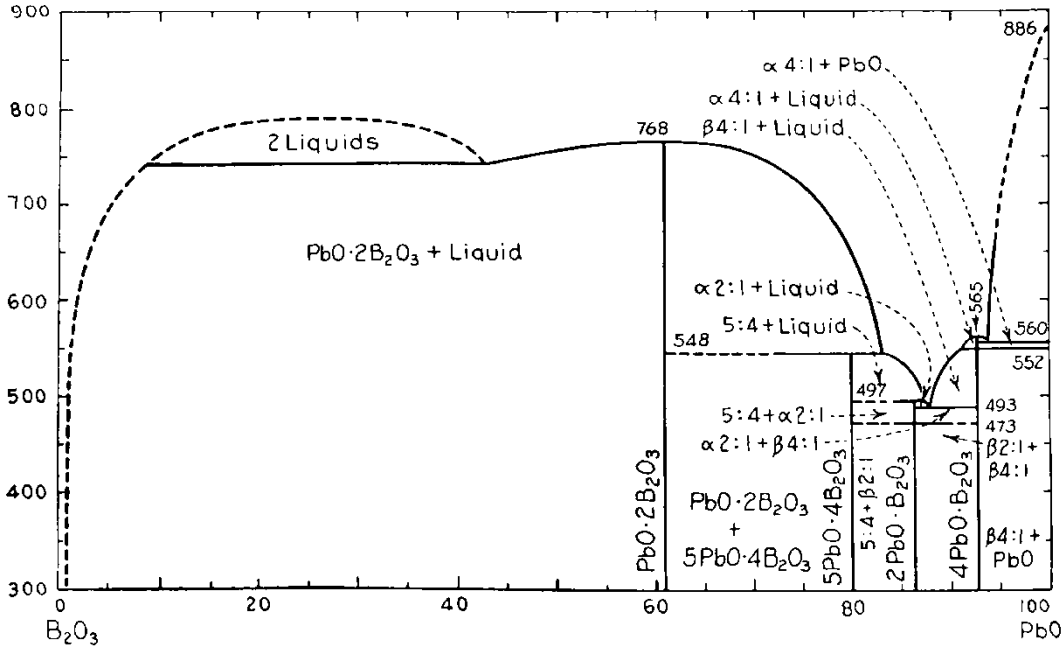

Figure 13: Phase diagram of PbO – B_2O_3 binary system.[39]

The products of reaction between PZT and PbO-B_2O_3 glasses at 850°C were studied using powder and bulk PZT samples.[39] The use of this additive has not been reported yet in PZT thick films.

2. Objective of the Thesis

As stated in the previous chapter, piezoelectric lead zirconate titanate ceramics find currently numerous applications. In some of these applications, noble metals such as platinum and palladium are used as internal electrodes; for applications in which the ceramic is cofired with the metallic electrode low cost based electrodes such as silver, nickel and copper, among others, cannot be used due to their low melting points as compared to the sintering temperatures commonly employed for PZT. The use of these expensive metals adds significant costs to the components. This issue becomes even more relevant when there is the need to embed capacitors into the circuit. It is then imperative to lower the sintering temperature of the electroceramics and to make it compatible with low cost based metals. Concomitantly, sintering at low temperatures also brings other benefits, as well, regarding the reduced power consumption and lead losses during sintering thereby contributing for a better environment.[3]

Within this context, the topic of this work is related with the preparation of PZT thick films on flexible copper substrates for embedded circuit applications. And the main objective of this study is to decrease the sintering temperature of thick PZT films to make them compatible with the use of Cu substrates and concomitantly to improve the film quality and dielectric performance. One way of doing this is through the use of sintering aids. By adding a commercial glass powder and mixtures of PbO and B_2O_3 with different ratios, as sintering aids, a systematic study of the preparation and properties of PZT thick films on Cu is undertaken.

Another important objective is to lower the fabrication costs of thick films to add value in terms of commercialization. Within this context electrophoretic deposition (EPD) method is exploited for the fabrication of these thick films and the processing conditions such as voltage, deposition time and suspension composition are studied in order to fabricate high-quality and reproducible coatings on the conductive substrates utilising a commercially available PZT powder.

3. Experimental Procedure

In this work PZT thick films were fabricated by EPD on Cu metallic foils. In order to decrease the sintering temperature of the films, the effect of sintering aids was addressed. The sintering aids used were a lead containing-borosilicate glass and a mixture of boron oxide and lead oxide. Lead oxide is a glass former with low melting point (phase diagram, Figure 12), which will help to decrease the sintering temperature of PZT. B_2O_3, as V_2O_5, is also a low melting point oxide and a glass former one.

The obtained results were compared with previous ones reported within this group for a mixture of PbO and V_2O_5.[45]

The next table indicates the various compositions studied in this thesis.

Table 4: Compositions prepared in this work and sintering conditions used for the densification of the films. The glass composition corresponds to SiO_2, PbO, Al_2O_3, B_2O_3 (commercial glass). The properties of the prepared films were compared with previously obtained films [45] sintered with a mixture of PbO+V_2O_5.

Samples	Compositions	Additives	Sintering Conditions
Series 1	PZT + 5 wt % Glass	Dispex (5 wt %)	800, 850 and 900ºC for 30 and 60 minutes
	PZT + 10 wt % Glass	Dispex (5 wt %)	
	PZT + 20 wt% Glass	Dispex (5wt %)	
Series 2	PZT + 10 wt % Glass	Dispex (5 wt %) + PVB (5-7.5 wt %)	
	PZT + 20 wt % Glass	Dispex (5 wt %) + PVB (5-7.5 wt %)	
Series 3	PZT + 1 wt % (90%B_2O_3 + 10%PbO)	-	
	PZT + 1 wt % (80%B_2O_3 + 20%PbO)	-	
	PZT + 1 wt % (50% B_2O_3 + 50% PbO)	-	
Series 4	PZT + 3 wt % (50% B_2O_3 + 50% PbO)	-	800 and 850ºC for 30 and 60 minutes
Comparison	PZT + 1 wt % (50 %PbO + 50 %V_2O_5)	-	800, 850 and 900ºC for 30 and 60 minutes

A powder suspension was prepared using commercial PZT powders (TRS600FG, TRS Technologies Inc., State College, PA) as starting materials and glacial acetic acid (Pronalab, 100%, Lisbon, Portugal) as the suspension medium. Glacial acetic acid was reported to improve

the electric properties of thick films prepared by EPD over aqueous and alcoholic media on platinised alumina substrate.[24]

A commercial borosilicate glass powder, Glass Powder 8465, manufactured by Schott Electronic Packaging was used in this study. Its transformation temperature is 385ºC and the dielectric constant of this glass is 15 and loss tangent is 0.0027. The glass powder 8465 was added to PZT in the amounts of 5, 10 and 20 weight percent (wt %) of PZT. PZT and glass powders were milled separately in acetone during 6 hours. The final particle size of 0,377 μm for PZT and 5,12 μm for Glass was determined by Coulter LS230 Instrument (Coulter LS 230, Coulter Electronic Limited, Luton, U.K.),

Lead oxide (Panreac, 99%) and boron oxide B_2O_3 (commercial oxide) were used for the second set of compositions. The particle size of these oxides was also assessed by the Coulter LS230 Instrument.

The mixture of PZT powders with sintering aids (glass or oxide powders) were ultrasonically mixed and dispersed in glacial acetic acid (Pronalab, 100%, Lisbon, Portugal) to form a suspension with a concentration of 3 wt % of PZT in acetic acid.

In this work, an electrophoretic light scattering (ELS) spectrophotometer (Delsa-440 SX, Beckman Coulter, Inc., USA) was used to determine the zeta potential of the PZT suspensions. For that, a sample is typically placed in a disposable plastic cuvette and platinum electrodes inserted. The entire cell is placed into the internal chamber of Delsa 440 SX and the measurement automatically conducted.

As it is well know, the dispersability of the glass powders in suspension is very difficult and because of that two one dispersant was used in this work. Commercial Dispex A 40 (0,01g/mL) was used in the amount of 5 wt % and 5 - 7.5 wt % of polyvinyl butyral (PVB) (commercial product), was used as binder, added to a 10 and 20 wt % of glass suspension.

Electrophoretic deposition was carried out in optimized conditions through varying the current, voltage and time of deposition. Figure 14 illustrates the electrophoretic deposition apparatus used in this work.

Figure 14: Representative image of the equipment used in this work for the EPD process. Left dispositive: ultrasonic bath; Middle dispositive: two electrodes cell, one positively charged and other negatively charged. Right dispositive: voltage supply.[Adapted from reference 40]

The distance between the metal foil cathode and the stainless-steel anode was kept at 2 cm. A dc voltage supply (Glassman High Voltage Inc., Portugal) was used to generate the dc voltage required for the deposition, ranging from 200 to 400 V.

Prior to each EPD cycle the suspensions were ultrasonically dispersed and magnetically stirred for 5 and 10 min, respectively, followed by settling for 0,5 min in order to sediment the coarse particles.

To fabricate >1μm thick films for which the properties are shown below, the suspension was sonicated for 10 min and the deposition was carried out over 0.5 min at 200V.

A mask with 10 mm diameter hole in centre (Figure 15 illustrates the mask with 10 mm diameter in centre) was used for the deposition. The metal foil substrate (Cu) used for film deposition was hold between the stainless steel and the mask.

Figure 15: Cell for electrophoretic deposition showing the mask with a 10 mm diameter hole in the centre.[Adapted from reference 40]

In previously works at this group it was observed that the rate of formation of the consolidated layer during EPD is directly proportional to the amount of charge that passed through the cell. When EPD is operated under constant current conditions, the deposited weight increases linearly with time. However, in order to maintain constant-current conditions, the voltage has to be continuously increased as the deposit induces an increased electrical resistance to the system. Under constant-voltage conditions, the potential between the electrodes is maintained constant, which thus results in a decreased deposition rate as the deposit builds up.[42]

After deposition, the obtained films were dried at room temperature overnight. The dried films were isostatically pressed at 2000 kg/cm^2 during five minutes. The films were then sintered between 800 and 900 ºC under a low oxygen partial pressure (pO_2) (between 5 x 10^{-5} and 8 x 10^{-7} atm), during 30 to 60 minutes.

The thickness of the films was estimated by a Micrometer, and the structure and phase assembly were analyzed by X-ray diffraction (XRD) (Rigaku, ‘‘Geigerflex’’ D/Max- B, Tokyo, Japan) operated at 40 kV and 30 mA, scanned from 20° to 80° with a scan speed of 1°/ min and step interval 0.02° using Cu K radiation with a wavelength of λ=1.5406 Å. The microstructure of the films was analysed by scanning electron microscopy (SEM, Hitachi S-4100, Japan) operated at 20 kV.

Dielectric properties (dielectric permittivity and loss) were obtained using an HP 4284A precision LCR meter, measuring 5 dots for each condition.

Capacitance–voltage dependence was measured with a Keithley current/voltage source meter. Before the measurements, gold (Au) top electrodes were sputtered onto the thick films through a shadow mask.

4. Results and Discussion

4.1 Characterization of the Precursor Powders and Suspensions

As mentioned before, there are three basic steps in EPD: formation of a stable suspension of the particles, electrophoretic migration of the particles to the opposite electrode, and deposition of the particles in the desired arrangement on the electrode surface. First step includes the preparation of a stable suspension in which the particles can move independently. In the second step a DC electric field is applied to the suspension causing the electrophoretic motion of charged particles toward the oppositely charged electrode. In the final step the inter-particle repulsion forces that keep the particles stably suspended must be overcome. EPD is purely a method of moving and arranging particles. To produce a dense mechanically strong layer or object it must be combined with some other process such as sintering and, sometimes a pre-sintering isostatic pressing step to eliminate the pores between the particles and to densify the film.[41]

EPD should not be confused with electrodeposition, here ions are deposited and discharged at the electrode. EPD requires colloidal stable suspensions where the particles carry a substantial charge. There are several suspension and dispersant media that can be used in EPD, that include aqueous, organic, acid and basis. Although aqueous media are important from the point of view of costs and environmental issues, due to electrolysis that tend to occur in water based suspensions under an electric field, which causes bubbles and pores in the deposited layer, aqueous media is seldom used. Although electrostatic stabilization is considered most effective in aqueous medium, a substantial surface charge density – with the associated countering layer in solution – can also be created in organic and other suspension media, through the use of special additives. This is the case of the present work.

4.1.1 Particle Size Distribution

Another important aspect that accounts for the stability of the suspension is the particle size. The particle size distribution of glass before and after milling and with and without Dispex is presented in the next graph (Figure 16). The curve of the glass particles without milling is characterised by three main peaks and the average particle size is 8.28 μm. After milling a bimodal curve was obtained with an average particle size of 3.58 μm. The dispersant effect of Dispex is not obvious, since similar results were obtained for dispersed and non dispersed suspension and the average particle size is 3.48 μm. This observation allowed us to conclude that Dispex was not effective in dispersing the glass particles.

Concerning the PZT powders, the particle size distribution illustrated in Figure 17 reveals a bimodal distribution with a first major peak in the submicron region (peak at 0.2 μm) and a

second one peaking at 1.7 μm that might correspond to some particle agglomerates. The average particle size is 0.414 μm. The addition of Dispex is not particularly effective in removing the second peak and only a very subtle increase of the volume % of the finer particles is observed. For this last case the average particle size is 0.337μm. Combined with SEM observations (Figure 18 and 19), it is believed that the two peaks reveal a weak and stronger agglomeration of the original particle size, respectively.

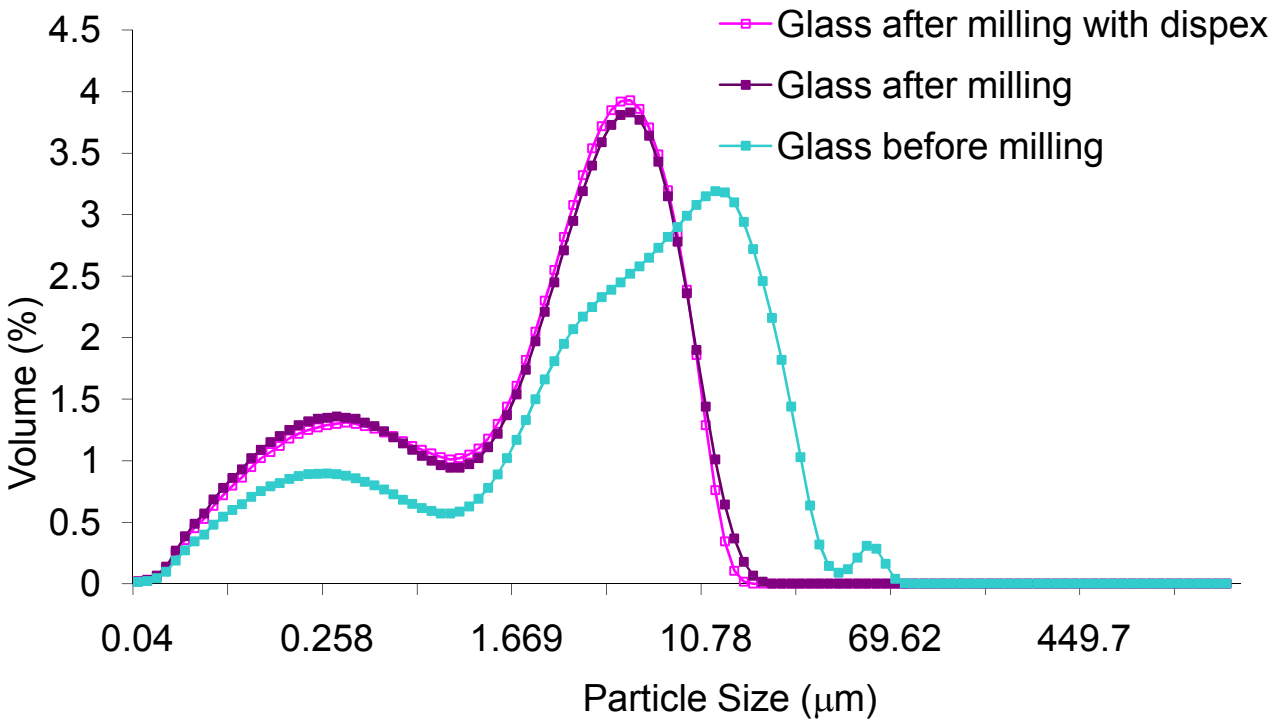

Figure 16: Particle size distribution of Glass particles before and after milling and with and without Dispex.

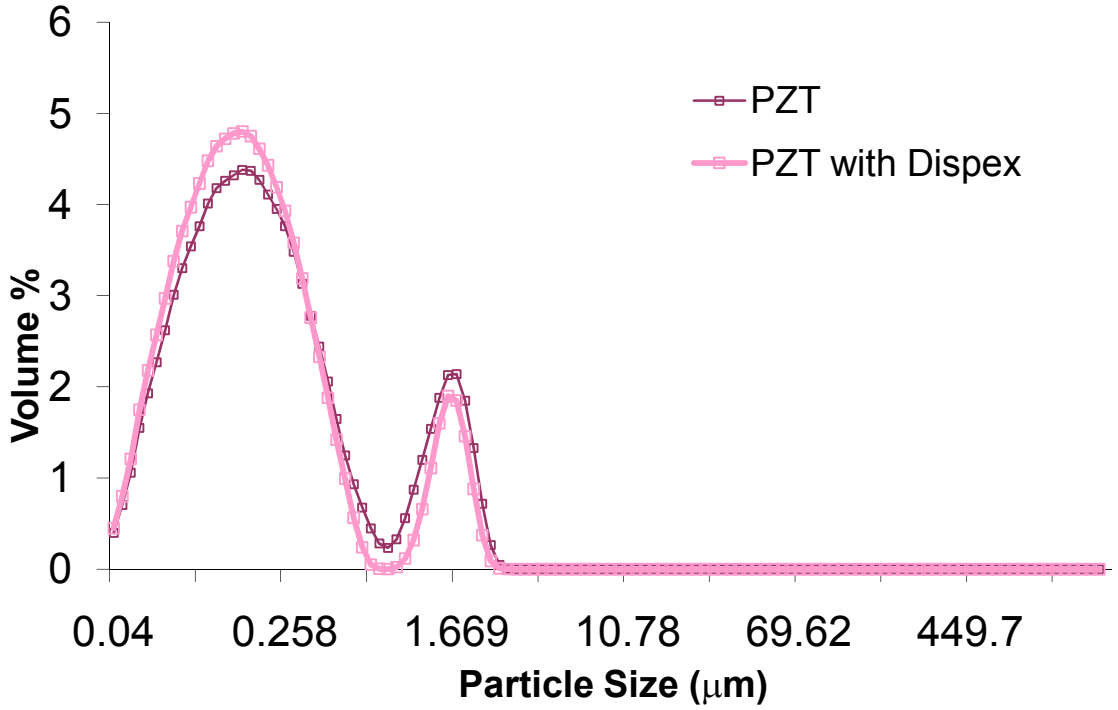

Figure 17: Particle size distribution of Lead Zirconate Titanate powders with and without Dispex.

The morphology of the PZT powders was analysed by SEM and the micrographs are presented in Figure 18, in which individual PZT particles (Figure 18) and agglomerates (Figure 19) can be identified, corroborating the particle size distribution analysis.

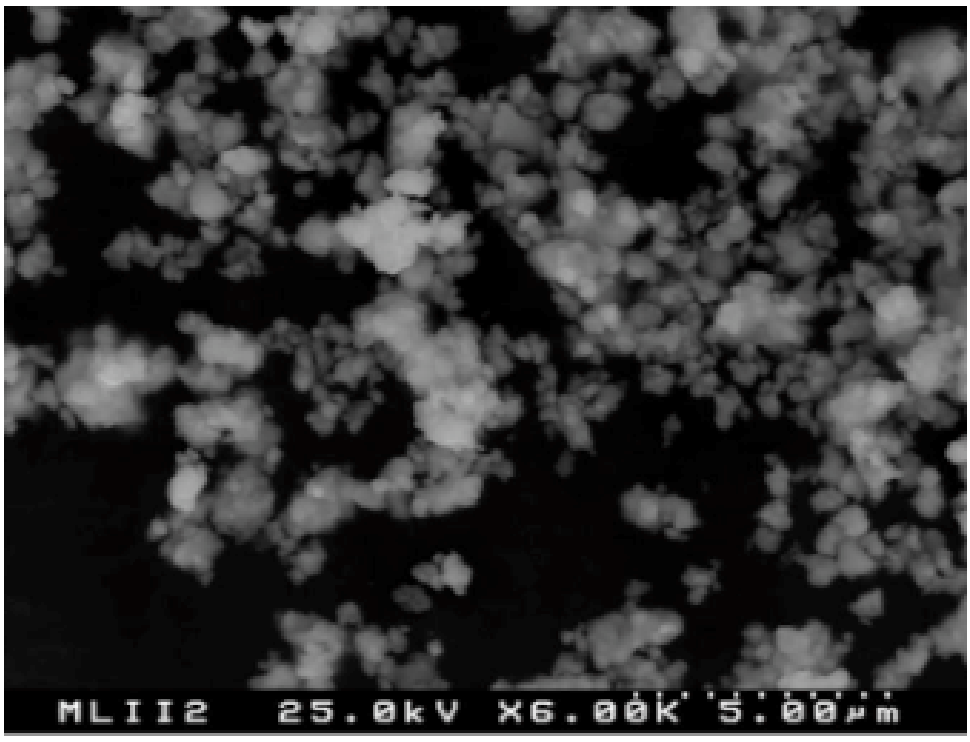

Figure 18: SEM morphology of PZT green powders.

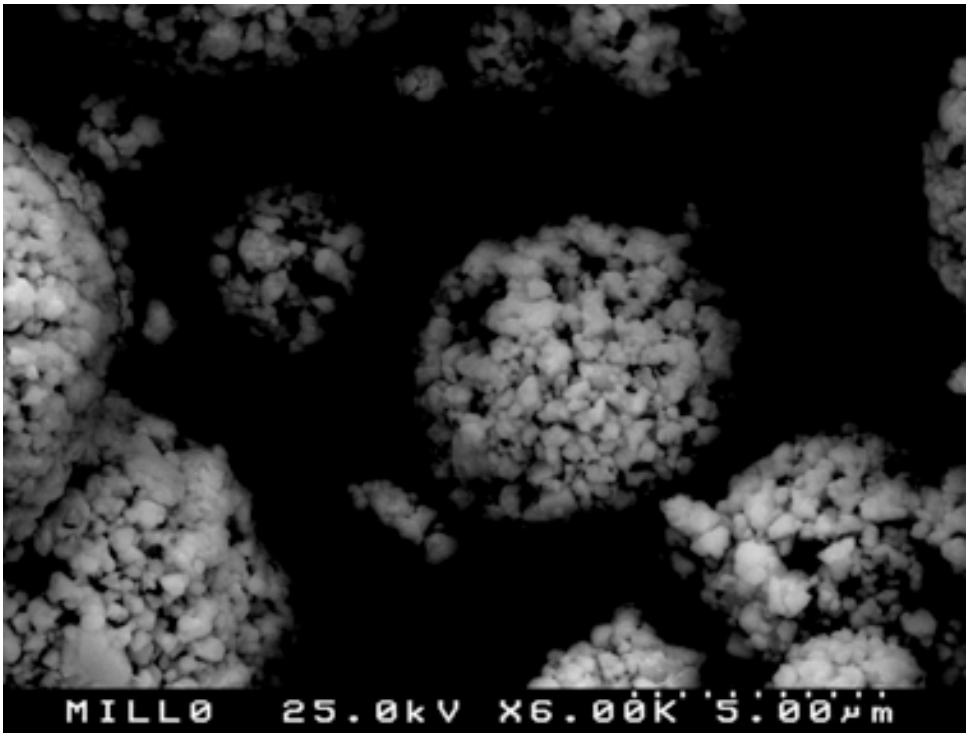

Figure 19: SEM morphology of PZT green powders.

4.1.2 Zeta Potential

4.1.2.1 Brief Introduction to Zeta Potential

Colloidal particles dispersed in a solution are electrically charged due to their ionic characteristics and dipolar attributes. In such a suspension each particle is surrounded by a layer of oppositely charged ions called the Stern layer. Outside the Stern layer, there are ions of opposite polarities which concentration varies, forming a cloud-like volume. This volume is called the diffuse double layer, and the whole volume is electrically neutral.[43]

When a voltage is applied to the solution in which particles are dispersed, particles are attracted to the electrode of the opposite polarity, accompanied by the fixed layer and part of the diffuse double layer, usually called as the "sliding surface" (Figure 20).

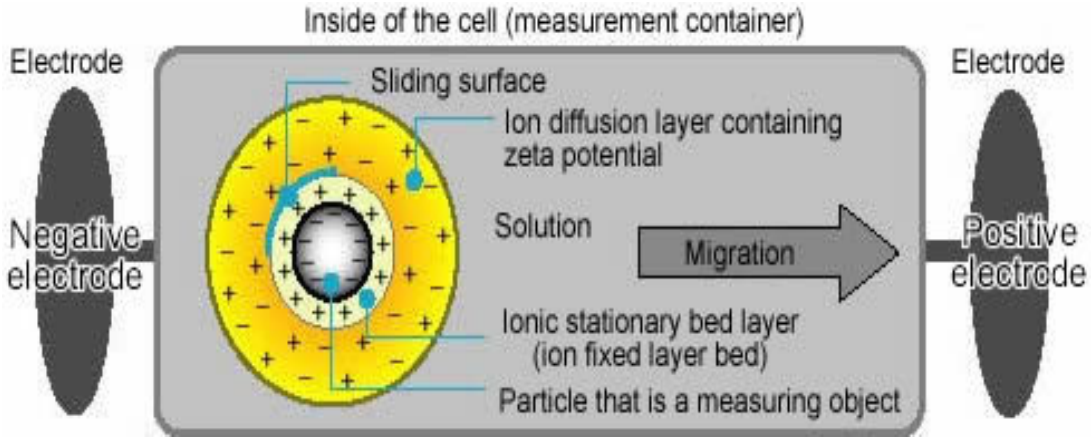

Figure 20: Movement of charged particles under the electric field.[Adapted from reference 43]

In the double layer model, the Zeta potential is considered to be the electric potential of this inner volume including this conceptual "sliding surface". As this electric potential approaches zero, particles tend to aggregate.

The static layer is computed using the following formula.[Adapted from reference 43]

$$\frac{hs}{b} = \sqrt{\frac{1}{3} + \frac{128}{\pi^5 K}}$$

K = (Width of Cell)/(Thickness of Cell)
b = A half of Thickness of Cell
hs = Static Layer (Distance from center of Cell)

Zeta Potential (Smoluchowski's Formula)

$$\zeta = \frac{4\pi\eta}{\varepsilon} \times U \times 300 \times 300 \times 1000$$

ζ=Zeta Potencial (mV)

η = Viscosity of Solution

ε = Dielectric Constant

$$U = \frac{\nu}{V/L}$$

Eletrophoretic Mobility

ν = Speed of Particle (m/sec)

V = Voltage (V)

L = The distance between eletrodes

To eliminate errors due to electroosmotic flow caused by any electrostatic charge on the measurement cell, the zeta potential is measured at the static layer, whose position can be calculated from the width and depth of the cell (the software performs this calculation automatically).

Some considerations to have in mind that are important for EPD:

- The magnitude of the zeta potential gives an indication of the potential stability of the colloidal system;
- If all the particles have a large negative or positive zeta potential they will repel each other and there is a dispersion stability;
- If the particles have low zeta potential values then there is no force to prevent the particles coming together and there is a dispersion instability;
- A dividing line between stable and unstable dispersions is generally taken at either +30 or -30mV (Figure 21), being suspensions with zeta potentials > +30mV or < -30mV normally considered stable.

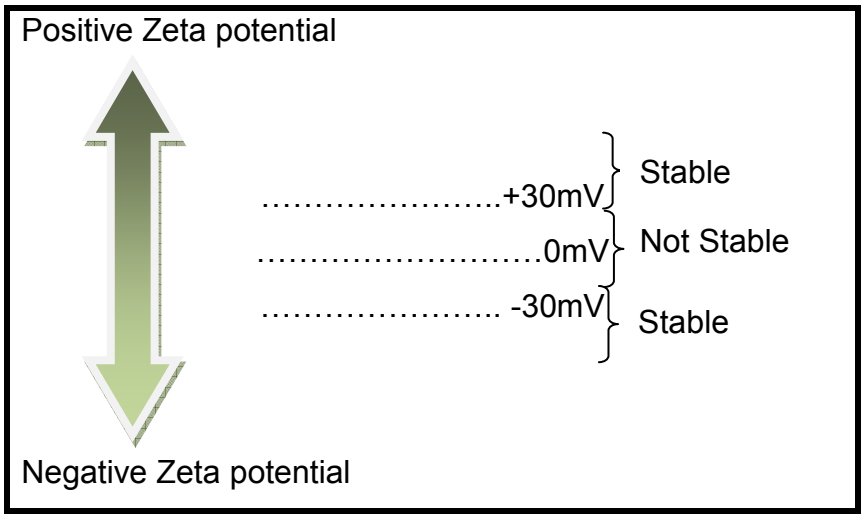

Figure 21: Zeta Potential Stable Zone.[Adapted from reference 44]

To guarantee the required suspension stability and a constant flow of particles under the applied electric field, during EPD, zeta potential curves are a good indicator of the surface charges and stability of the suspensions. Meanwhile, zeta potential sign (positive or negative) determines the direction and migration velocity of the powder particles during EPD. Moreover, because high green densities are required for these thick films a very well dispersed suspension is needed. It is then crucial to maximize the repulsive forces between the particles to prevent their coagulation and consequent flocculation that will markedly affect the quality of the deposited films.

The surface charge of these PZT suspensions was analyzed by zeta-potential measurements and the zeta potential of PZT powders dispersed in Potassium Chloride (KCl) as a function of pH is depicted in Figure 22. At low pH, PZT is positively charged and presents a quite high zeta potential value, > +30 mV, indicating its suitability for electrophoretic deposition; under an electric field the powders will be deposited onto the cathode. As the pH value increases zeta potential decreases being zero (isoelectric point) for pH ≈ 10.15 and then the negative surface charges increase for higher pH values.

The zeta potential behaviour of the glass and oxide powders was analysed as well. The zeta potential curve for unmilled and milled glass is plotted in Figure 23. Similarly to the previous curve, the zeta potential of glass powders decreases as pH increases with an isoelectric point for pH ≈ 10.15 for glass before milled and pH ≈ 10.9 for glass after milled. For low pH values the zeta potential is around +30 mV, suggesting a good compatibility with PZT powders in terms of suspension stability towards an effective EPD. In accordance with the particle size distribution, milled glasses present slightly higher zeta potential values.

Based on these results of zeta potential, suspensions of the films in this work were prepared in acetic acid media and under a pH value < 5, and a cathodic EPD took place.

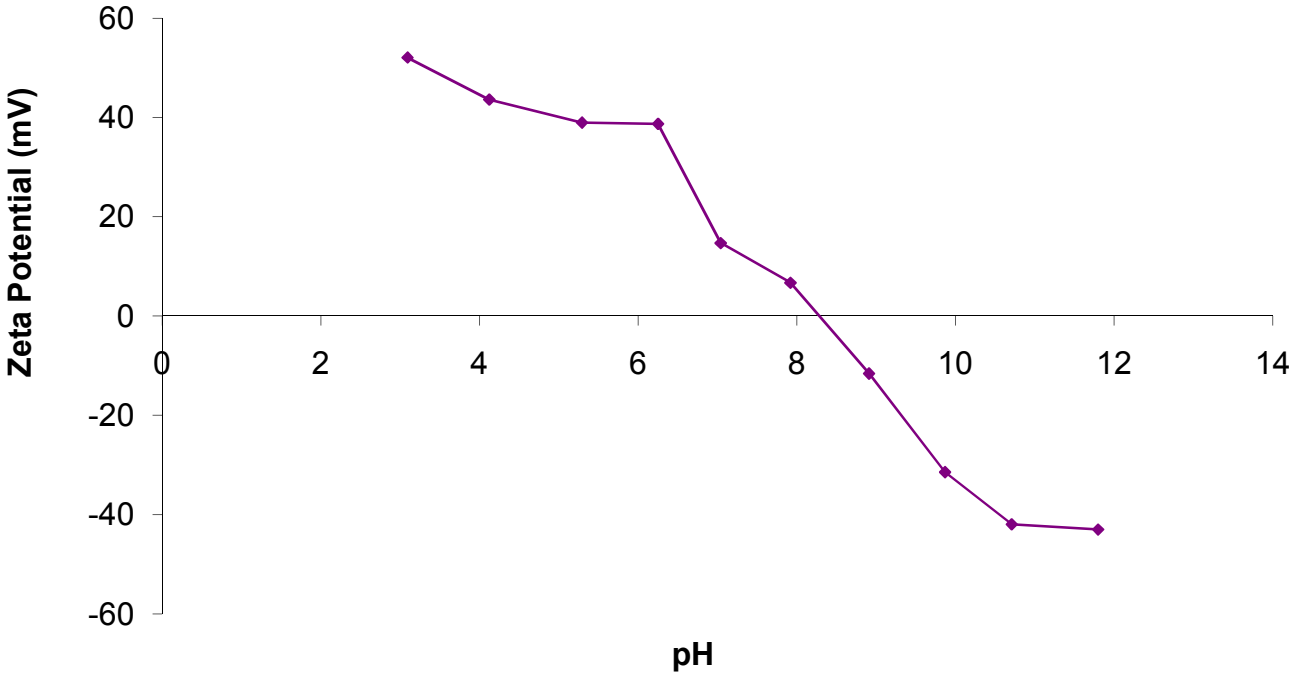

Figure 22: Zeta potential of Lead Zirconate Titanate powders in Potassium Chloride based suspension media.

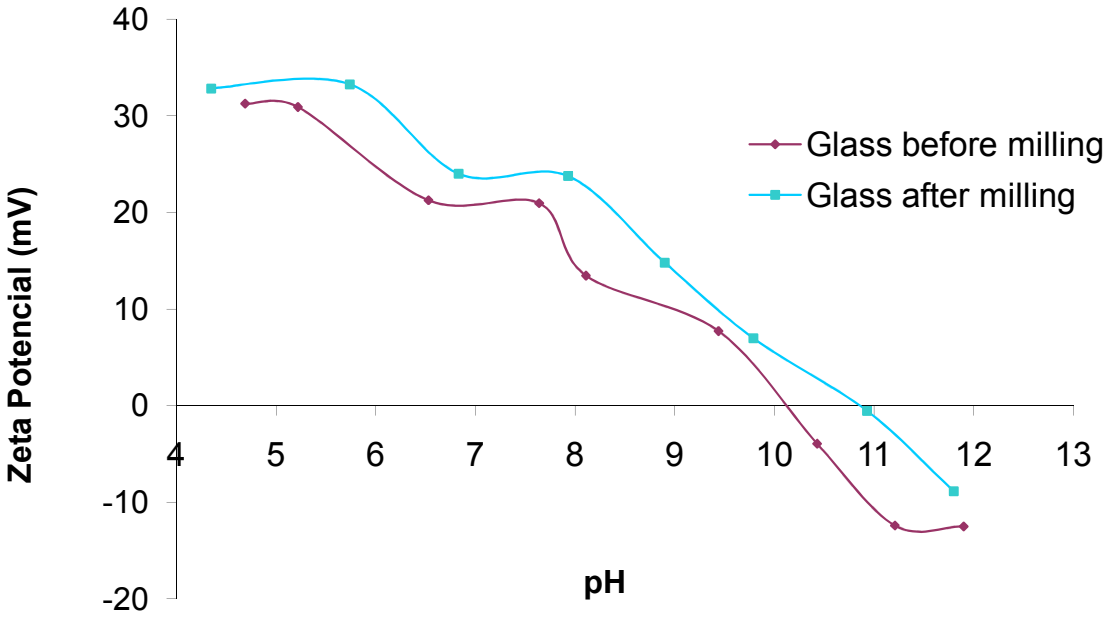

Figure 23: Zeta Potential of a Glass after and before milling in Potassium Chloride based suspension media.

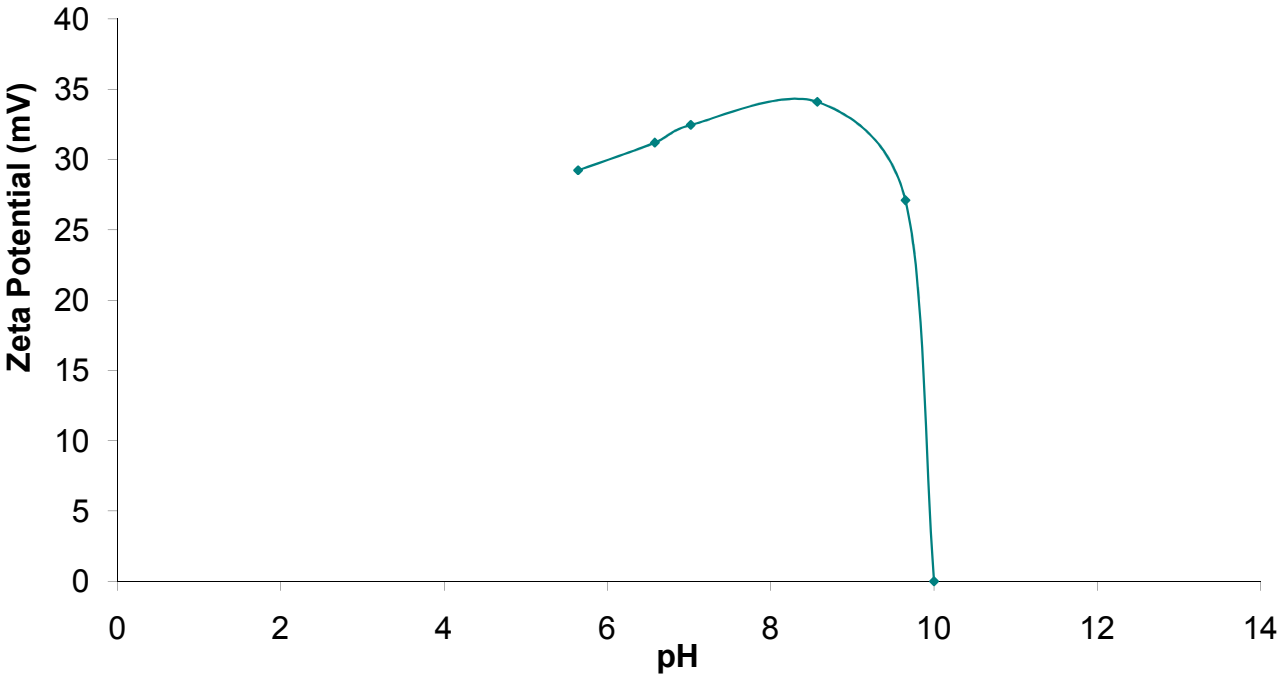

Figure 24: Zeta potential of Lead Oxide in Potassium Chloride based suspension media.

4.2 Characterization of the Films

4.2.1 Structure and Phase Analysis

The XRD patterns of sintered PZT films with addition of 5 wt % Glass additions deposited on Cu are depicted in Figure 25. The crystalline phases present in the film after sintering at 800ºC for 30 minutes are PZT, ZrO_2, Cu, PbO, and $PbTiO_3$. To be noted here is the high intensity of the Cu peaks, what may related with the low thickness of the films deposited with glass addition. Similar phases were identified for the films sintered with the other glass contents and at different temperatures. No significant changes were observed and no phases resulting from the reaction of the glass with PZT or with Cu were observed.

All this bad results for formed crystalline phases, the appearance of second phases and dominant phases being copper were probably the reason for such bad results on dielectric properties and the abandonment of these compositions for deposition of these films with glass addition.

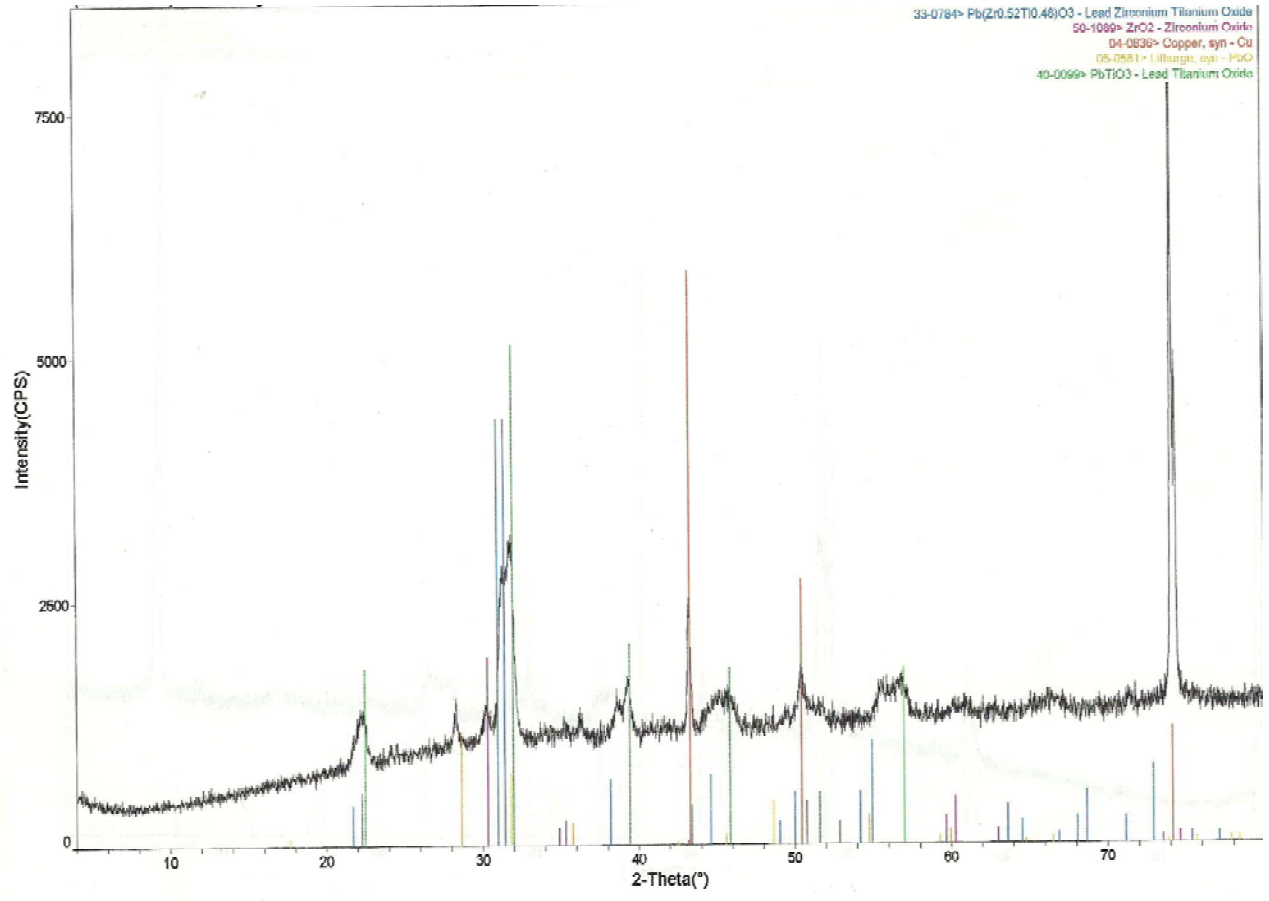

Figure 25: XRD patterns of PZT films with PZT with 5 wt % of Glass, sintered at 800ºC for 30 minutes.

The XRD patterns of sintered PZT films with B_2O_3 + PbO on Cu are represented in Figures 26, 27, 28 and 29.

Figure 26 depicts the XRD patterns of PZT films with 1 wt % of (90% B_2O_3 and 10% PbO) and sintered at 800ºC and 900ºC for 30 and 60 minutes. For the low sintering temperatures (800ºC) three crystalline phases were identified as PZT, PbO and Cu, being PZT the dominant phase. The presence of PbO in these films is related with the used additives. The absence of boron based crystalline phases should be related with the glass formation character of boron oxide, implying an effectiveness of the role of PbO – B_2O_3 additions as sintering aid. Important to note here is the nonappearance of any cuprite phase, resulting from the oxidation of the Cu substrate, what indicates that the used reducing atmosphere was effective in preventing the oxidation of the substrate, at least under the current XRD detection limit. As the sintering temperature increases to 900ºC besides the phases previously detected, peaks corresponding to Pb and ZrO_2 were identified as well. This may be due to a reaction between PZT and Cu leading to the separation of the PZT with the formation of lead oxide and zirconium oxide, and as a consequence may degrade the electrical response of these films. Another indication of the degradation of PZT is that the intensity of the peaks correspondent to PZT decreased as the sintering temperature increases to 900ºC. Indeed in a previous work [4] for PZT films deposited on Cu foils and sintered at temperatures higher than 950 ºC ZrO_2 was detected as well. [34] It was then postulated that the formation of a Cu_x-Pb when sintering above 950 °C caused the decomposition PZT accompanied by the Ti enrichment of PZT and formation of ZrO_2. [4]

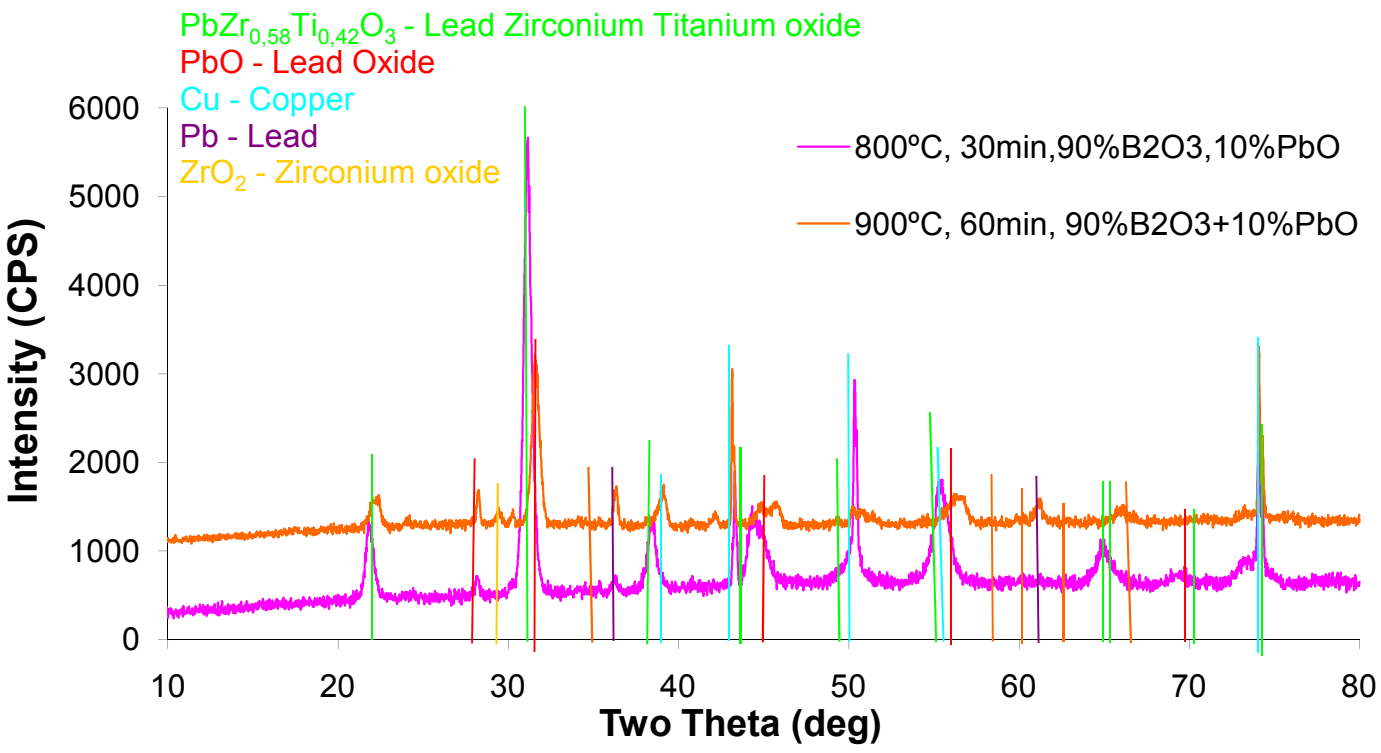

Figure 26: XRD patterns for PZT films with 1 wt % of (90% B_2O_3 and 10% PbO) sintered at 800ºC and 900ºC for 30 and 60 minutes.

The XRD patterns plotted in next figure (Figure 27) correspond to the PZT films with 1 wt % of (80% B_2O_3 and 20% PbO) sintered at 800ºC and 900ºC for 30 and 60 minutes. Similarly to the previous films, for the low sintering temperature only the phases corresponding to PZT, PbO and Cu were detected. As the sintering temperature increases the identified phases are PZT, Cu, PbO, ZrO_2 and Pb, as observed before.

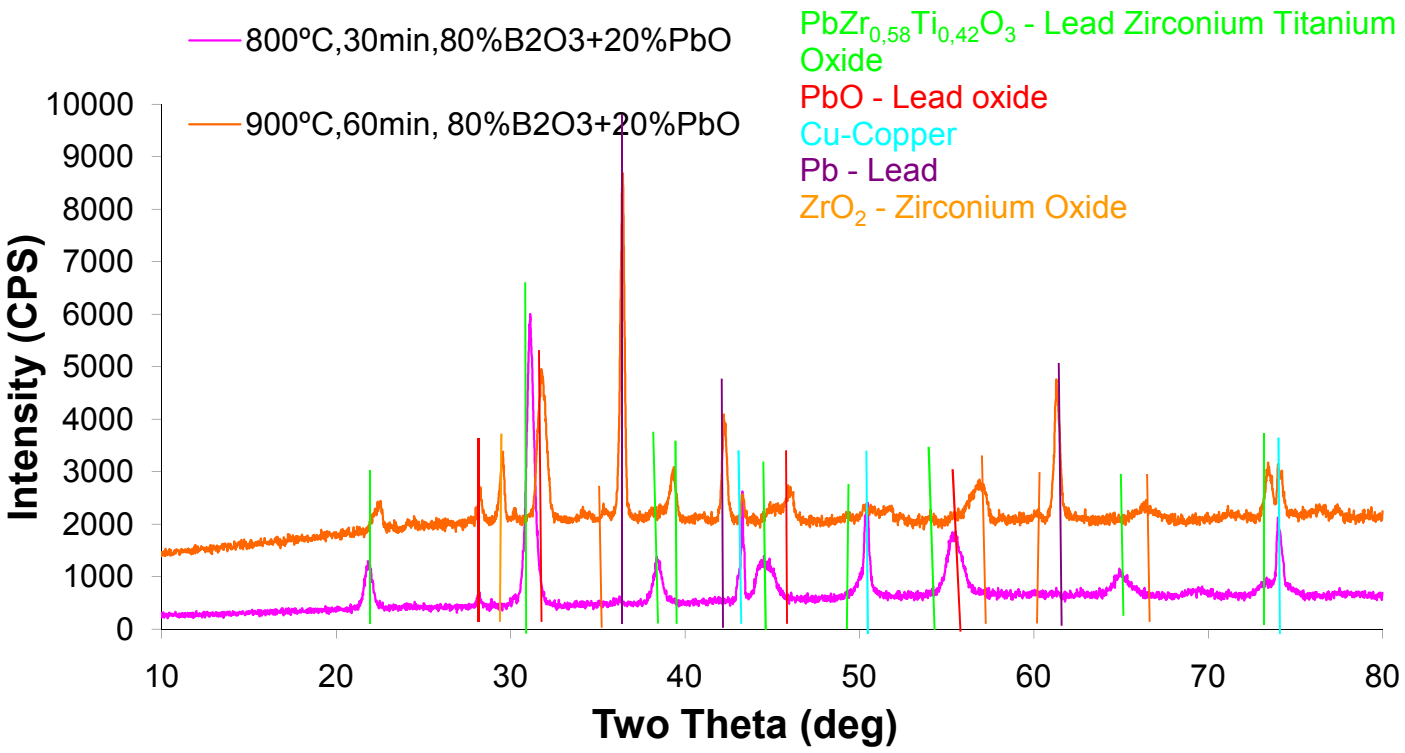

Figure 27: XRD patterns of PZT films with 1 wt % of (80% B_2O_3 and 20% PbO) sintered at 800ºC and 900ºC for 30 and 60 minutes.

Figure 28 illustrates the XRD patterns of PZT films with 1 wt % of (50% B_2O_3 and 50% PbO) sintered at 800ºC and 900ºC for 30 and 60 minutes. The crystalline phases identified in these films are the same as in the two previous cases: PZT, Cu and PbO for the films sintered at 800 ºC and plus ZrO_2 and Pb for the films sintered at 900ºC. In this case the intensity of the PZT degrades as well with the sintering temperature.

From the above XRD results there are no obvious differences in terms of phases formed and in terms of crystallinity (inferred by peaks intensity) between the PZT films prepared with different B_2O_3 + PbO proportions. For all of the studied oxide mixtures the highest sintering temperature (900ºC) promotes reactions with the substrate and the formation of secondary phases. Due to the excess of PbO used as sintering aid, residual PbO is present in these films. In terms of phase formation the low sintering temperature of 800 ºC corresponds to the most adequate situation in terms of formed phases.

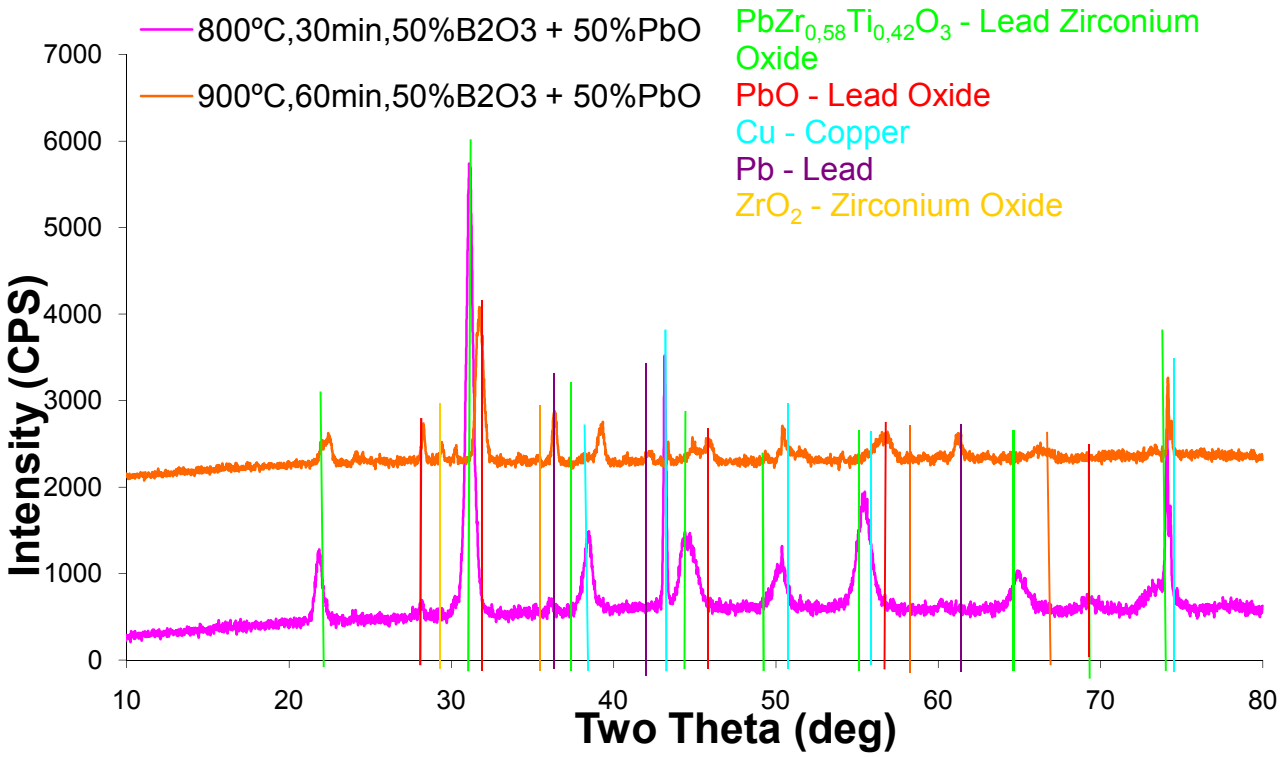

Figure 28: XRD patterns of PZT films with 1 wt % of (50% B_2O_3 and 50% PbO) sintered at 800ºC and 900ºC for 30 and 60 minutes.

XRD patterns of PZT films with 3 wt % (50% B_2O_3 + 50% PbO) sintered at 800ºC for 30 minutes are plotted in Figure 29. Six crystalline phases were identified as, PZT, ZrO_2, Cu, PbO and cuprite (Cu_2O), being the most intense peaks those correspondent to the PZT phase.

For films sintered at 850ºC for 30 minutes the identified phases are PZT, ZrO_2, PbO and Cu. In this case cuprite was not detected. Under the same sintering conditions but longer sintering times the same phase's we present together with some peaks of TiO_2.

Differently from the previous cases is the detection of the peaks of cuprite in the films sintered at low temperatures that indicate the oxidation of the Cu substrate; as stated before this oxidation was not visible in some of the previous patterns. The oxidation of the substrate may be related with the experimental sintering conditions used in the course of this work, in which the control of the low oxygen partial pressure *(pO_2)* is indeed not very accurate.

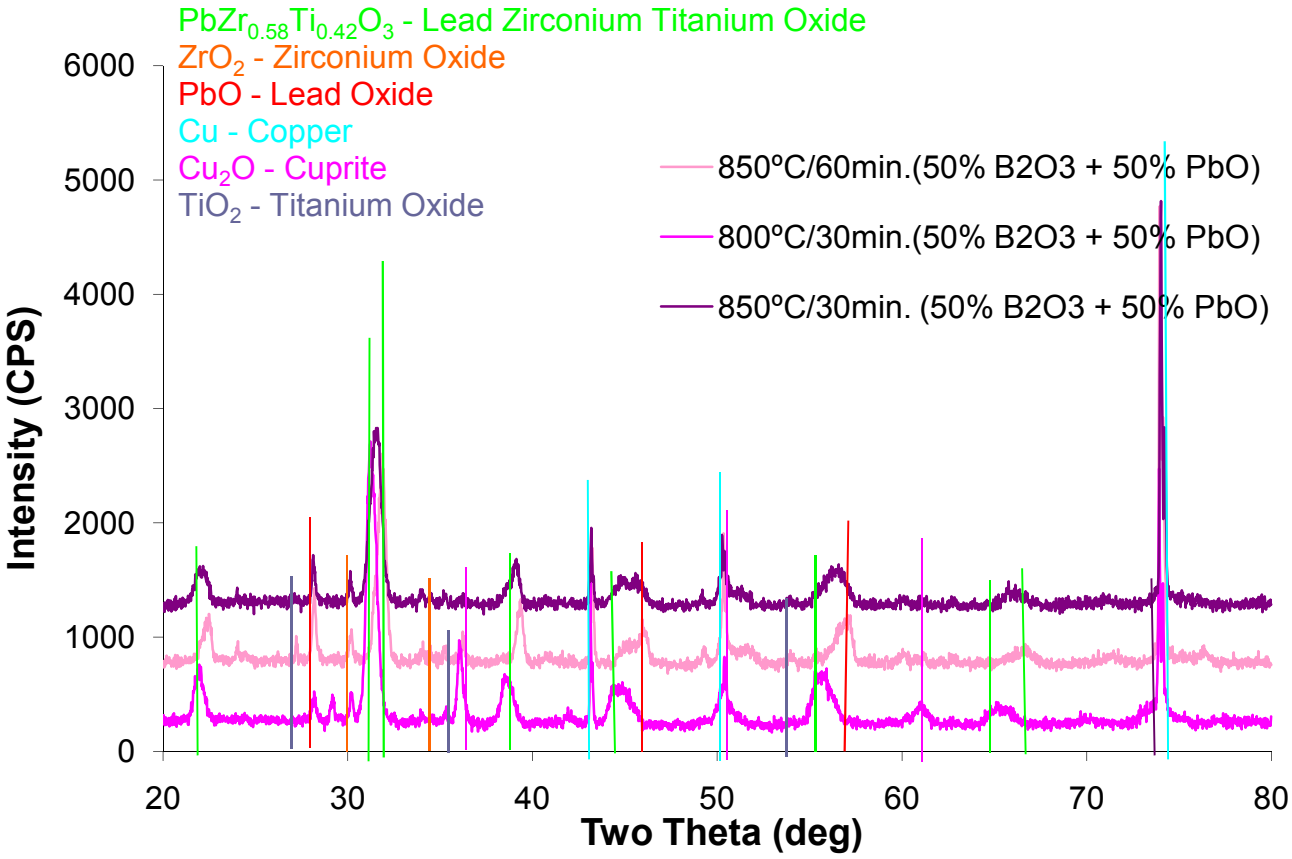

Figure 29: XRD patterns of PZT films with 3 wt % of (50% B_2O_3 and 50% PbO) sintered at 800ºC and 850ºC for 30 and 60 minutes.

The next table summarises the phase content determined by DRX analysis for the different films compositions.

Table 5: Phase content of the different PZT films with mixture oxide addition and determined by XRD analysis.

Compositions of PZT films with	Detected Phases
1 wt % (90% B_2O_3 + 10 % PbO) for 800ºC and 30 minutes	PZT, PbO and Cu
1wt % (90% B_2O_3 + 10% PbO) for 900ºC and 60 minutes	PZT, PbO, Cu, ZrO_2 and Pb
1wt % (80% B_2O_3 + 20% PbO) for 800ºC and 30 minutes	PZT, PbO and Cu
1wt % (80% B_2O_3 + 20% PbO) for 900ºC and 60 minutes	PZT, PbO, Cu, ZrO_2 and Pb
1wt % (50% B_2O_3 + 50% PbO) for 800ºC and 30 minutes	PZT, PbO and Cu
1wt % (50% B_2O_3 + 50% PbO) for 900ºC and 60 minutes	PZT, PbO, Cu, ZrO_2 and Pb
3 wt % (50% B_2O_3 + 50 % PbO) for 800ºC and 30 minutes	PZT, PbO, Cu_2O, ZrO_2 and Cu
3 wt % (50% B_2O_3 + 50 % PbO) for 850ºC for 30 minutes	PZT, PbO, ZrO_2, Cu and PbO
3 wt % (50% B_2O_3 + 50 % PbO) for 850ºC for 60 minutes	PZT, PbO, ZrO_2, Cu, PbO and TiO_2

4.2.2 Film Microstructure and Thickness

Figure 30 illustrates the optical micrographs of some of the PZT films as deposited and after drying. Thin and fluffy layers with irregular edges and surfaces cover some parts of the substrate for films prepared from PZT and glass powders suspensions. In these cases the film thickness was not uniform and in some cases it was even impossible to have a continuous layer of powder on the surface of the substrate. These observations support very well the XRD results obtained for these films (Figure 25). It is then expected that for some of these films the ability to measure the dielectric properties will be difficult.

On the other hand conformal and uniform PZT films were obtained for the films with oxides additions. These observations are in agreement with the examinations during the electrophoretic deposition, with the results of the suspension studies and with the XRD results.

a)

b)

Figure 30: Optical micrographs of films prepared from PZT and Glass powders suspensions **(a)** and Optical micrographs of film prepared from PZT and a mixture of (B_2O_3 + PbO) **(b)**, after drying.

Typical microstructures of the PZT green films are represented in Figure 31 (a and b) for PZT films with (50% B_2O_3 + 50% PbO) additions. As expected, green films show higher porosity than those fabricated from milled powders, which show relatively close packed microstructures.

To illustrate typical microstructures, samples sintered at 800 °C with 1wt % of (50% B_2O_3 and 50% PbO) were selected for SEM analysis and the micrographs are presented in Figure 32. From the low magnification image it is clear that homogeneous and crack free films were obtained. However the film microstructure is not very dense and, as depicted in the high magnification micrograph the grains are loosely packed. The cross section micrograph of these films (Figure 32 c)) indicates that the thickness of these films is around 10 μm, the surface is quite smooth, the grains are very fine and the porosity is clearly seen.

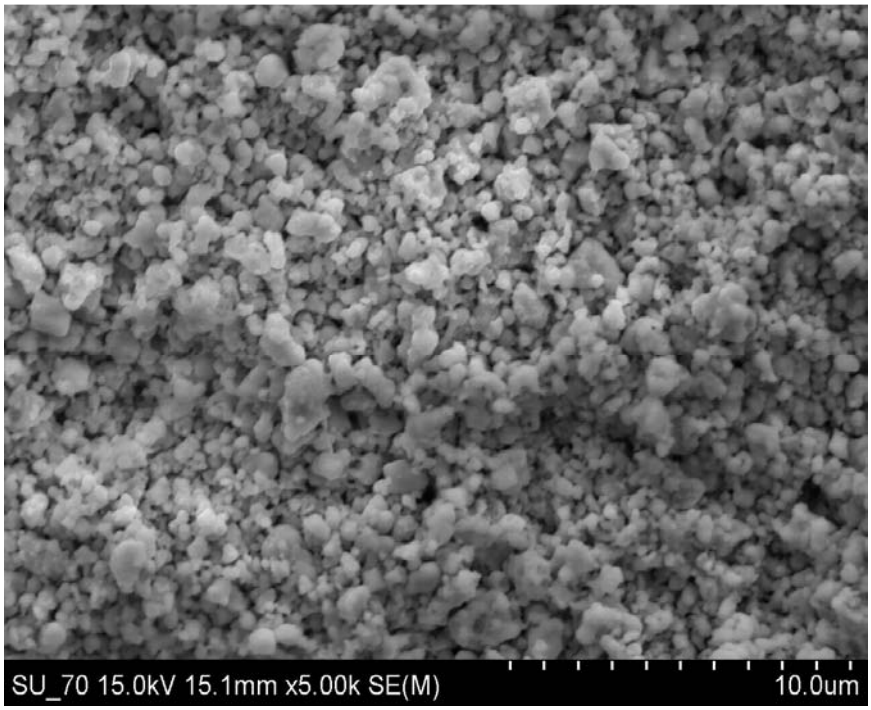

a)

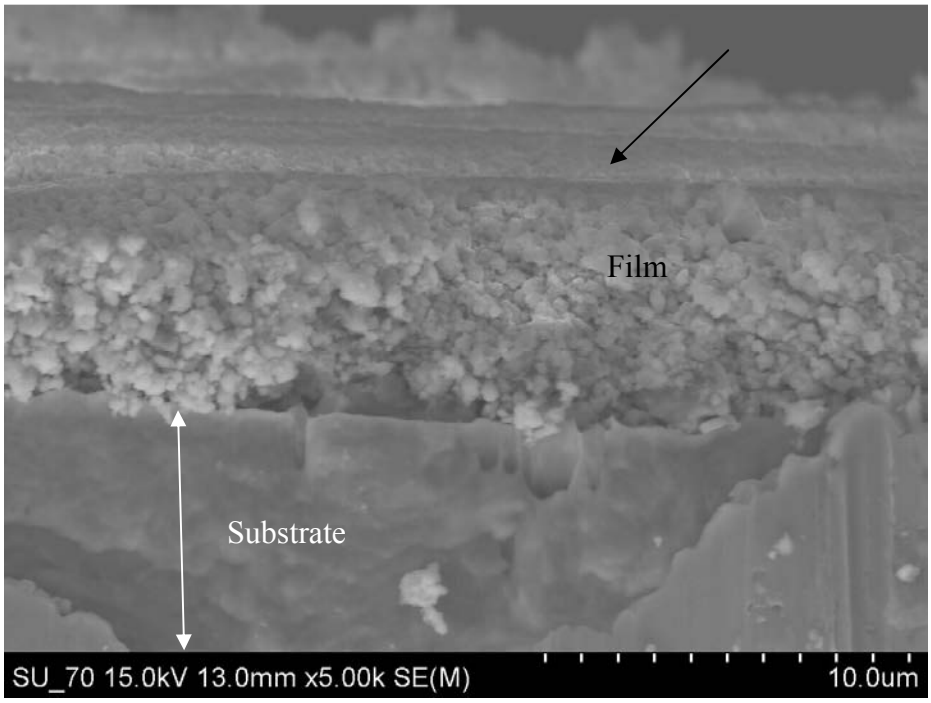

b)

Figure 31: Microstructure of PZT green films with 1 wt % addition of (50% B_2O_3 and 50% PbO); a) low magnification, b) cross section.

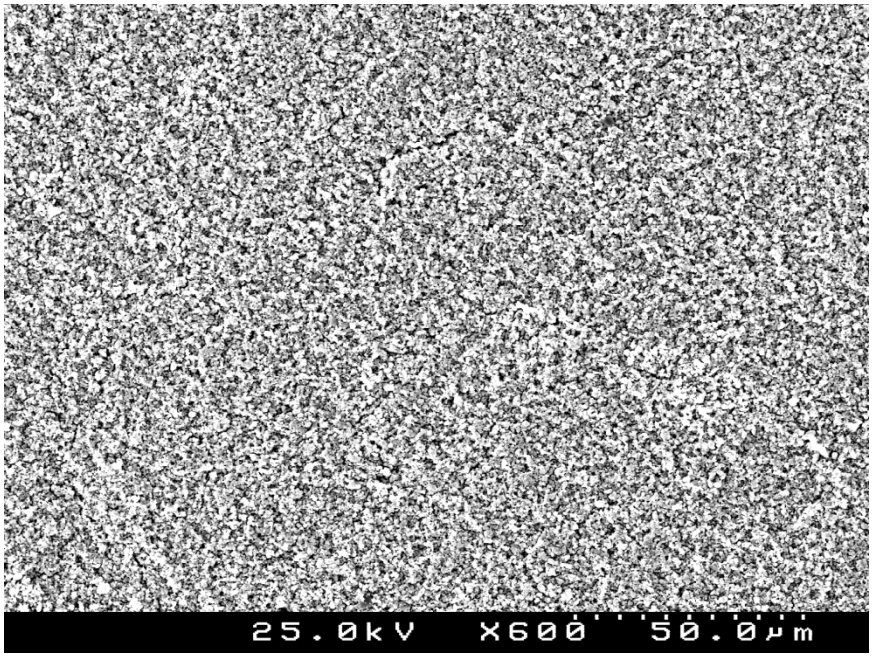

a)

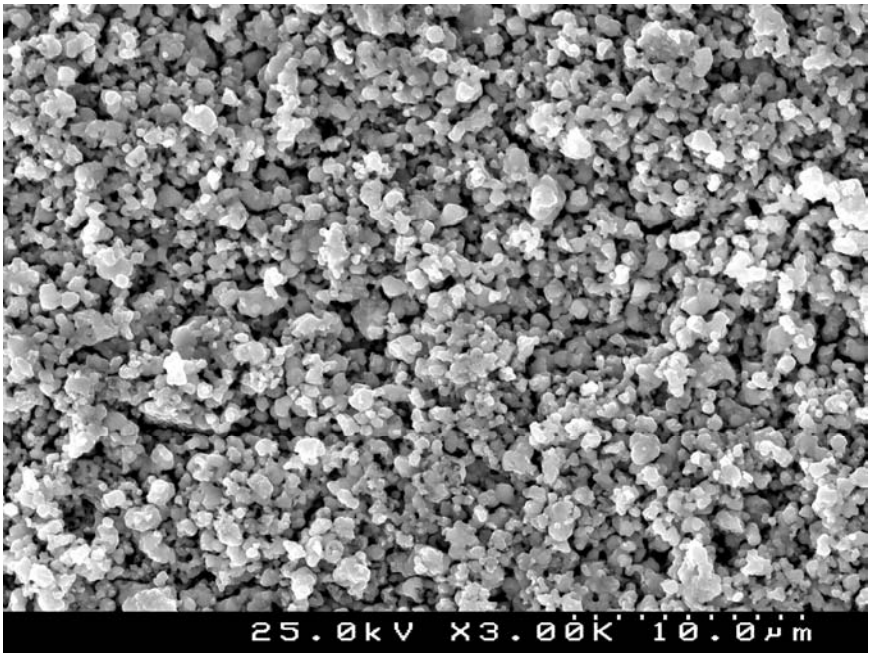

b)

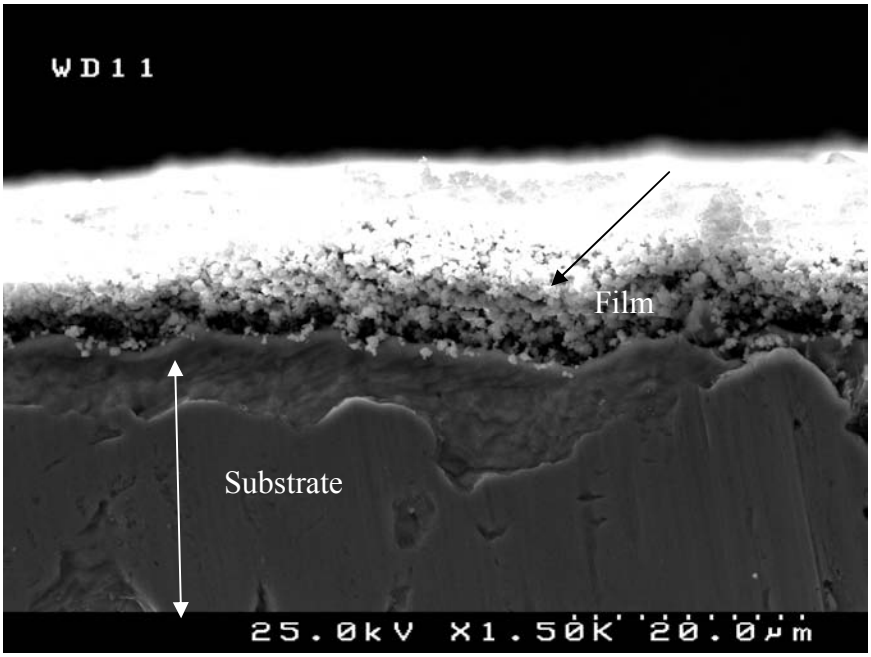

c)

Figure 32: Microstructure of PZT films with 1 wt % addition of (50% B_2O_3 and 50% PbO) sintered at 800ºC and 30 minutes; a) low magnification, b) high magnification and c) cross section.

The next micrographs correspond to films of PZT with 1wt % of (80% B_2O_3 and 20% PbO) and 1 wt% of (90% B_2O_3 and 10% PbO) sintered at high temperatures, 900ºC for 60 minutes. As clearly seem from the images and as expected at this high sintering temperature films are denser and grains are bigger. For some of these films, cracks were observed at these high temperatures, what might be related with the preparation conditions.

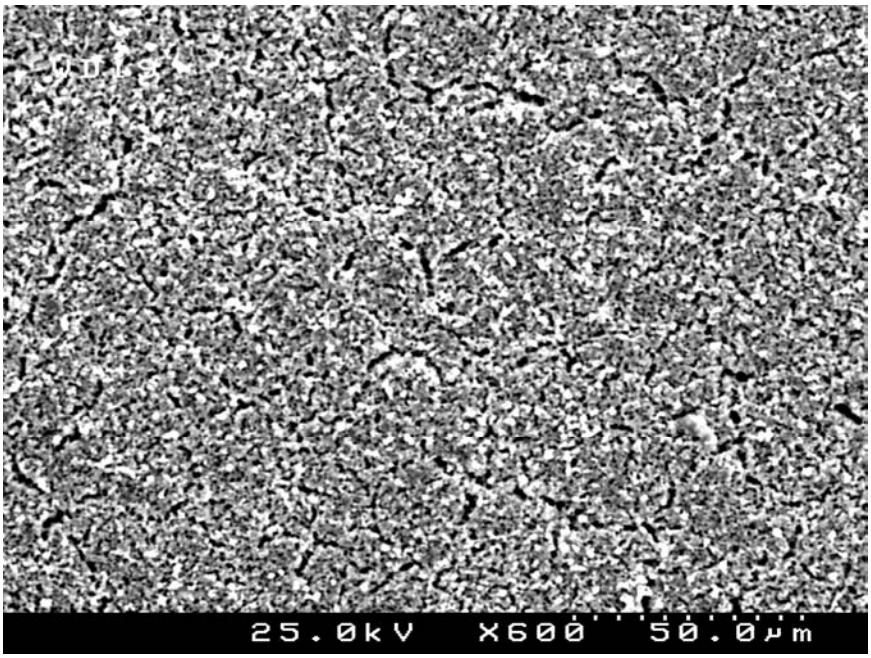

a)

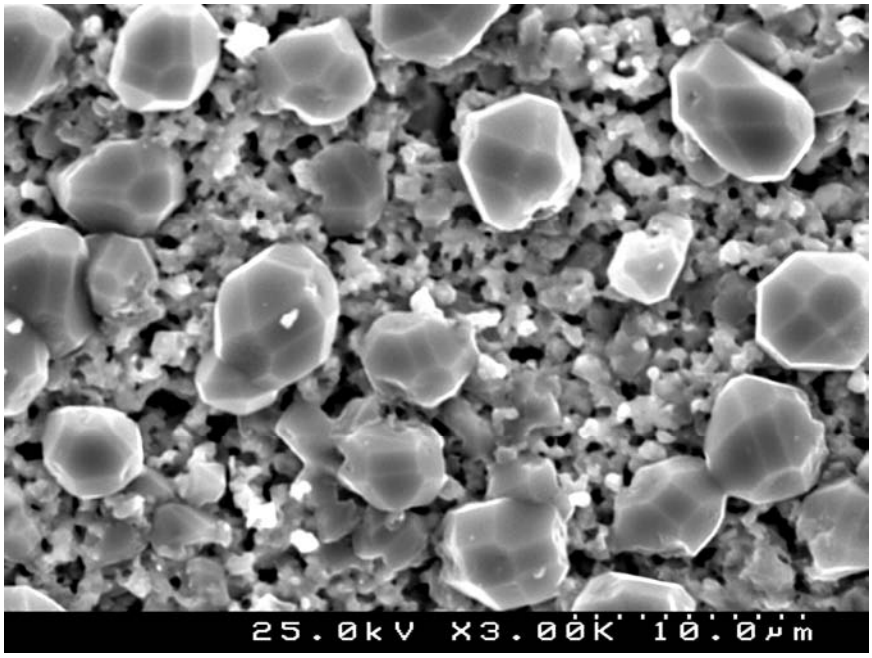

b)

Figure 33: Microstructure of: a) PZT films with 1 wt % of (80% B_2O_3 and 20% PbO) sintered at 900ºC for 60 minutes and b) PZT films with 1 wt % of (90% B_2O_3 and 10% PbO) sintered at 900ºC for 60 minute (by EDS analyse, one can see that bigger grain correspond to ZrO_2).

4.2.3 Electrical Properties

4.2.3.1 Electrical properties of PZT + 5, 10 and 20 wt % Glass Frit

The dielectric permittivity and losses as a function of the frequency and at room temperature of PZT films with glass additions and sintered at different temperatures are depicted in Figures 34 and 35. For very low frequencies, as the frequency increases the dielectric permittivity slightly decreases, keeping almost constant until 381 at 1 kHz. Similar behaviour is observed for the losses. The dielectric permittivity ranges from 50 to 350 and the losses from 0.05 to almost 2. In comparison with the values obtained in this work for the other PZT films and reported in the literature this range of permittivity values is quite low [1], [4], [39]

As it can be seen there is no consistent variation of the dielectric response with the sintering cycle. For the films with 20 wt % of glass addition it was not possible to obtain any dielectric data. In this case the films presented very high porosity and almost all of the capacitors were short circuited when the electric field was applied.

These observations are a result of the difficult deposition of PZT powders and glass and are consistent with the structural and microstructural analysis reported before.

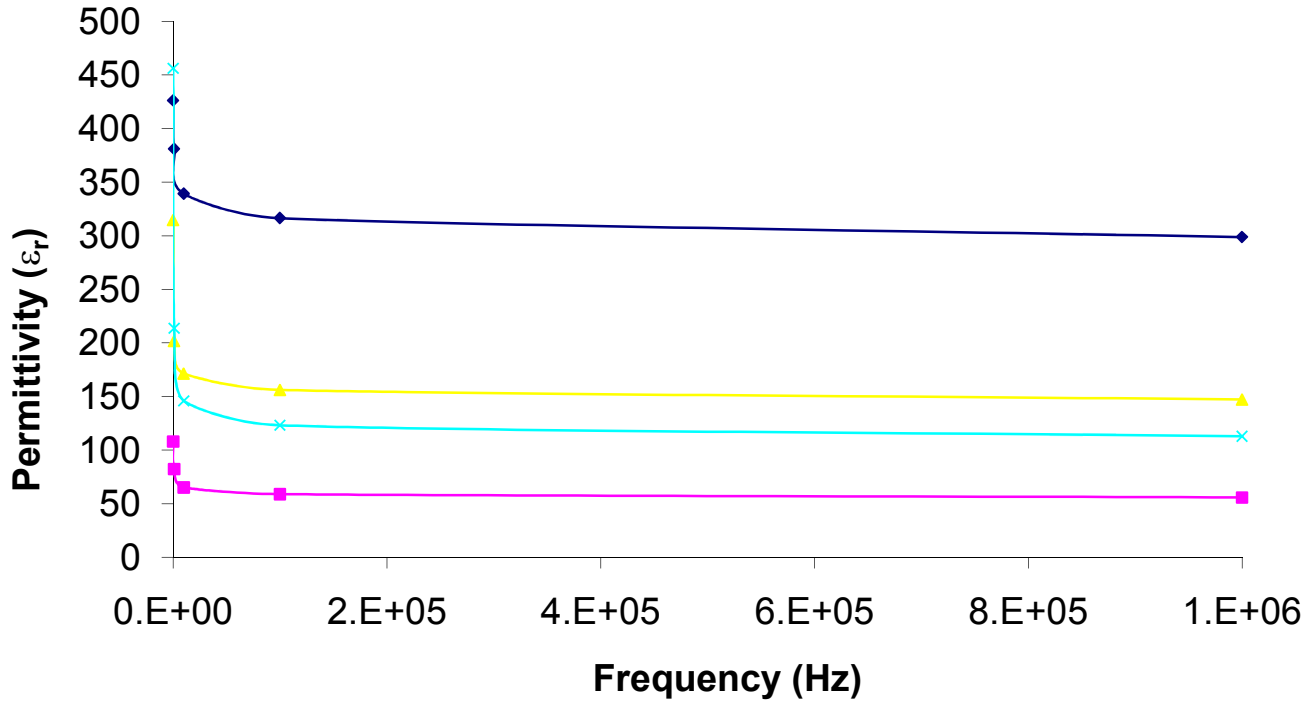

Figure 34: Permittivity versus frequency for PZT + 10 wt % Glass (SiO_2, PbO, Al_2O_3, B_2O_3) films sintered at 800ºC, 850ºC and 900ºC for 30 and 60 minutes. __ 800 ºC for 30 minutes, with 0.0045 mm of film thickness; __ 850 ºC for 30 minutes, with 0.0042 mm of film thickness; __900 ºC for 30 minutes, with 0.0035mm of film thickness; __ 900 ºC for 60 minutes, with 0.025 mm of film thickness.

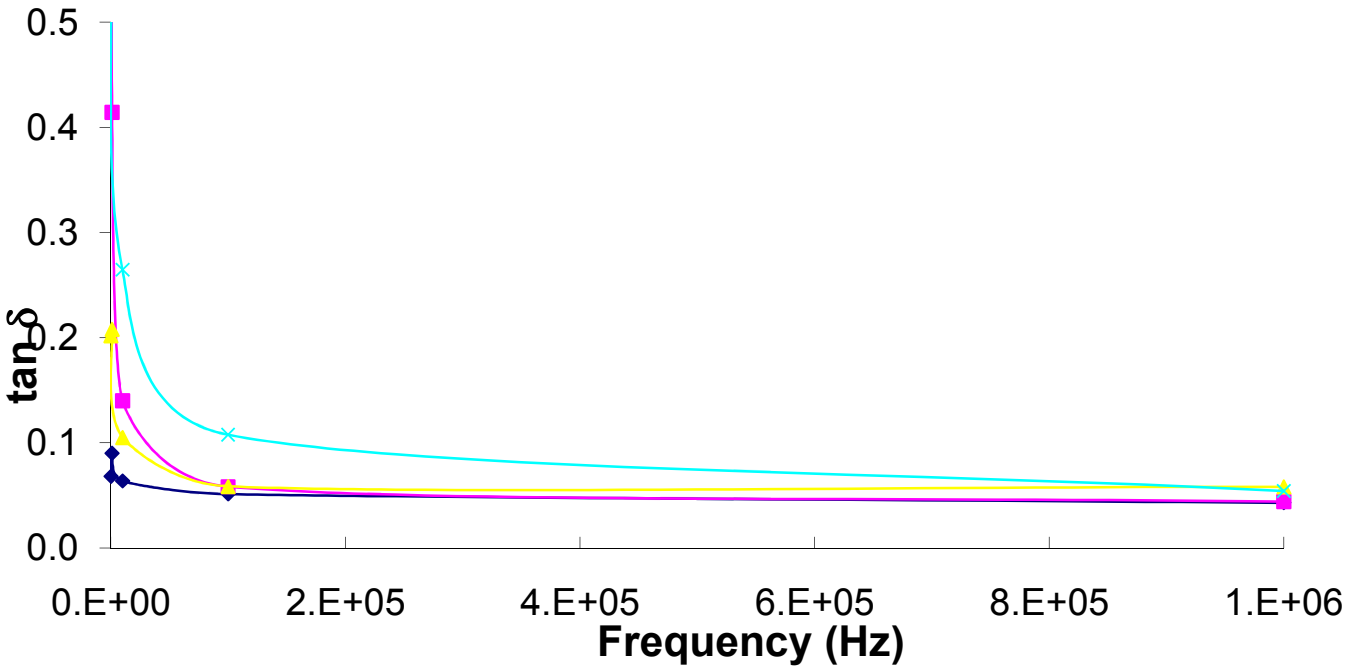

Figure 35: Losses versus frequency for PZT + 10 wt % Glass (SiO_2, PbO, Al_2O_3, B_2O_3) films sintered at 800ºC, 850ºC and 900ºC for 30 and 60 minutes. __ 800 ºC for 30 minutes, with 0.0045 mm of film thickness; __ 850 ºC for 30 minutes, with 0.0042 mm of film thickness; __900 ºC for 30 minutes, with 0.0035mm of film thickness; __ 900 ºC for 60 minutes, with 0.025 mm of film thickness.

As expected from the microstructures these properties are quite poor and reflect well the difficulties in getting homogeneous microstructures for these films, what is indeed related with the difficulty in depositing by EPD a homogeneous composite microstructure of PZT and glass powders.

In order to improve the quality of the deposition binders were used. However the dielectric permittivity and losses of PZT films with glass additions and PVB were very poor, being the obtained dielectric permittivity quite small, ranging from 25 to 35, and the losses, consequently quite high, around 6, as depicted in Figures 36 and Figures 37, as an example. These results clearly indicate that the use of PVB was indeed not effective in improving films quality. The use of PVB didn´t improve the adhesion of the particles to the substrate, on the contrary it decreased the mobility under the electric field during EPD avoiding the deposition of continuous thick layers. The degree of sedimentation of these suspensions was still high. The decomposition of the binders, in the present case, left open residual porosity what hindered the densification of the films and somehow contradicted the sintering aid effect of the glass.

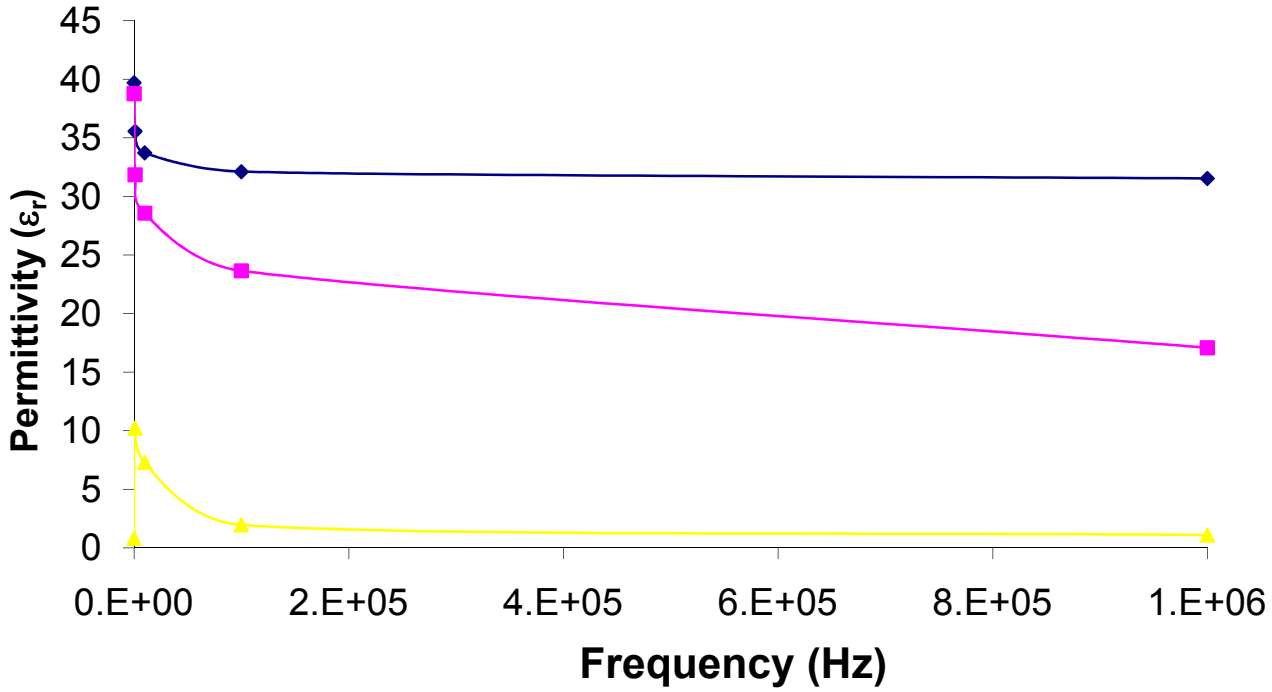

Figure 36: Permittivity versus frequency for PZT + 10 and 20 wt % Glass + 7.5 wt % PVB films sintered at 800ºC and 900ºC for 30 minutes. __ (10%), 800 ºC for 30 minutes, with 0.0046 mm of film thickness; __ (20%), 850 ºC for 30 minutes, with 0.0042 mm of film thickness; __ (20%), 900 ºC for 30 minutes, with 0.0035mm of film thickness.

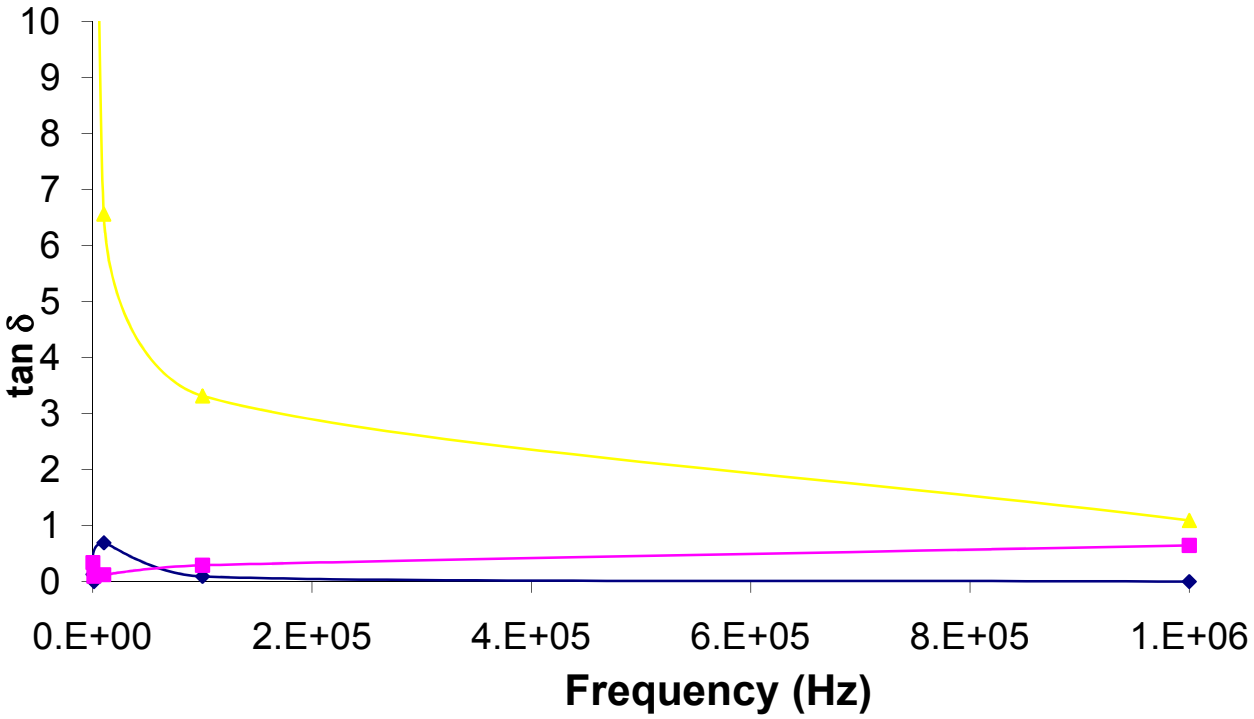

Figure 37: Losses versus frequency for PZT + 10 and 20 wt % Glass + 7.5 wt % PVB films sintered at 800ºC and 900ºC for 30 minutes. __ (10%), 800 ºC for 30 minutes, with 0.0046 mm of film thickness; __ (20%), 850 ºC for 30 minutes, with 0.0042 mm of film thickness; __ (20%), 900 ºC for 30 minutes, with 0.0035mm of film thickness.

4.2.3.2 Electrical properties of PZT + 1 wt % (B_2O_3 + PbO)

The electrical properties of PZT thick films with different amounts of oxide mixtures are presented in this section.

The comparison between the permittivity of PZT with 1 wt % (xB_2O_3 + (100-x)PbO) films sintered at different temperatures and for different periods of time as a function of lead oxide and boron oxide content is depicted in Figures 38 and 39. As the sintering temperature increases the permittivity decreases. A similar statement holds for the effect of the sintering time: higher permittivities were measured for the films sintered for 30 minutes against films sintered for 60 minutes. The dielectric response of the films corroborates well the observations of the phase analysis (Figures 26 to 28). Prolonged sintering time or high sintering temperatures favoured the reaction between PZT and Cu, with the formation of secondary phases (ZrO_2 and Pb) and modification of the stoichiometry of PZT, which damages the dielectric properties.

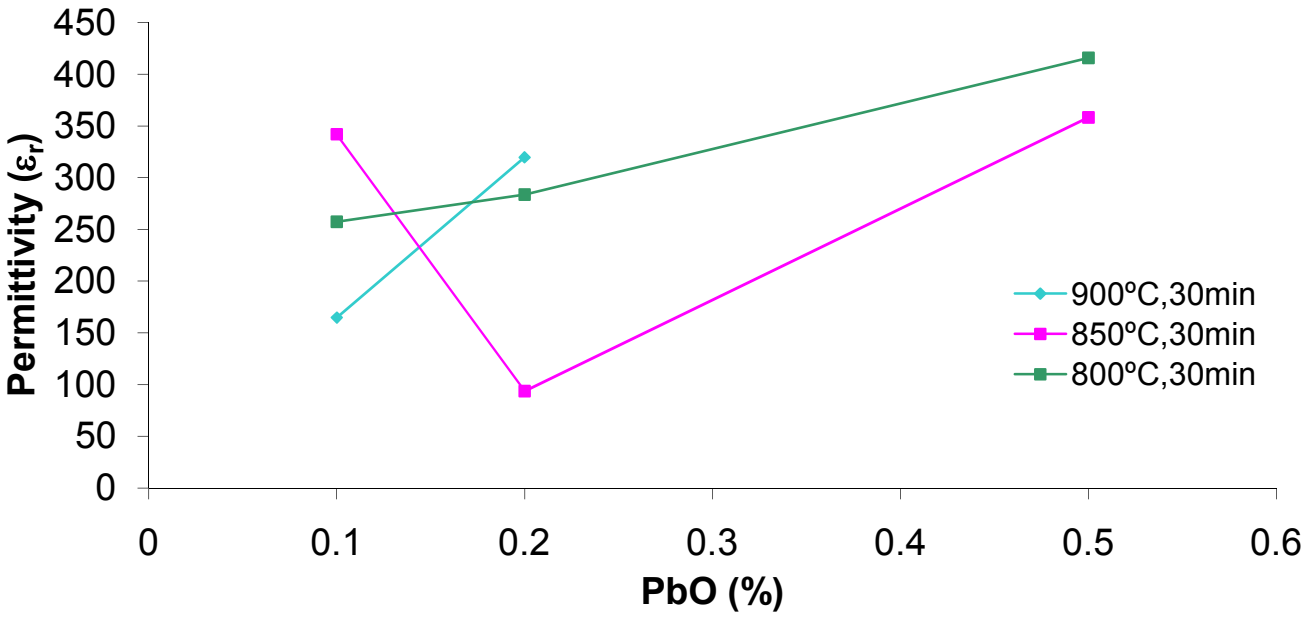

Figure 38: Permittivity versus PbO % of PZT films with 1 wt % of (xB_2O_3 + (100-x) PbO), being x = 90, 80 and 50) and sintered at different sintering temperatures, 800ºC, 850ºC and 900ºC for 30 minutes.

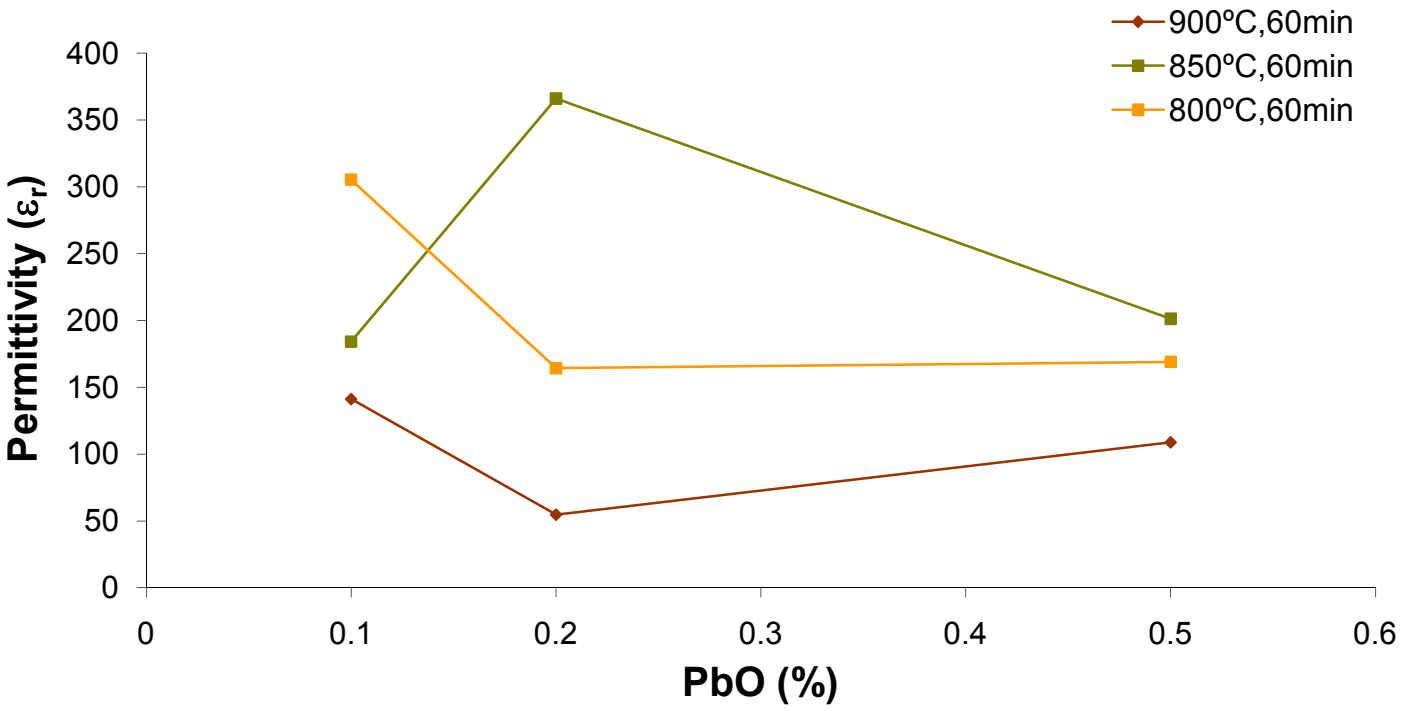

Figure 39: Permittivity versus % PbO of PZT films with 1 wt % of (xB_2O_3 + (100-x) PbO), being x= 90, 80 and 50) and sintered at different sintering temperatures, 800ºC, 850ºC and 900ºC for 60 minutes.

In the next graph of the permittivity versus frequency (Figure 40) for PZT films with 90% B_2O_3 and 10 % PbO one can observe that high permittivities are obtained for the films sintered at 850ºC for 30 minutes and the permittivity at 1 kHz was approximately 342. The lowest values of permittivity were obtained at 900ºC and 60 minutes.

Figure 41 depicts the curves of dielectric losses versus frequency in which a similar tendency is observed with the highest losses being observed for the films sintered at 900 ºC and 60 minutes of sintering time.

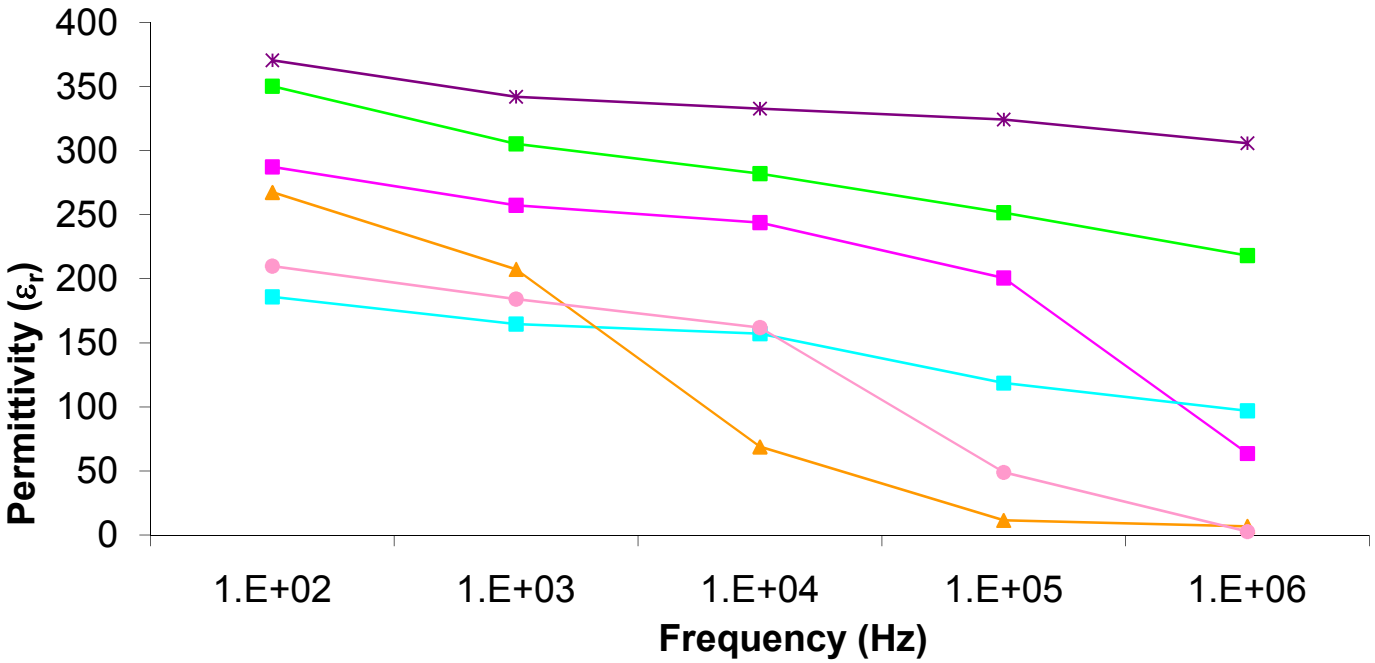

Figure 40: Permittivity versus frequency for PZT films with 1wt % of (90% B_2O_3 and 10% PbO) and sintered at 800ºC, 850ºC and 900ºC for 30 and 60 minutes. __ 800 ºC for 30 minutes, with film thickness of 0.0162 mm; __ 800 ºC for 60 minutes, with film thickness of 0.0165 mm; __ 900 ºC for 30 minutes, with film thickness of 0.0172 mm; __ 900 ºC for 60 minutes, with film thickness of 0.0072 mm; __ 850 ºC for 30 minutes, with film thickness of 0.0172 mm; __ 850 ºC for 60 minutes, with film thickness of 0.0165 mm.

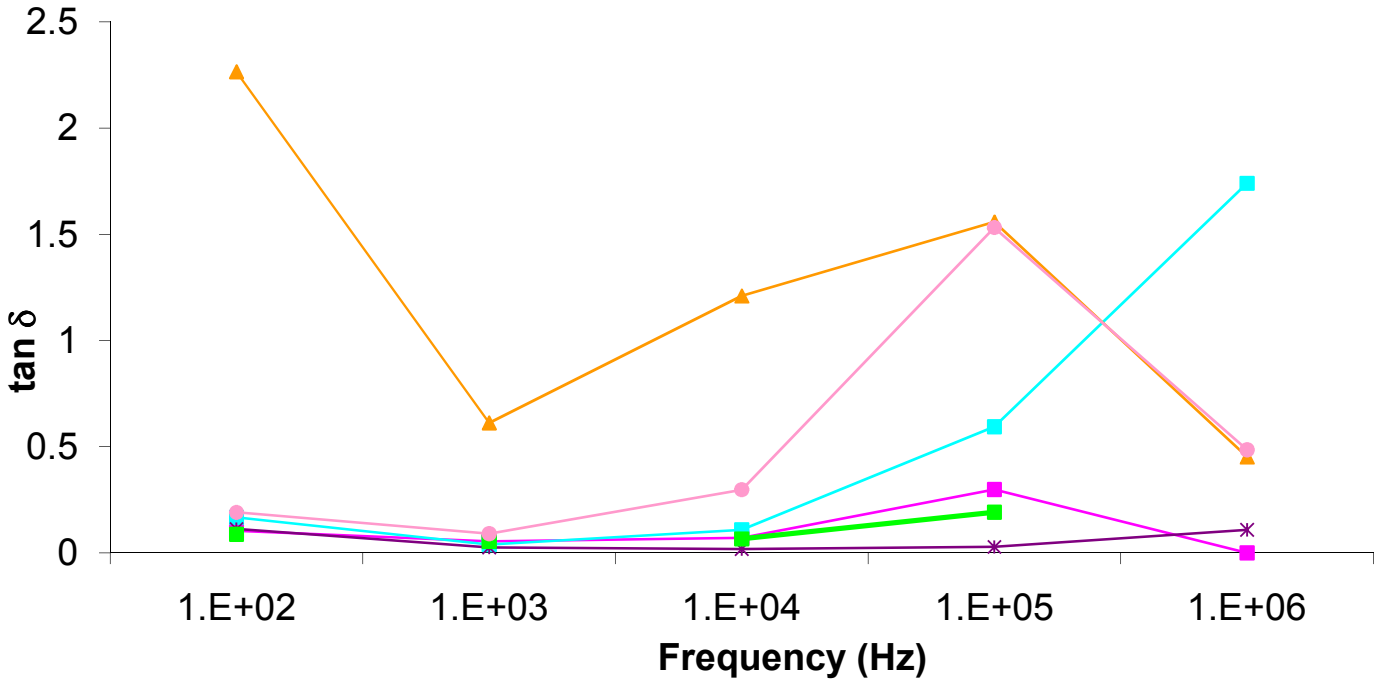

Figure 41: Dielectric losses (tan δ) versus frequency for PZT films with 1wt % of (90% B_2O_3 and 10% PbO) and sintered at 800ºC, 850ºC and 900ºC for 30 and 60 minutes. . __ 800 ºC for 30 minutes, with film thickness of 0.0162 mm; __ 800 ºC for 60 minutes, with film thickness of 0.0165 mm; __ 900 ºC for 30 minutes, with film thickness of 0.0172 mm; __ 900 ºC for 60 minutes, with film thickness of 0.0072 mm; __ 850 ºC for 30 minutes, with film thickness of 0.0172 mm; __ 850 ºC for 60 minutes, with film thickness of 0.0165 mm.

The dielectric response of PZT films with 1wt % of (80% B_2O_3 and 20% PbO) and sintered at different temperatures are represented in Figures 42 and 43. A similar trend is observed for the variation of the permittivity with the frequency and with the sintering temperature. The best dielectric permittivity and losses were observed for the films sintered at 850ºC and 60 minutes and the inferior response observed for those sintered at 900ºC and 60 minutes. The dielectric losses of these films followed this behaviour.

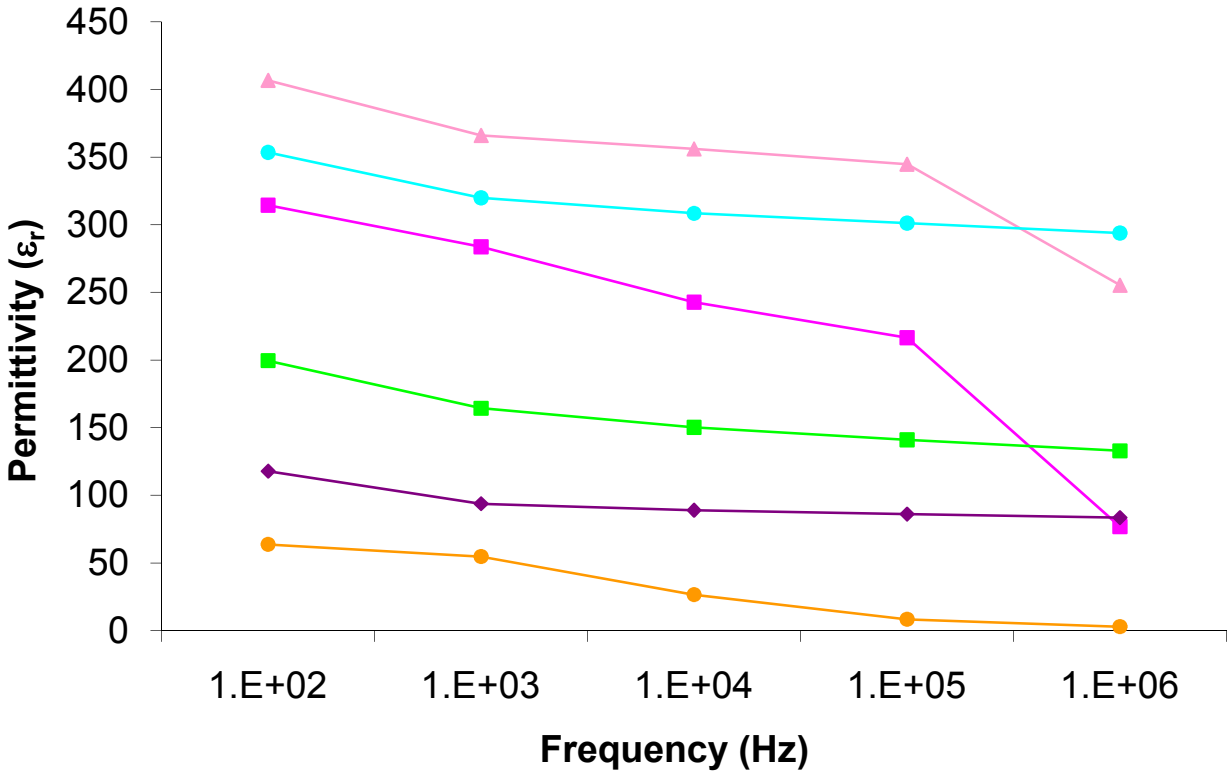

Figure 42: Permittivity versus frequency for PZT films with 1wt % of (80% B_2O_3+ 20% PbO) films sintered at 800ºC, 850ºC and 900ºC for 30 and 60 minutes. __ 800 ºC for 30 minutes, with film thickness of 0.0202 mm; __ 800 ºC for 60 minutes, with film thickness of 0.0146 mm; __ 900 ºC for 30 minutes, with film thickness of 0.0106 mm; __ 900 ºC for 60 minutes, with film thickness of 0.0092 mm; __ 850 ºC for 30 minutes, with film thickness of 0.0124 mm; __ 850 ºC for 60 minutes, with film thickness of 0.0265 mm.

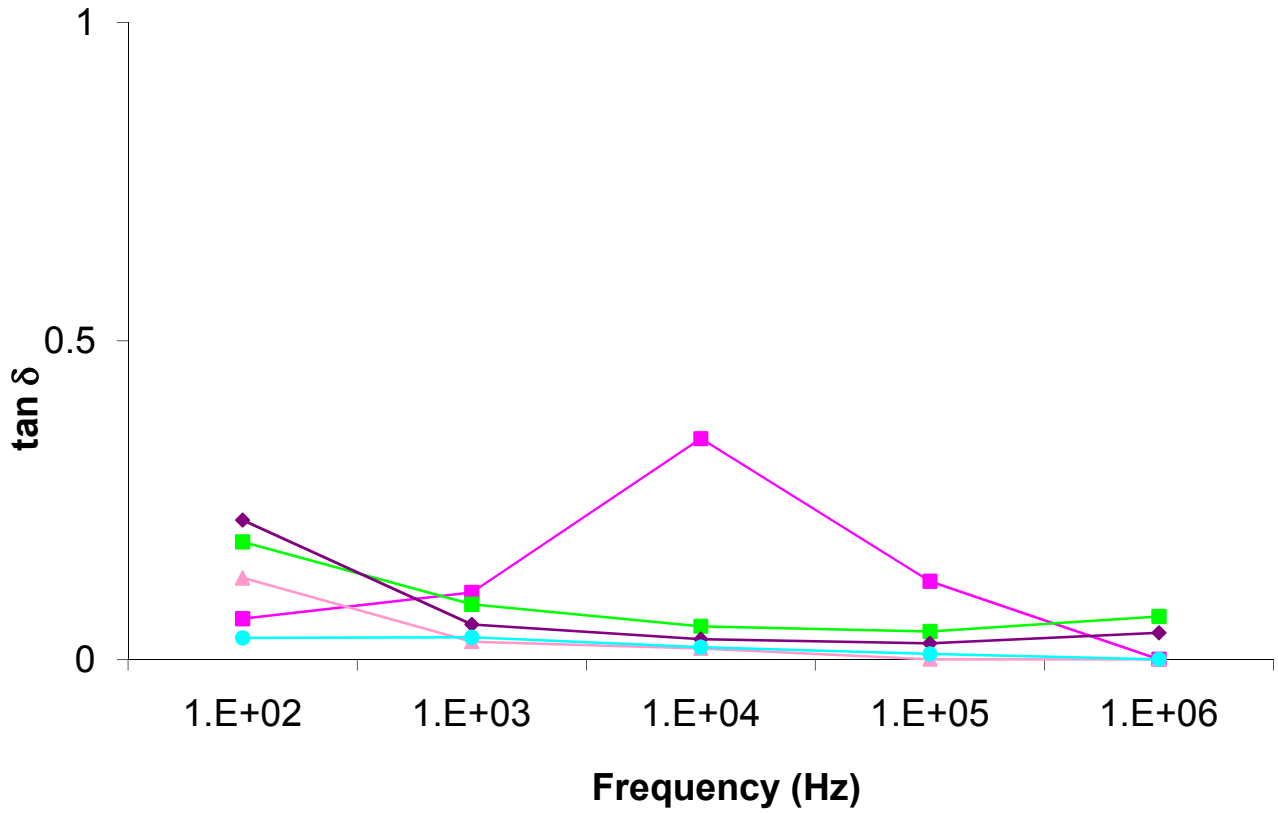

Figure 43: Dielectric losses (tan δ) versus frequency for PZT films with 1wt % of (80 B_2O_3+ 20 PbO films sintered at 800ºC, 850ºC and 900ºC for 30 and 60 minutes. __ 800 ºC for 30 minutes, with film thickness of 0.0202 mm; __ 800 ºC for 60 minutes, with film thickness of 0.0146 mm; __ 900 ºC for 30 minutes, with film thickness of 0.0106 mm; __ 900 ºC for 60 minutes, with film thickness of 0.0092 mm; __ 850 ºC for 30 minutes, with film thickness of 0.0124 mm; __ 850 ºC for 60 minutes, with film thickness of 0.0265 mm.

Next graph (Figure 44) represents the dielectric permittivity for PZT films with 1 wt % (50% B_2O_3 + 50% PbO) and 3 wt % of (50% B_2O_3 + 50% PbO) as a function of the frequency. Two distinct zones in the graph can be clearly observed: i) films with 1wt% of (50% B_2O_3 + 50% PbO) and ii) films with 3 wt % of (50% B_2O_3 + 50% PbO) indicating the obvious role of the amount of the sintering aids in the dielectric response, that is optimised for 3wt% of the oxide addition.

For the same frequency (1 kHz) but with a composition of 3 wt % of (50% B_2O_3 + 50% PbO) the value obtained for permittivity was 1195 at 850ºC and 30 minutes. Indeed, the best dielectric response of this work was obtained for the composition of 3 wt % of (50% B_2O_3 + 50% PbO), that corresponds to the best film densification.

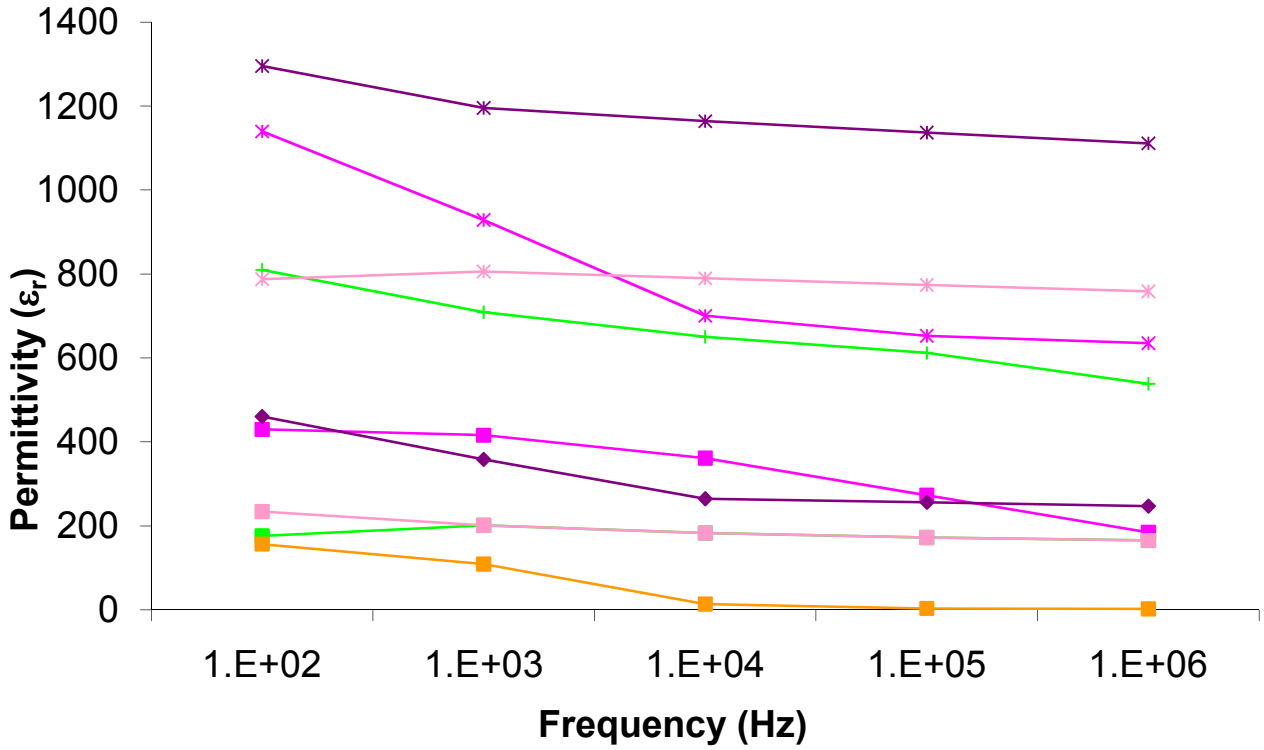

Figure 44: Permittivity versus frequency for sintered PZT films with 1 and 3 wt % of (50 B_2O_3 + 50 PbO) films sintered at 800ºC, 850ºC and 900ºC for 30 and 60 minutes. __ (1wt %), 800 ºC for 30 minutes, with film thickness of 0.0238 mm; __ (1wt %), 800 ºC for 60 minutes, with film thickness of 0.0112 mm; __ (1wt %), 900 ºC for 60 minutes, with film thickness of 0.0044 mm; __ (1wt %), 850 ºC for 30 minutes, with film thickness of 0.0154 mm; __ (1wt %), 850 ºC for 60 minutes, with film thickness of 0.0130 mm; _*_ (3wt %), 800 ºC for 30 minutes, with film thickness of 0.010 mm; _'_ (3wt %), 800 ºC for 60 minutes, with film thickness of 0.009 mm; _*_ (3wt %), 850 ºC for 30 minutes, with film thickness of 0.009 mm; _*_ (3wt %), 850 ºC for 60 minutes, with film thickness of 0.009 mm.

In terms of loss, better results were once again obtained for 3 wt % of (50% B_2O_3 + 50% PbO) (Figure 45). For the composition with the best permittivity, losses at 1 kHz are 0.02.

Capacitance versus voltage curves of these films are shown in Figure 46. The best capacitance response was observed for the films sintered at low temperatures: a capacitance of 0.503 pF for PZT films with 1wt % of (50 B_2O_3 + 50 PbO), sintered at 800ºC and 850ºC of sintering temperature 30 and 60 minutes, respectively.

The discrepancies between the capacitance and dielectric response for the films with 1 and 3 wt% may be related with microstructural details of the films, such as film thickness and interface layers, that under the applied electric field can affect differently the polarization and as a consequence the maximum capacitance is not observed for the film that exhibits the maximum permittivity.

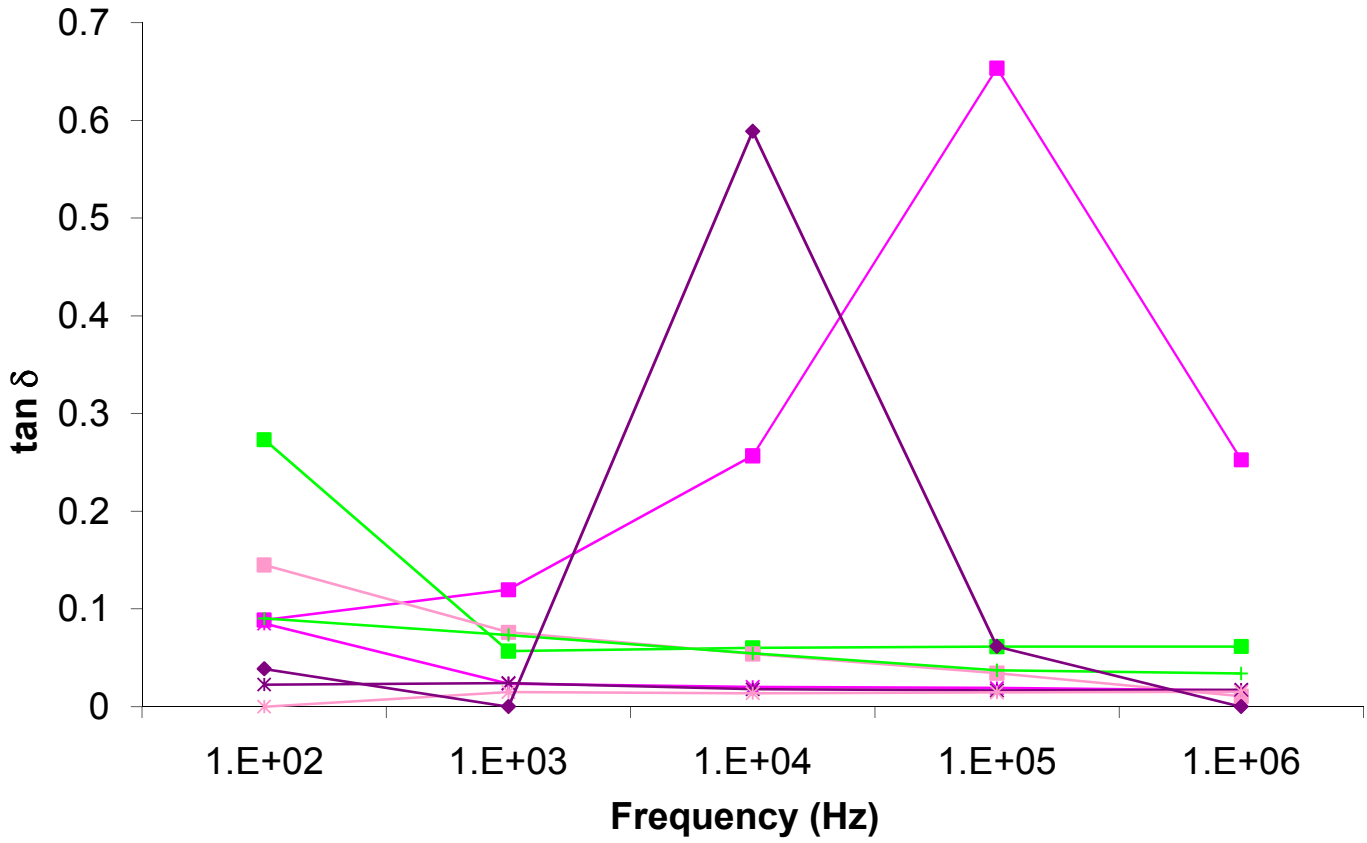

Figure 45: Dielectric losses (tan δ) versus frequency for PZT films with 1 and 3 wt % of (50% B_2O_3+ 50% PbO) films sintered at 800ºC, 850ºC and 900ºC for 30 and 60 minutes. __ (1wt %), 800 ºC for 30 minutes, with film thickness of 0.0238 mm; __ (1wt %), 800 ºC for 60 minutes, with film thickness of 0.0112 mm; __ (1wt %), 850 ºC for 30 minutes, with film thickness of 0.0154 mm; __ (1wt %), 850 ºC for 60 minutes, with film thickness of 0.0130 mm; _*_ (3wt %), 800 ºC for 30 minutes, with film thickness of 0.010 mm; _'_ (3wt %), 800 ºC for 60 minutes, with film thickness of 0.009 mm; _*_ (3wt %), 850 ºC for 30 minutes, with film thickness of 0.009 mm; _*_ (3wt %), 850 ºC for 60 minutes, with film thickness of 0.009 mm.

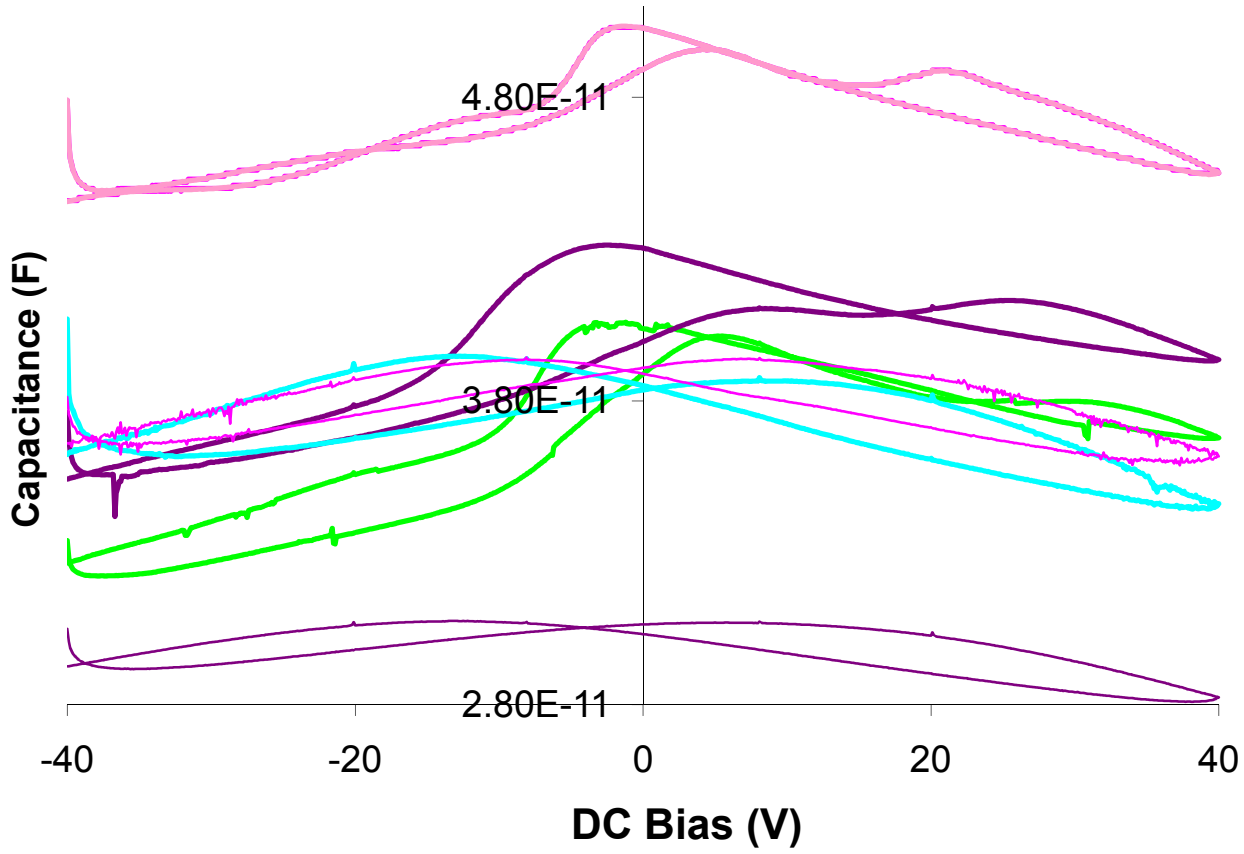

Figure 46: Capacitance versus voltage PZT films with 1and 3 wt % of (50% B_2O_3+ 50% PbO) sintered at 800ºC, 850 and 900ºC for 30 and 60 minutes. __ (1wt %), 800 ºC for 30 minutes, with film thickness of 0.0238 mm; __ (1wt %), 800 ºC for 60 minutes, with film thickness of 0.0112 mm; __ (1wt %), 900 ºC for 30 minutes, with film thickness of 0.0078 mm; __ (1wt %), 850 ºC for 30 minutes, with film thickness of 0.0154 mm; __ (1wt %), 850 ºC for 60 minutes, with film thickness of 0.0130 mm; __ (3wt %), 800 ºC for 30 minutes, with film thickness of 0.010 mm; __ (3wt %), 850 ºC for 30 minutes, with film thickness of 0.009 mm.

4.2.3.3 Electrical properties of PZT + 1wt % (V_2O_3 + PbO)

For comparison equivalent films with a mixture of V_2O_5 and PbO [45] were prepared and their dielectric properties measured and are presented in Figures 47 and 48. In general and as expected the permittivity and the losses decrease as the frequency increases, within the frequency range used in this work.

As observed for the films with B_2O_3 and PbO, the best dielectric performance of PZT with 1wt % (V_2O_3 + PbO) was observed for the films sintered at low sintering temperatures and times (permittivity of 381 and losses of 0.09 at 1 kHz,). While for PZT with (xB_2O_3 + (100-x) PbO), the best values of permittivity were in general obtained at 850ºC and 30 minutes, for PZT with (V_2O_5 + PbO) the highest values were obtained at 800ºC and 30 minutes. These differences reflect the different behaviour of the sintering aids, being the vanadium lead oxide mixture more effective in terms of dielectric response at lower temperatures than the boron lead oxide mixtures, although films with this last mixture presented the highest values of dielectric permittivity.

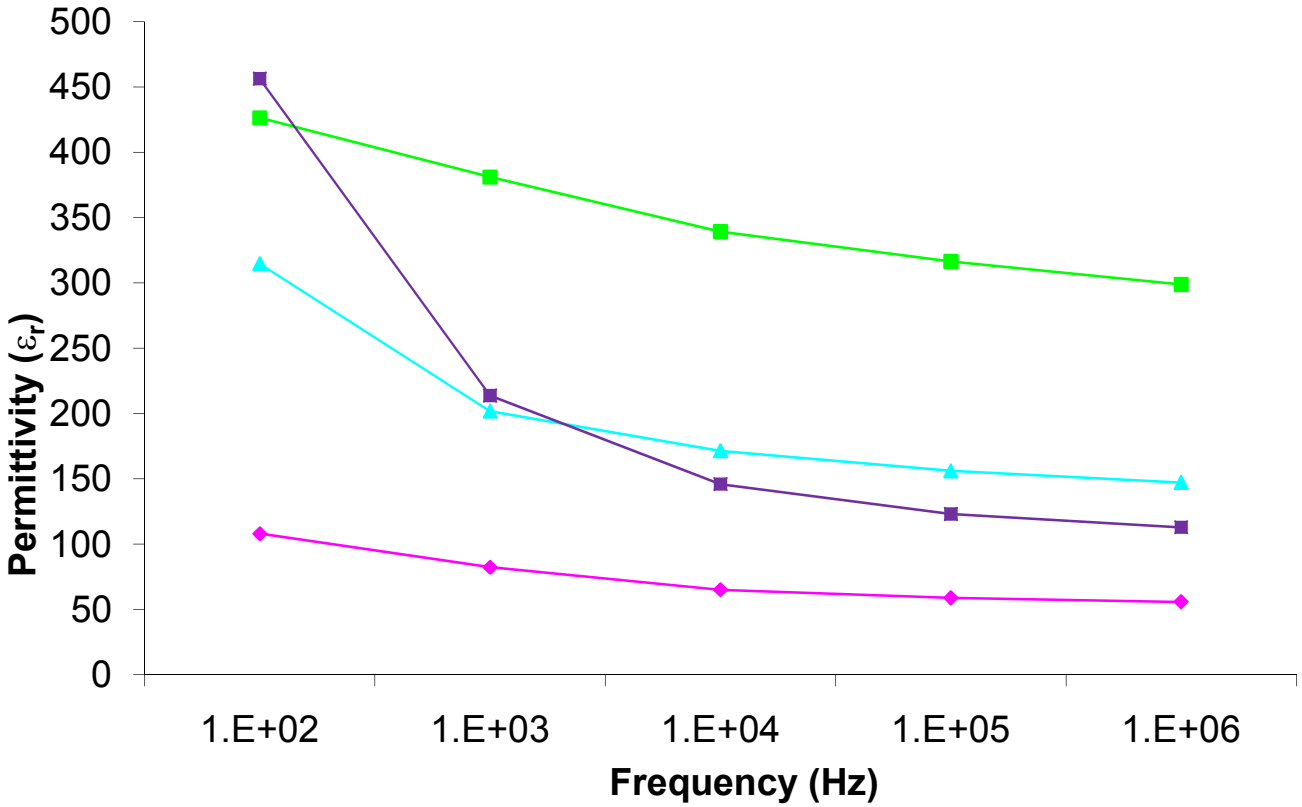

Figure 47: Permittivity versus frequency for PZT films with 1wt % of (V_2O_5 + PbO) and sintered at 800ºC, 850ºC and 900ºC and for 30 and 60 minutes. __800 ºC for 30 minutes, with film thickness of 0.007 mm; __850 ºC for 30 minutes, with film thickness of 0.010 mm; __900 ºC for 30 minutes, with film thickness of 0.011mm; __900 ºC for 60 minutes, with film thickness of 0.009 mm.

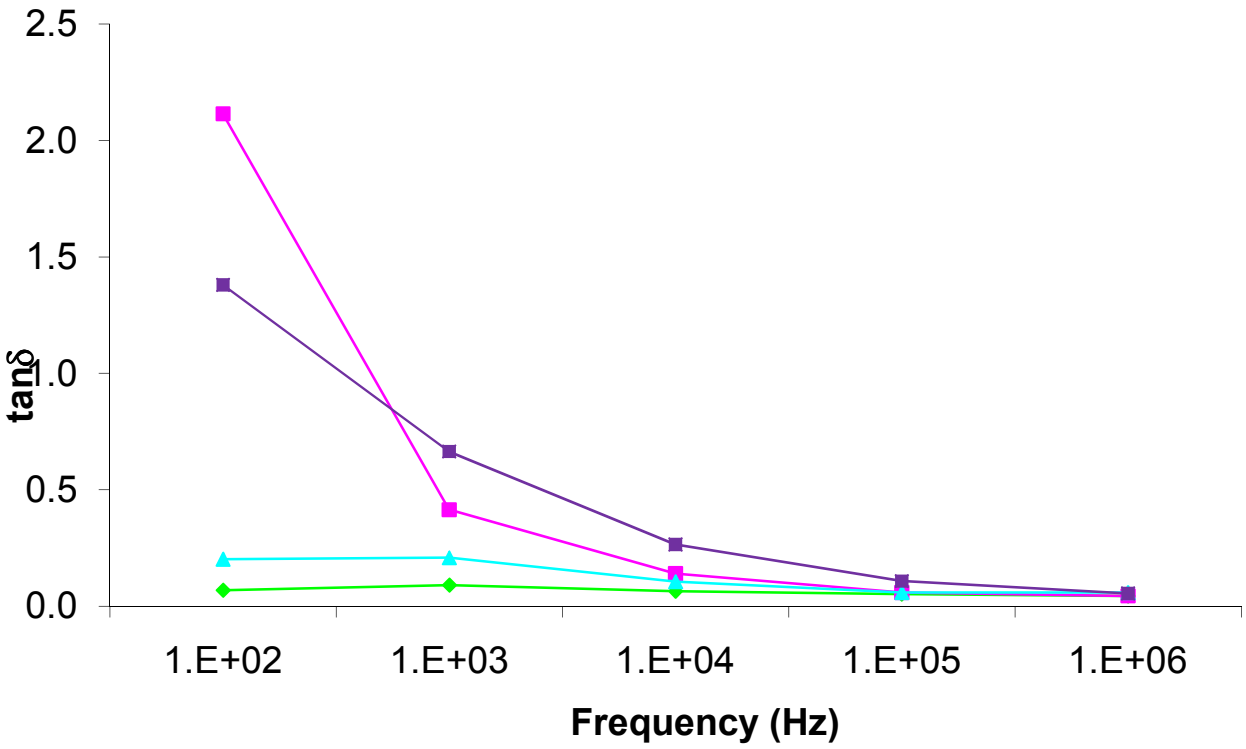

Figure 48: Dielectric losses (tan δ) versus frequency for PZT films with 1wt % of (V_2O_5 + PbO) and sintered at 800ºC, 850ºC and 900ºC and for 30 and 60 minutes. __800 ºC for 30 minutes, with film thickness of 0.007 mm; __850 ºC for 30 minutes, with film thickness of 0.010 mm; __900 ºC for 30 minutes, with film thickness of 0.011mm; __900 ºC for 60 minutes, with film thickness of 0.009 mm.

For comparison the next graph depicts the variation of the dielectric permittivity and losses as a function of frequency of PZT thick films on Cu foil sintered at 1000 ºC for 30 min at pO_2 ~5 x10^{-5} atm. The dielectric permittivity at a frequency of 10 kHz is 90 and the dielectric loss was 0.2. It´s obvious from these results that PZT thick films on Cu substrates sintered without sintering aids have not the required properties required to embed them into electronic systems. On the other hand and based on the above results, PZT films on Cu sintered with a mixture of B_2O_3 + PbO posses enhanced properties making these films good candidates for embedding microelectronics applications.These observations are well visible in the next table.

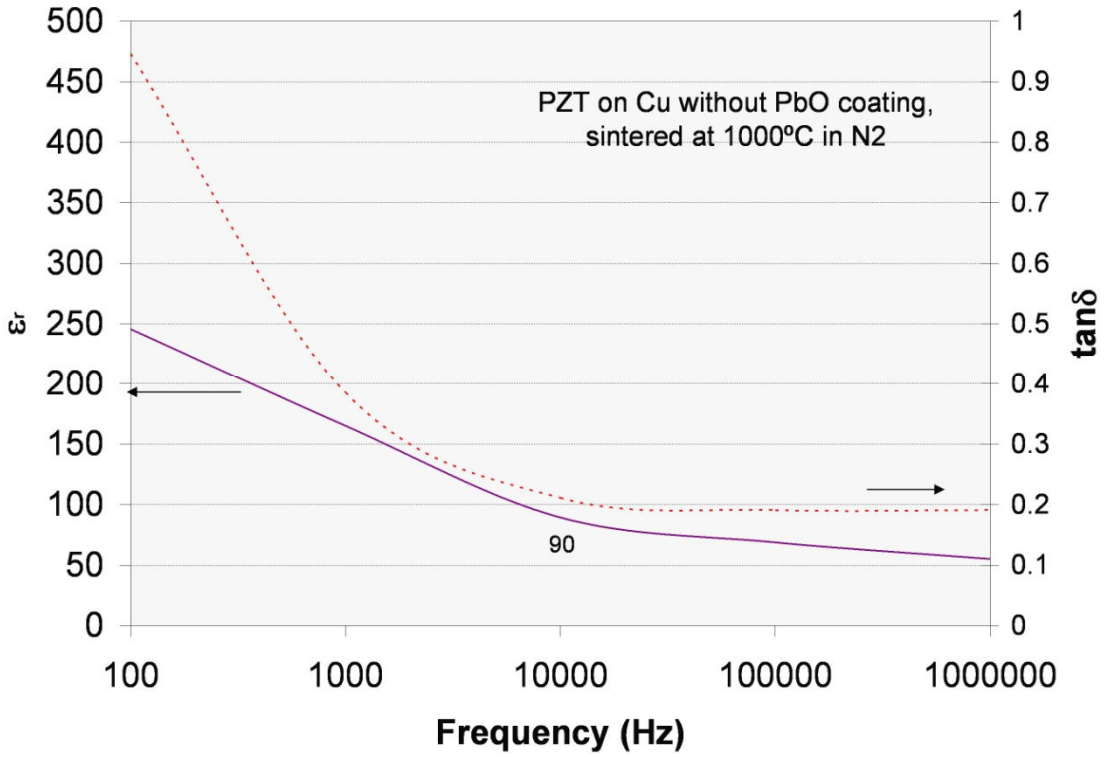

Figure 49: Dielectric Permittivity and Dielectric Loss of PZT thick films on Cu foil sintered at 1000 ºC for 30 min at pO_2 ~5 x10^{-5} atm as a function of frequency. [34]

Table 6 presents the dielectric permittivity and dielectric loss of PZT thick films deposited on Cu foils without any additive, with glass, with a mixture of 1 and 3 wt % (B_2O_3 + PbO), with a mixture of 1 wt % (V_2O_5 + PbO) and with additions of PbO and sintered at different temperatures.

Comparing all values one can see that the best dielectric response was obtained for the films with 3 wt % (50% B_2O_3 + 50% PbO) and sintered at 850ºC, 30 min and for PZT deposited on Pt foils and sintered 1150ºC and 30 minutes.

Table 6: Permittivity and dielectric loss for PZT thick films deposited on Cu foils, with additions of glass, a mixture of 1 and 3 wt % (B_2O_3 + PbO), a mixture of 1 wt % (V_2O_5 + PbO) and PbO and PZT thick films deposited on Pt foils and sintered at different temperatures.

Composition and conditions of the films	Frequency 1000 (HZ)	
	Permittivity (ε_r)	Loss (tan δ)
PZT + glass for 800ºC, 30 min.	316.5	0.05
PZT + glass for 850ºC, 30 min.	58.9	0.06
PZT + glass + PVB for 800ºC, 30 min.	35.6	0.00
PZT + glass + PVB for 850ºC, 30 min.	31.9	0.10
1wt % ($90B_2O_3$ + 10PbO) for 800ºC, 30 min	257.4	0.05
1wt % ($90B_2O_3$ + 10PbO) for 850ºC, 30 min.	342.0	0.03
1wt % ($50B_2O_3$ + 50PbO) for 800ºC, 30 min.	415.9	0.12
1 wt % ($50B_2O_3$ + 50PbO) for 850ºC, 30 min.	358.4	-
1 wt % ($80B_2O_3$ + 20PbO) for 800ºC, 30 min.	283.8	0.10
1 wt % ($80B_2O_3$ + 20PbO) for 850ºC, 30 min	93.7	0.05
3 wt % ($50B_2O_3$ + 50PbO) for 800ºC, 30 min.	928.5	0.02
3 wt % ($50B_2O_3$ + 50PbO) for 850ºC, 30 min.	1195.2	0.02
1 wt % (V_2O_5 + PbO) for 800ºC, 30 min.	381.0	0.09
1 wt % (V_2O_5 + PbO) for 850ºC, 30 min.	82.3	0.41
PZT for 1000ºC, 30 min.	160	0.32
PZT + PbO for 1000ºC, 30 min.	240	0.03
PZT on PT foil for 1150ºC, 30 min.	1330	0.06

5. Conclusions

In order to decrease the sintering temperature of thick PZT films to make them compatible with the use of Cu substrates and to improve the film quality and dielectric performance for embedded circuit applications, using a low cost based process, the following approaches were tested in this work: fabrication of PZT films by EPD and utilization of two different types of sintering aids: borate-based glass powders and a mixture of lead and boron oxide.

It was verified that the addition of glass powders was not very effective as a sintering aid. The main reason behind this observation is associated with the difficulties in depositing homogenous thick films by EPD, what is related with problems in keeping stable the suspension of PZT and glass powder. The stability of the suspension depends on the interaction between electrostatic and van der Waals forces acting on the individual particles. The coagulation of a disperse system (suspension) is the result of the interaction of such forces. High electrostatic repulsion forces occur for highly charged particles what was impossible to obtain in these PZT + borate glass suspensions. To improve the quality of the deposition, binders were added, but weren't effective and there was not any improvement in the quality of the deposition. As a consequence these films presented a poor dielectric response. More research is necessary to optimise the stability of the suspension what implies the understanding of the mechanism of charging glass particles.

On the other hand, it was verified that under controlled pO_2 atmosphere dense thick PZT films on Cu were obtained in the presence of 1 and 3 wt % of a mixture of B_2O_3 and PbO. In this case the stability of the suspension, related with the high zeta potential, was very good and homogeneous and compact films were deposited on Cu foils. The addition of B_2O_3 + PbO was indeed effective in reducing the sintering temperature of PZT thick films and the best dielectric behaviour was obtained for 3 wt % of (50% B_2O_3 + 50% PbO) and films sintered at 850ºC for 30 minutes. For sintering temperatures higher than 850ºC the dielectric properties deteriorate, what may be related with the reaction of PZT with the Cu substrate.

In conclusion, using EPD technology, crack-free PZT thick films with 3 wt % of addition of (50 % B_2O_3 + 50 % PbO) on Cu foils were obtained after sintering at temperatures lower than 900ºC under controlled pO_2 atmosphere and present dielectric permittivities ~1195 and dielectric losses ~0.02. The obtained dielectric performance is superior to the one of PZT films previously prepared in which lead oxide and vanadium oxide were used as sintering aids. In this case after sintering at 900ºC for 30 min a dielectric permittivity of ~450 and loss tangent of 1.39 was reported.[45]

References

[1] R. P. Tandon, V. Singh, N. Narayanaswami and V. K. Hans, *Low temperature sintering of PZT ceramics using a glass additive*, Ferroelectrics, **196**, 117 – 120 (1997).

[2] P.K. Davies, H. Wu, A.Y. Borisevich, I.E. Molodetsky, L. Farber, *Crystal Chemistry of complex perovskites: New Ordered Dielectric Oxides*, Annual Review Material Res, **38**, 369-401 (2008)

[3] A. Saphary, R. K. Panda and V. F. Janas, *Ferroelectric Ceramics: Processing, Properties & Applications*, Applications of Ferroelectric Ceramic Materials, **1**, 1-46 (2005).

[4] A. Wu, P. M. Vilarinho and A. I. Kingon, *Ceramic Processing Strategies* for *Thick Films on Copper Foils,* Acta Materialia, **58**, 2282-2290 (2010).

[5] S. W. Or, Y. F. Duan, Y. Q. Ni, Z. H. Chen and K. H. Lam, Development Magnetorheological Dampers with Embedded Piezoelectric Force Sensors for Structural Vibration Control, Journal of Intelligent Material Systems and Structure, **19**, 1327-1338 (2008).

[6] www.msm.cam.ac.uk/doitpoms/tlplib/piezoelectrics/pzt.php (as in December, 2009).

[7] C. A. Randall, N. Kim, J. P. Kucera, W. Cao and T. R. Shrout, *Intrinsic and Extrinsic Size Effects in Fine-Grained Morphotropic-Phase-Boundary Lead Zirconate Titanate Ceramics*, Journal of the American Ceramic Society, **81** [3] 677–88 (1998).

[8] M. W. Hooker, *Properties of PZT-Based Piezoelectric Ceramics between 150 and 250 Degrees Celsius*, Center for Aerospace Information, 301, 1-30 (1998).

[9] B. Jaffe, W. Cook and H. Jaffe, *Piezoelectric Ceramics*, (1971).

[10] H. M. Liu,Q.L. Zhao, M. S. Cao, J. Yuan, Z. X. Duan, C. J. Qiu, *Electromechanical Properties of Microcantilever Actuated by Enhanced Piezoelectric PZT Thick Film*, China Physics Letters, **25**, 4128-4130 (2008).

[11] L. Jin, Z. He and D. Damjanovic, *Nanodomains in Fe^{+3} doped lead zirconate titanate ceramics at the morphotropic phase boundary do not correlate with high properties*, Applied Physics Letters, **95**, 012905 – 012905-3 (2009).

[12] G. H. Hardling, *Ferroelectric Ceramics: History and Technology*, Journal of the American Ceramic Society*,* **82** [4] 797–818 (1999).

[13] J. F. Ihlefeld, *Synthesis and Properties of Barium Titanate Solid Solution Thin Films deposited on Copper Substrates,* Thesis in Doctor of Philosophy, North Carolina State University, (2006).

[14] V. R. Cooper, I. Grinberg, N. R. Martin and A. M. Rappe, *Local Structure of PZT*, Fundamental Physics of Ferroelectrics, American Institute of Physics, **626**, 26-35 (2002).

[15] P. M. Vilarinho, *Functional Materials: Properties, Processing and Applications*, Scanning Probe Microscopy: Characterization, Nanofabrication and Device Application of Functional Materials, **186**, 3 -33 (2005).

[16] J. Gao, *Sol-Gel* $(Ba_xSr_{1-x})TiO_3$ *Thin Films for Microelectronic Applications*, Master Thesis in Material Science, University of Aveiro (2007).

[17] Y. Bing, *Synthesis structure and properties of high piezoelectrics and ferroelectrics complex perovskite systems,* Master Thesis in Material Science, Shandong University, (2005).

[18] N. Izyumskaya, Y. I. Alivov, S. J. Cho, H. Morko, H. Lee and Y. S. Kang, *Processing, Structure, Properties, and Applications of PZT Thin Films*, Critical Reviews in Solid State and Material Science, 32, 111-202 (2007).

[19] N. Setter and R. Waser, *Eletroceramic Materials*, Acta Materialia, 48, 151-178 (2000).

[20] H. Li, *Sodium Potassium Niobate-based Lead-free Piezoelectric Ceramics: Bulk and Freestanding Thick Films*, Thesis in Doctor of Philosophy, Faculty of Drexel University (June 2008).

[21] A. L. Kholkin, A. Wu and P. M. Vilarinho, *Piezoelectric thick film composites: Processing and applications*, Material Science, **5**, 1-24 (2004).

[22] Y.Takahashi, *Synthetic process of the sol-gel derived* $Pb(Zr_{0.53}Ti_{0.47})O_3$ *films using polyvinyl butyral binder*, Thin Solid Films, **370**, 5-9 (2000).

[23] M. D. Losego, L. H. Jimison, J. F. Ihlefeld and J. P. Maria, *Ferroelectric response from lead zirconate titanate thin films prepared directly on low-resistivity copper substrates*, Applied Physics Letters, **86**, 172906 – 172906-3 (2005).

[24] I. Corni, M. P. Ryan and A. R. Boccaccini, *Electrophoretic deposition: From traditional ceramics to nanotechnology*, Journal of the European Ceramic Society, **28**, 1353–1367 (2008).

[25] A. Wu, P.M. Vilarinho, *Eletrophoretic Deposition of Lead Zirconate Titanate Films on Metal Foils for Embedded Components*, Journal of the American Ceramic Society, **89** [2] 575–581 (2006).

[26] A. R. Boccaccini, J. A. Roether, B. J. C. Thomas, M. S. P. Shaffer, E. Chaves, E. Stoll and E. J. Minay, *The Electrophoretic Deposition of inorganic nanoscaled Material*, Journal of the Ceramic Society of Japan, **114**, 1-14 (2006).

[27] S.Y. Ng and A. R. Boccaccini, *Lead zirconate titanate films on metallic substrates by electrophoretic deposition*, Materials Science and Engineering, **116**, 208–214 (2005).

[28] L. Besra and M. Liu, *A review of fundamentals and applications of Electrophoretic Deposition*, Progress in Materials Science, **52**, 1–61 (2007).

[29] F. Zhi, A. Wu, P. M. Vilarinho and A. I Kingon, *Low dielectric loss $BaNd_2Ti_5O_{14}$ thick Films prepared by electrophoretic deposition technique*, Applied Physics Letters, **90**, 52912 - 052912-3 (2007).

[30] X. Su, A. Wu and P. M. Vilarinho, *Titanium tellurite thick films prepared by electrophoretic deposition and their dielectric properties*, Scripta Materialia, **61**, 536–539 (2009).

[31] P. Sooksaen, I. M. Reaney, D. C. Sinclair, *Engineered sintering aids for PbO-based* electroceramics, Journal of Electroceramics, **18**, 77–85 (2007).

[32] http://www.metalprices.com/ (as in July 2009).

[33] T. Sweeney and R. W. Whatmore, *Electrophoretic depositions of PZT ceramic films*, IEEE Xplore, **1**, 193-196, (1996).

[34] A. Wu, P. M. Vilarinho, S. Srinivasan, A. I. Kingon, I. M. Reaney, D. Woodward, A.R. Ramos and E. Alves, *Microstructural studies of PZT thick films on Cu foils*, Acta Materialia, **54,** 3211–3220 (2006).

[35] W. F. Smith and J. Hashemi “Foundations of Materials Science and Engineering”, Hardcover edition from McGraw-Hill Science/Engineering/Math (2005), www.amazon.com/Foundations-Materials-Science-Engineering-Student/dp/0073107638#reader_0073107638 (as in December 2009

[36] D. J. Chakrabartl and D.E. Laughlin, *The Cu-Pb based system*, Bulletin of Alloy Phase Diagrams*,* **5**, 503 – 510 (1984).

[37] www.metallurgy.nist.gov/phase/solder/cupb-w.html (as in July 2009).

[38] C.H. Wang and L. Wu, *4PbO·B_2O_3 - A New Sintering Agent For Pb(Zr, Ti)O_3 Ceramics*, Japanese Journal of Applied Physics, 32, 3209-3213 (1993).

[39] B. S. Purwasasmita and T. Kimura, *Effect of glass composition on chemical reaction between lead zirconate titanate and glasses (part 1): Lead-borate glasses*, Journal of the Ceramic Society of Japan, **108**, 966-972 (2000).

[40] F. Zhi, P.M. Vilarinho, A. I. Kingon, *$BaNd_2Ti_5O_{14}$ thick Films for Microelectronics Fabricated by Electrophoretic Deposition*, Thesis in Doctor of Materials Science and Engineering, Aveiro University (2008).

[41] F. Zhi, P. M. Vilarinho, A. Wu and A. I. Kingon, *Textured Microstructure and Dielectric Properties Relationship of $BaNd_2Ti_5O_{14}$ Thick Films Prepared by Electrophoretic Deposition*, Advanced Functional Materials, **19**, 1–11 (2009).

[42] L. Bergström, *Colloidal Processing of Ceramics*, Handbook of Applied Surface and Colloid Chemistry, **9**, 201-217 (2001).

[43 A. V. Delgado, F. Gonzalez-Caballero, R. J. Hunter, L. K. Koopal, and J. Lyklema, *Measurement and Interpretation of Electrokinetic Phenomena*, Pure and Applied Chemistry, **77**, 1753–1805 (2005).

[44] http://www.malvern.com/LabEng/technology/zeta_potential/zeta_potential_LDE.htm (as in February 2010).

[45] A. Wu, P. M. Vilarinho, A. Kingon, Internal Report, 2009.